IWLiME 2024

11th INTERNATIONAL CONFERENCE ON LITHIUM, INDUSTRIAL MINERALS AND ENERGY

November 27th to 29th Antofagasta, Chile

POSTERS

Organized by

Sponsored by

TABLE OF CONTENTS

INFLUENCE OF DIFFERENT MONOMERS ON THE AMPHIPHILIC PROPERTIES OF JANUS PARTICLES APPLIED IN PHASE CHANGE SLURRIES 1

INFLUENCE OF EXTERNAL COMPRESSIVE PRESSURE ON POUCH STACKED $LiFePO_4$ BATTERIES 4

MODELING OF THE PHYSICOCHEMICAL PROPERTIES OF THE Li_2SO_4 – $LiNO_3$ – H_2O SYSTEM 8

THE CORRELATION BETWEEN SURFACE SCALING BEHAVIOR WITH SOLAR OPTICAL PROPERTIES OF SILICON NANOWIRES: AN INVESTIGATION BASED ON FRACTAL CONCEPTS 11

STUDY OF ELECTRODIC REACTIONS TO PRODUCE LITHIUM HYDROXIDE FROM LITHIUM SULPHATE BY MEANS OF REACTIVE ELECTRODIALYSIS 14

PERFORMANCE EVALUATION OF $Li\text{-}O_2$ CELLS WITH Fe_2O_3-MODIFIED CATHODES USING ATOMIC LAYER DEPOSITION 17

MODELING AND SIMULATION OF THE Co-PRECIPITATION SYNTHESIS PROCESS OF THE JANUS NANOPARTICLES IN BATCH REACTOR 20

SYNTHESIS AND CHARACTERIZATION OF A NICKEL AND LITHIUM FERRITE FOR ELECTROCHEMICAL APPLICATIONS 23

PURIFICATION OF LiCl BRINES FROM EDL THROUGH ELECTROCHEMICAL ALKALINIZATION 26

SIMULATION OF THE PROCESS FOR OBTAINING POTASSIUM SULFATE FROM REGIONAL RAW MATERIALS 29

SYNTHESIS AND CHARACTERIZATION OF $LiNi_{0.5}Mn_{1.5}O_4$: A COMPARATIVE STUDY OF THE EFFECT OF LITHIUM SOURCES 32

EXPERIMENTAL EVALUATION OF NITRATE MIXTURES AS PCMs IN THERMAL ENERGY STORAGE FOR INDUSTRIAL APPLICATIONS ...35

INDUSTRIAL PROCESS STEAM SUPPLY – DEMONSTRATION OF AN ULTRA-DYNAMIC THERMAL ENERGY STORAGE 38

CELLULAR AUTOMATON MODEL FOR CORROSION SIMULATION AND OXIDE ION INFLUENCE IN THERMAL STORAGE SYSTEMS WITH MOLTEN SALTS..41

STUDY AND EVALUATION OF THE THERMAL BEHAVIOR IN THE SYNTHESIS OF THE CATHODE MATERIAL Na_XMnO_2 BY THE SOLID-STATE METHOD 44

ASSESSMENT OF DUST DEPOSITION EFFECTS ON PHOTOVOLTAIC MODULES USING AN ACCELERATED SOILING CHAMBER SIMULATING ATACAMA DESERT ENVIRONMENTAL CONDITIONS .47

VOLUMETRIC PROPERTIES MODELLING IN UNSATURATED SOLUTION OF Li–Na–K–Cl–H_2O SYSTEM FROM 288.15 TO 323.15 K USING THE PITZER EQUATIONS 50

POTENTIAL ELECTROACTIVE MATERIAL FOR LITHIUM-ION BATTERIES 53

STUDY OF ELECTROCRYSTALLIZATION OF PALLADIUM ON TITANIUM FOR WATER REDUCTION ELECTROCATALYSIS 56

SOLID-LIQUID EQUILIBRIUM MODELLING OF METHANOL + LITHIUM HYDROXIDE + WATER SYSTEM AT THREE TEMPERATURES 59

Influence of different monomers on the amphiphilic properties of Janus particles applied in phase change slurries

M. Cruz[1,2], S. Ushak[1,2], Y.E. Milian[1,3]
[1]*Center for Advanced Research in Lithium and Industrial Minerals, University of Antofagasta, Avenue Universidad de Antofagasta 02800, Antofagasta, Chile.*
[2]*Mineral Process Engineering, University of Antofagasta, Avenue Universidad de Antofagasta 02800, Antofagasta, Chile*
[3]*Iberian Energy Storage Research Center, Polígono 13, Parcela 31, "El Cuartillo", 10004 Cáceres, Spain.*

Thermal energy storage (TES) has gained considerable attention due to the persistent demand for energy, the requirement to improve the efficiency of renewable energy sources, and the necessity for effective auxiliary storage systems. [1]. In this sense, the interest in phase change slurries (PCS) as advanced TES and heat transfer media is growing. PCS are latent heat storage media that combine the high TES density of Phase Change Materials (PCMs) and the transport properties of conventional heat transfer fluids (HTF). In addition, PCS necessitates the use of a stabilizing agent that not only promotes effective interaction among components but also improves heat transfer efficiency. This agent plays a crucial role in maintaining system stability and optimizing thermal dynamics. Janus particles (JPs) are characterized by their asymmetrical structure due to different physical and/or chemical compositions, which confers amphiphilic properties. The dual nature of JPs makes them effective stabilizing agents; therefore, this study aims to evaluate the effects of different monomers on the amphiphilic properties of Janus particles in relation to PCMs and HTFs to support the advancement of novel PCS.
For the synthesis of JPs, the method proposed by Luo and collaborators [2] was modified by employing four silane-based monomers for the lipophilically modified face: trimethoxyphenylsilane, trimethylpropargylsilane, isobutyltrimethoxysilane and trimethoxyoctadecylsilane; meanwhile γ–glycidyloxypropyltrimethoxysilane was employed for conferring the hydrophilically modified face. Fourier-transform infrared spectroscopy (FTIR) analysis was used to determine the functionalization of JPs; the particle diameter were estimated using Dynamic Light Scattering (DLS) technique, and the amphiphilic behavior of the obtained JPS were evaluated using the dispersion/aggregation of particles in different solvents (water, ethanol, tetrahydrofuran, n-dodecane, and benzene) with different polarities at the interface of two immiscible solvents [3].
The FTIR results for the best synthesis of JPs with trimetoxifenilsilano is shown in the figure 1, the signals at 2974 and 2890 cm^{-1} are more pronounced in the first spectra because these Janus particles have a greater amount of alkyl groups on their surface due to less modification or a different treatment compared to the later spectra. In the last three spectra, the lower intensity of these signals indicates that the alkyl groups have been partially replaced or modified by other functional groups, such as silanes, which reduces the intensity of the C–H vibrations. This change due to a functionalization process, such as silanization, which introduces new functional groups

on the surface and decreases the amount of alkyl groups, which explains the lower intensity of these signals. Respect to particle diameter distribution (Figure 2), Trimethoxyoctadecylsilane has a lower polydispersity index compared to the other three compounds and that the largest size distribution of JPs as located between 200 and 400 nm indicating that it has a relatively uniform size distribution. Additionally, a dodecane-in-water (o/w) slurry system was chosen to probe the amphiphilic character, the higher the stabilization of the dodecane checked the higher the Janus character of JPs.

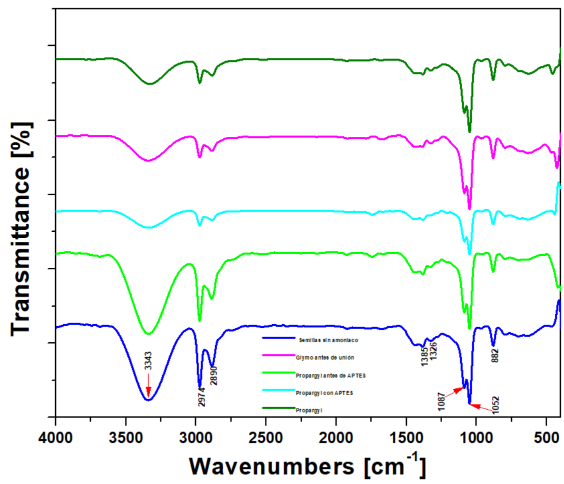

Figure 1. FTIR of JPs synthetized with Trimetoxifenilsilano

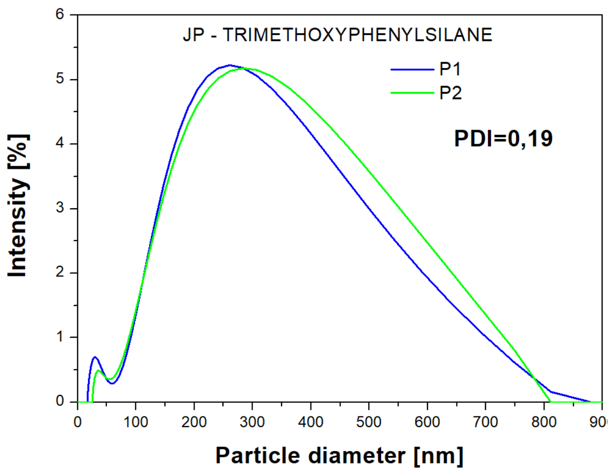

Figure 2. Particle diameter of Janus particles using Trimethoxyphenylsilane

The synthesis of JPs was developed, the best monomer for the synthesis is trimetoxiphenylsilane. The synthesized of JPs demonstrate that they are a promising material for the formation of PCS and these can be used as sources of energy storage.

Keywords: Janus Particles**,** Slurries, Thermal energy storage.

Acknowledgments: *Authors thank to ANID/FONDAP Nº 15110019, PUENTE Nº 1523A0006, and projects ANID/FONDECYT REGULAR 1231721project.*
M. Cruz would like to thank the ANID 21230140 year 2023.

References:

[1] *Y. Zhou, L. Duan, X. Ding, Y. Bao, F. Tian. Economic feasibility assessment of a solar aided liquid air energy storage system with different operation strategie. Journal of Energy Storage (72)2023.*
[2] J. Luo, B. Jiang, L. He, P. Wang, B. Peng, J. Yang, B. Ding, Y. Li, X. Geng, Nano -silica dispersion having amphiphilic properties and a double-particle structure and its production method. Patent Application N° US2019/046939A1, 2019.
[3] *E. Borri, N. Hua, A. Sciacovelli, D. Wu, Y. Ding, Y. Li, V. Brancato, Y. Zhang, A. Frazzica, W. Li, Z. Yu, Y.E. Milian, S. Ushak, M. Grageda and L.F. Cabeza. Phase Change Slurries for Cooling and Storage: An Overview of Research Trends and Gaps. Energies (15) 2022.*

11th INTERNATIONAL CONFERENCE IN LITHIUM, INDUSTRIAL MINERALS AND ENERGY

November 27-29, Antofagasta, Chile

Influence of different monomers on the amphiphilic properties of Janus particles applied in phase change slurries

M. Cruz[1,2], S. Ushak[1,2], Y.E. Milian[1,3]

[1]Center for Advanced Research in Lithium and Industrial Minerals, University of Antofagasta, Avenue Universidad de Antofagasta 02800, Antofagasta, Chile.
[2]Mineral Process Engineering, University of Antofagasta, Avenue Universidad de Antofagasta 02800, Antofagasta, Chile
[3]Iberian Energy Storage Research Center, Polígono 13, Parcela 31, "El Cuartillo", 10004 Cáceres, Spain.

Introduction

Thermal energy storage (TES) has gained considerable attention due to the persistent demand for energy, the requirement to improve the efficiency of renewable energy sources,and the necessity for effective auxiliary storage systems. [1] The charging/discharging time and capacity of some of the energy storage systems are shown in Figure 1.

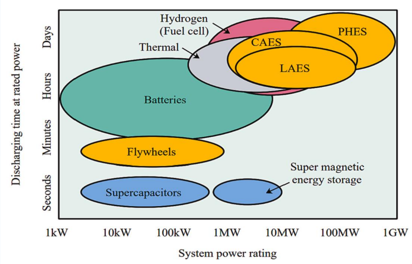

Figure 1. Capacity of some of the energy storage systems.. Source: Economic feasibility assessment of a solar aided liquid air energy storage system with different operation strategies, Zhou et al, 2023.

PCM (Phase Change Slurries)

The interest in phase change slurries (PCS) as advanced TES and heat transfer media is growing. PCS are latent heat storage media that combine the high TES density of Phase Change Materials (PCMs) and the transport properties of conventional heat transfer fluids (HTF). A recent scheme of the operation of a phase change material PCM is described in Figure 2. The combination of a phase change material and a heat transfer fluid results in an emulsion or a phase change slurry whose characteristics are shown in Figure 3.

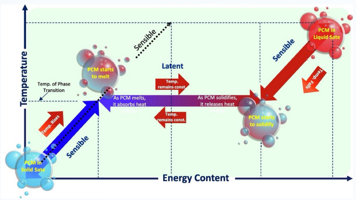

Figure 2. PCM Working. Source: Progress in research and development of phase change materials for thermal energy storage in concentrated solar power. Khan et al, 2023.

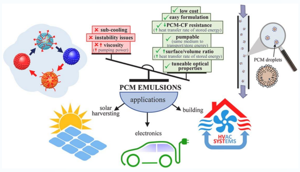

Figure 3. PCM Emulsions characteristics. Source: Review on phase change material emulsions for advanced thermal management: Design, characterization and thermal performance. Cabaleiro et al, 2022.

JPs (Janus Particles)

PCS necessitates the use of a stabilizing agent that not only promotes effective interaction among components but also improves heat transfer efficiency. This agent (Janus particles) plays a crucial role in maintaining system stability and optimizing thermal dynamics.

Janus particles (JPs) are characterized by their asymmetrical structure due to different physical and/or chemical compositions, which confers amphiphilic properties. The dual nature of JPs makes them effective stabilizing agents. Some Janus particles applications are shown in figure 4.

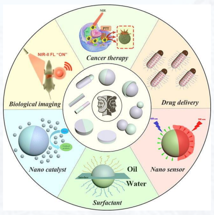

Figure 4. Applications of Janus particles. Source: Preparation and application of Janus nanoparticles: Recent development and prospects, Li et al, 2022.

Methodology

For the synthesis of JPs, the method proposed by Luo and collaborators [2] was modified by employing four silane-based monomers described below:

STEP 0

- Preparation of silicon oxide nanospheres using hydrolysis condensation process.

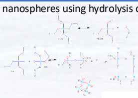

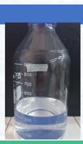

Silicon oxide nanoparticles

STEP 1

- Hydrophobic modification using 4 compounds.

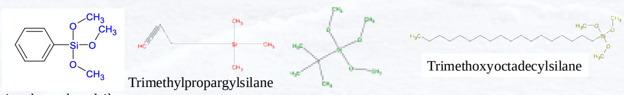

Trimethoxyphenylsilane

Trimethylpropargylsilane

Isobutyltrimethoxysilane

Trimethoxyoctadecylsilane

STEP 2

- Hydrophilic modification

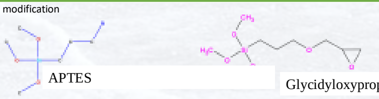

APTES

Glycidyloxypropyltrimethoxysilane

Fourier-transform infrared spectroscopy (FTIR) analysis was used to determine the functionalization of JPs; the particle diameter were estimated using Dynamic Light Scattering (DLS) technique

Results

FTIR results for the best synthesis of JPs with trimetoxifenilsilano is shown in the figure 5, the signals at 2974 and 2890 cm^{-1} are more pronounced in the first spectra because these Janus particles have a greater amount of alkyl groups on their surface due to less modification or a different treatment compared to the later spectra. In the last three spectra, the lower intensity of these signals indicates that the alkyl groups have been partially replaced or modified by other functional groups, such as silanes, which reduces the intensity of the C–H vibrations. This change due to a functionalization process, such as silanization, which introduces new functional groups on the surface and decreases the amount of alkyl groups, which explains the lower intensity of these signals.

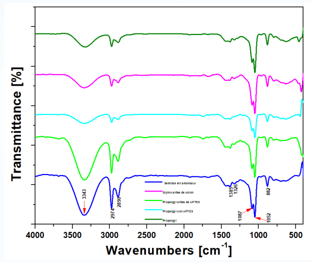

Figure 5. FTIR of JPs synthesized with trimethoxiphenilsilane

Particle diameter distribution (Figure 6), shown that Trimethoxyoctadecylsilane has a lower polydispersity index compared to the other three compounds and that the largest size distribution of JPs is located between 200 and 400 nm indicating that it has a relatively uniform size distribution.

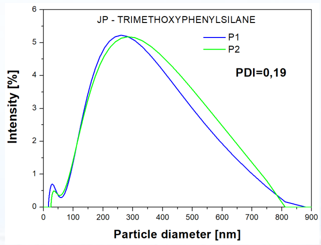

Figure 6. Particle diameter distribution of JPs synthesized with trimethoxiphenilsilane.

Additionally, a dodecane-in-water (o/w) slurry system was chosen to probe the amphiphilic character (Figure 7), the higher the stabilization of the dodecane checked the higher the Janus character of JPs.

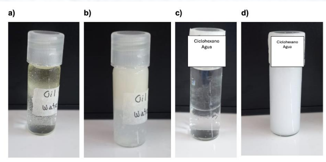

Figure 7. Emulsification experiments to test the dual functionality of Janus particles a and b oil wáter system, c and d cyclohexane and wáter system with/without JPs.

Conclusions

The synthesis of JPs was developed, the best monomer for the synthesis is trimetoxiphenylsilane. The synthesized of JPs demonstrate that they are a promising material for the formation of PCS and these can be used as sources of energy storage.

Acknowledgments: Authors thank to ANID/FONDAP N° 15110019, PUENTE N° 1523A0006, and projects ANID/FONDECYT REGULAR 1231721project.
M. Cruz would like to thank the ANID 21230140 year 2023.

References

[1] Y. Zhou, L. Duan, X. Ding, Y. Bao, F. Tian. Economic feasibility assessment of a solar aided liquid air energy storage system with different operation strategie. Journal of Energy Storage (72)2023.
[2] J. Luo, B. Jiang, L. He, P. Wang, B. Peng, J. Yang, B. Ding, Y. Li, X. Geng, Nano -silica dispersion having amphiphilic properties and a double-particle structure and its production method. Patent Application N° US2019/046939A1, 2019.
[3] E. Borri, N. Hua, A. Sciacovelli, D. Wu, Y. Ding, Y. Li, V. Brancato, Y. Zhang, A. Frazzica, W. Li, Z. Yu, Y.E. Milian, S. Ushak, M. Grageda and L.F. Cabeza. Phase Change Slurries for Cooling and Storage: An Overview of Research Trends and Gaps. Energies (15) 2022.

Organized by:

Sponsors:

INFLUENCE OF EXTERNAL COMPRESSIVE PRESSURE ON POUCH STACKED LiFePO4 BATTERIES

A. Garcia[1], M.Gonzales[2]

[1]Center for Advanced Research in Lithium and Industrial Minerals, University of Antofagasta, Avenue Universidad de Antofagasta 02800, Antofagasta, Chile.

[2]Chemical Engineering Department, University of Antofagasta, Avenue Universidad de Antofagasta 02800, Antofagasta, Chile

INTRODUCTION:

Batteries serve to store and supply electrical energy and are essential in electronic devices, electric vehicles and renewable energy storage systems. Lithium-ion batteries with LiFePO4 (LFP) offer future benefits such as increased safety and thermal stability, reducing the risk of fire and explosion. In addition, their long lifetime and low cost make them attractive for applications in electric vehicles and renewable energy storage. This work aims to study how different levels of external pressure influence the electrochemical performance of batteries, and to determine an optimal external pressure to improve the lifetime and performance of lithium-ion batteries. A. Barai et al. (2017), authors investigate the impact of compressive loads on the cyclic life of pouch cells, highlighting that external pressure can prevent electrode delamination and cracking. Their work suggests that applying pressure during the charge-discharge cycle can optimize cell capacity and stability. External pressure during the fabrication of lithium-ion battery components affects mechanical properties and microstructure by improving particle-to-particle contact, reducing porosity, and improving overall electrode density.

External pressure refers to the force applied on a material or system from the outside, in this case, on lithium-ion battery (LIB) cells. It will be applied during cell cycling to increase the volumetric energy density, improve particle distribution and optimize the connection between the electrode materials and the current collector. However, excessive pressure can cause long-term capacity loss. In addition, pressure can help stabilize the solid-electrolyte interface (SEI) layer and limit the volumetric expansion of the active material.

Objectives of the External Pressure Study in Batteries

- Improve Electrochemical Performance: The aim is to understand how external pressure can optimize the discharge capacity, capacity retention and polarization resistance of batteries.
- Increase Lifetime: The study of external pressure helps identify conditions that minimize delamination, cracking and other mechanical phenomena that can affect cell durability. It helps limit particle and solid electrolyte interface (SEI) cracking, which can extend battery life. The application of external pressure can also expel the gases generated, improving the safety and overall performance of battery cells.

METHODOLOGY

In this research we worked with different pressures 29.43 and 90.74 kPa, which are applied to a unitary pouch battery that was manufactured in the form of stacking, with dimensions of 5.3 cm long by 4.3 cm wide, with LFP cathode electrodes and graphite anodes.

RESULTS

Table 1. Pressurized operating conditions for unit cell batteries.

Celda	POUCH
Initial specific capacity [mAh/g]	119,89
Final specific capacity [mAh/g]	107,41
Velocity	0,07C
Current [mA]	1.5
Pressure 1 [Kpa]	29,43
Pressure 2 [Kpa]	90,74

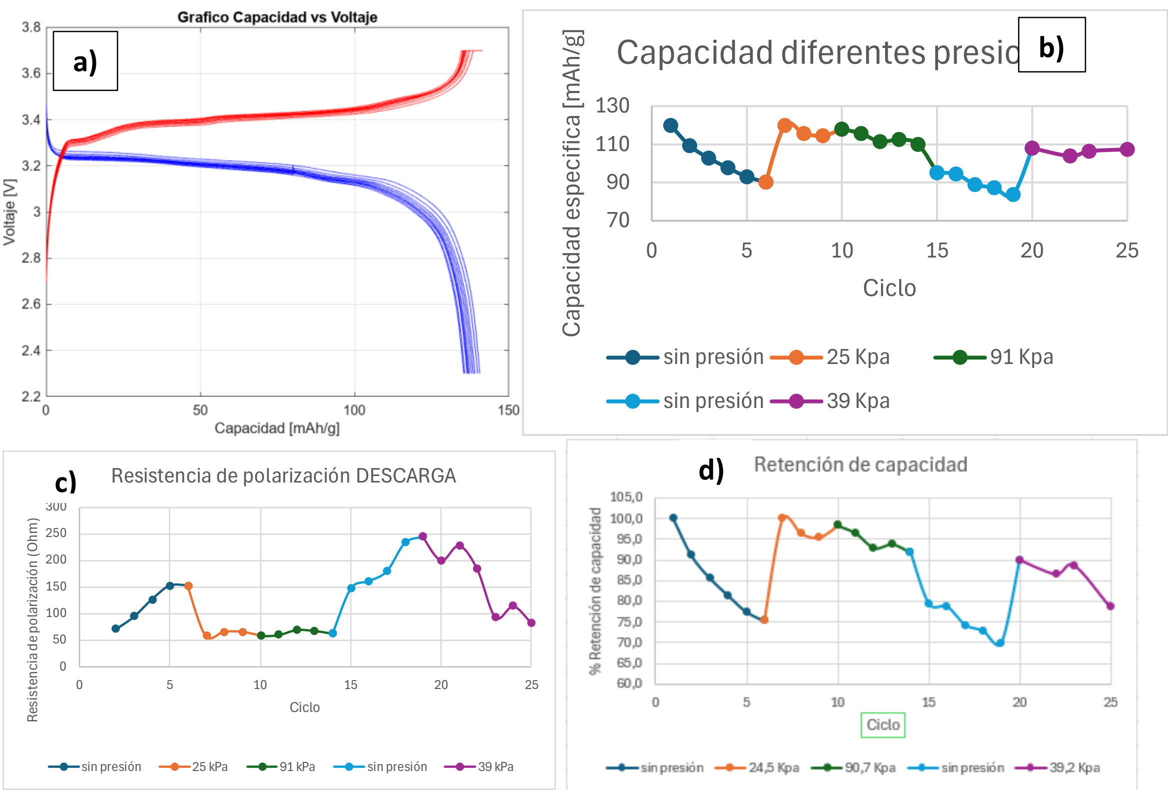

Figure 1. Electrochemistry of pouch battery. a) capacitance vs. voltage plot; b) capacitance by cell pressure interaction; c) polarization resistance and d) capacitance retention.

Keywords: lithium ion bacteria, LFP, external compression pressure, polarization resistance, capacity, retention.

2024 IWLiME
11th INTERNATIONAL CONFERENCE IN LITHIUM, INDUSTRIAL MINERALS AND ENERGY
November 27-29, Antofagasta, Chile

Influence of External Compressive Pressure on Pouch Stacked LiFePO4 Batteries

A. Garcia[1], M. Gonzales[2], M.Grageda[3]

[1] *Center for Advanced Research in Lithium and Industrial Minerals, University of Antofagasta, Avenue Universidad de Antofagasta 02800, Antofagasta, Chile.*

[2] *Chemical Engineering Department, University of Antofagasta, Avenue Universidad de Antofagasta 02800, Antofagasta, Chile*

INTRODUCTION

The application of external compression pressure to lithium-ion batteries has become a crucial area of research to improve their performance and longevity. As these batteries are increasingly used in portable electronic devices and electric vehicles, the need to optimize their life cycle becomes imperative. External pressure not only influences current distribution and electrochemical resistance, but also plays a key role in mitigating cell degradation, allowing for more efficient operation and increased durability in critical applications.

EXPERIMENTAL METHODOLOGY

Stacked pouch battery manufacturing :

1 MIXED — 2 COATING — 3 CALENDERING — 4 DIMENSIONING + STACKED — 5 ELECTROCHEMICAL MEASUREMENTS

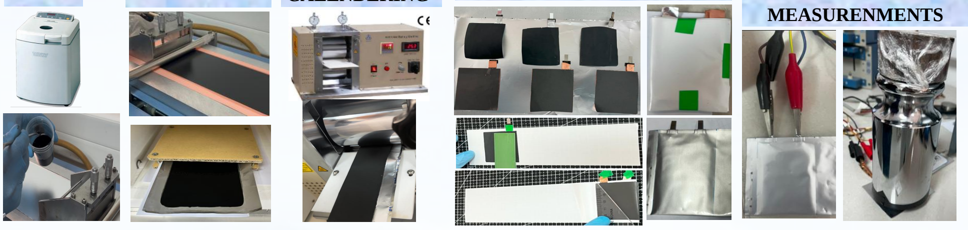

Fig 1. Manufacture of stacked pouch cell and its electrochemical connection.

RESULTS AND DISCUSSION

In this research we worked with different pressures, which are applied to the unitary pouch batteries manufactured in stacked form.

Table 1. Operating conditions with pressure for unit cell batteries.

Cell	POUCH
Velocity	0.1 C
Current [mA]	1.5
Pressure 1 [kPa]	30
Presure 2 [kPa]	90

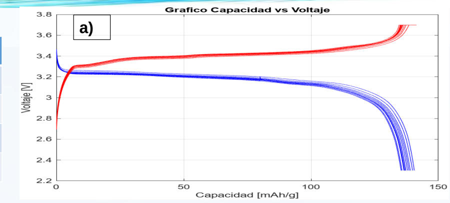

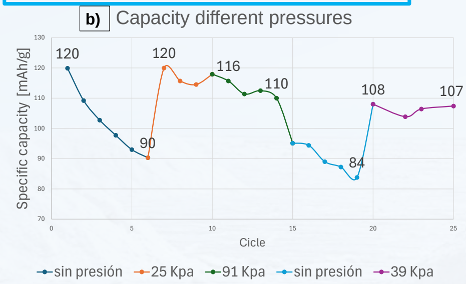

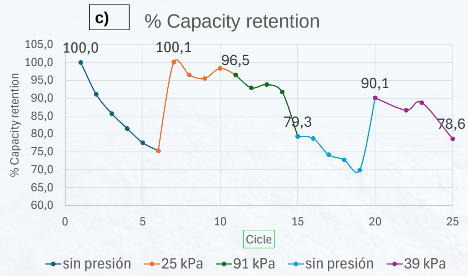

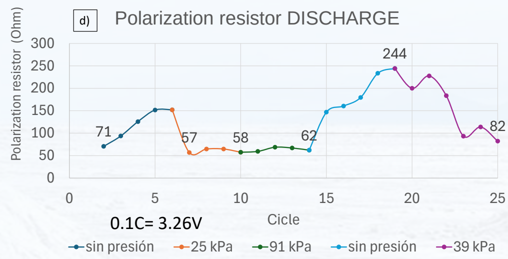

Fig 2. Electrochemical cell ; a) charge/discharge profile; b) specific capacity applying different pressures; c) % capacity retention d) polarization resistance.

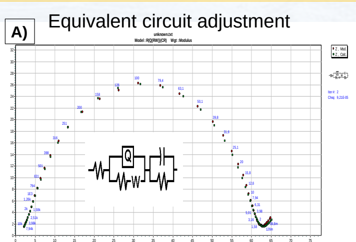

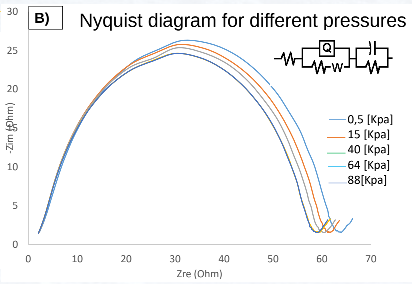

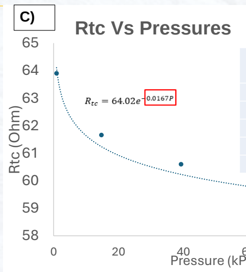

Table 2. Resistance due to applied pressure.

Rtc (Ohm)	P (kPa)
63,9	0,5
61,66	15
60,6	40
59,43	64
59,12	88

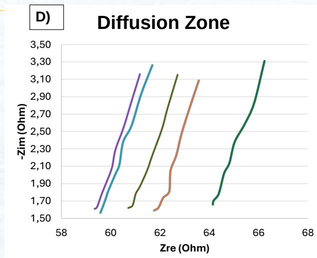

Fig 3. Impedance, A) equivalent circuit fit; B) Nyquist diagram for different pressures in the pouch cell, C) exponential fit and D) diffusion zone.

CONCLUSIONS

In Figure 1 b, when pressure of 30 [kPa] is applied, it recovers the initial capacity of 120 mAh/g, recovering 32% of the capacity.When the pressure is removed, the capacity drops from 110 to 83 mAh/g, a decrease of 24%.On the other hand, the specific capacity, capacity retention and polarization resistance have the same behavior, this tells us that we are improving the cyclability of the battery with a correct pressure.From Figure 3, the Nyquist Diagram determined that with low pressure the Charge Transfer Resistance is higher, but there is a limit pressure that generates changes in the cell and in this case it is 64 [kPa]. In addition, an exponential adjustment was determined, to know what pressure the battery needs. In the diffusion zone (Warburg) all have the same slope, therefore, the lithium ion diffusion in the active material is not modified.

Modeling of the physicochemical properties of the Li_2SO_4 – $LiNO_3$ – H_2O system

Braian S. Torres[1], Francisca J. Justel[1], Yecid P. Jimenez[2, 3]

[1]*Departamento de Ingeniería Metalúrgica y Materiales, Universidad Técnica Federico Santa María, Valparaíso, Chile.*

[2]*Departamento de Ingeniería Química y Procesos de Minerales, Universidad de Antofagasta, Antofagasta, Chile.*

[3]*Centro de Economía Circular en Procesos Industriales (CECPI), Facultad de Ingeniería, Universidad de Antofagasta, Av. Angamos 601, Antofagasta 1240000, Chile*

This work focuses on modeling the physicochemical properties of the Li_2SO_4 – $LiNO_3$ – H_2O system through experimental measurements of density, viscosity, sound velocity, and refractive index as a function of concentration and temperature. These measurements are conducted within an unsaturated range below the solubility curve of the ternary system, using empirical and semi-empirical models. The growing demand for lithium carbonate and hydroxide for lithium-ion battery production is driving electromobility and highlights the need for efficient processes to produce lithium salts and their derivatives, thus promoting scientific and technological advancement. Designing processes for producing lithium salts and valuable compounds requires, first and foremost, data that enable an understanding of brine properties and their thermodynamics, providing a basis for models in production processes. Due to the specific conditions of lithium brines and the challenges associated with measurements using conventional equipment, which often require specialized instruments, there is a lack of experimental data on physicochemical properties in both saturated and unsaturated ranges as a function of temperature. These models help to explain how concentration and temperature influence physicochemical and thermodynamic properties, providing a critical foundation for chemical and metallurgical processes. High-value elements, such as lithium sulfate, are produced as by-products in the production chain of lithium carbonate or hydroxide. Moreover, the Li_2SO_4 – $LiNO_3$ system is relevant for producing new batteries due to its high conductivity, with applications in energy storage and generation. [1]

The experimental design for measuring these physicochemical properties consists of a mapping of the unsaturated range of the ternary system below the solubility curve. In this study, density is modeled using the Pitzer model [2], which provides a good fit for volumetric and mixing parameters. Refractive index and sound velocity are modeled using Othmer's rule [3]. For dynamic viscosity, the multicomponent model by Laliberté [4] is applied as a function of concentration and temperature. Figure 1 summarizes the measurements of these properties at 298.15 K. Based on these results, it is concluded that the density of the Li_2SO_4 – $LiNO_3$ – H_2O ternary system increases with increasing $LiNO_3$ concentration under constant Li_2SO_4 conditions, and similarly, increasing the concentration of Li_2SO_4 under constant $LiNO_3$ conditions also increases the density, based on volumetric and mixing parameters. A similar analysis can be performed for refractive index, sound velocity, and dynamic viscosity. Additionally, measurements at 308.15 K and 318.15 K were conducted for the same properties, revealing that both density and refractive index decrease with increasing temperature across the unsaturated range. Meanwhile, sound velocity increases slightly with temperature, and dynamic viscosity decreases with rising temperature due to increased ion mobility and transport in the solution.

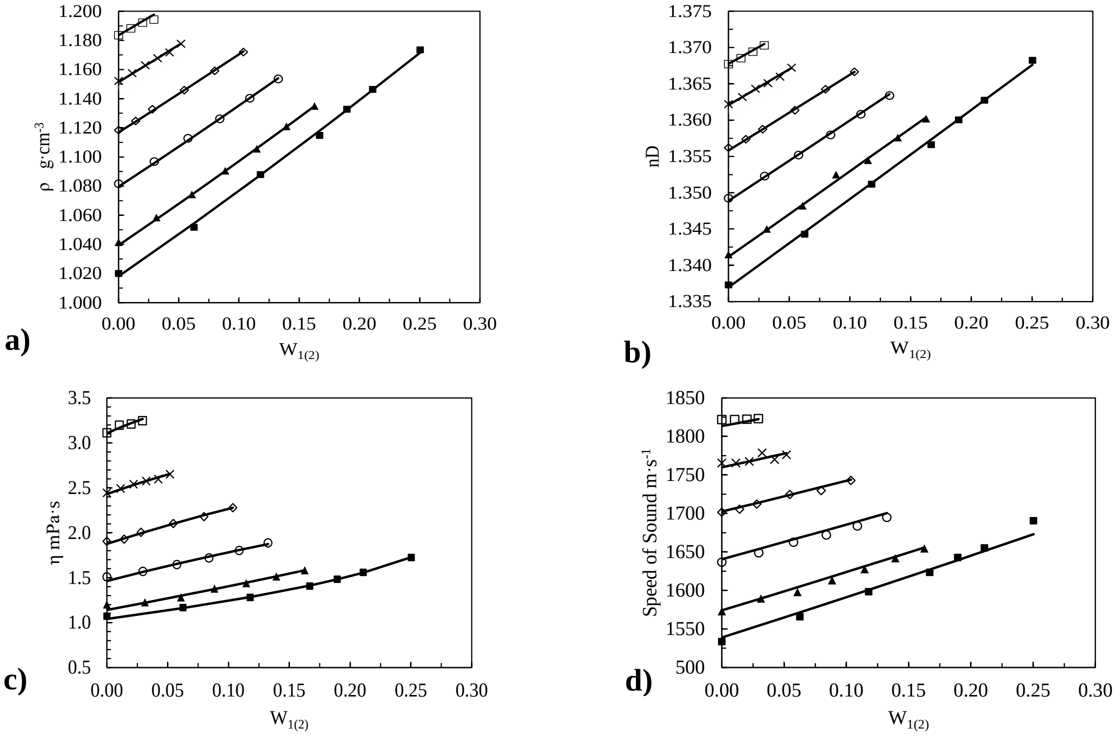

Figure 1. Physicochemical properties of the ternary system $Li_2SO_4 – LiNO_3 – H_2O$ at 298.15 K. (a) Density; (b) Refractive Index; (c) Dynamic Viscosity; (d) Speed of Sound.
$W_{1(2)}$: Mass Fraction of Lithium Nitrate. W_1 : Mass Fraction of Lithium Sulphate
(□, $W_1 = 0.205$; ×, $W_1 = 0.1704$; ◇, $W_1 = 0.132$;○, $W_1 = 0.091$; ▲, $W_1 = 0.047$; ■, $W_1 = 0.023$. This work. ─ (a) Density Pitzer Model; ─ (b, d) Othmer´s Rule. – (c) Viscosity (Laliberté et.al).

Keywords: Physicochemical properties, Lithium Sulphate, Lithium Nitrate.

Acknowledgments: *Fondecyt Iniciación N°1122073. DIM [1]. DIQUIMIN [2]*

References:

[1] M. El Guendouzi and A. Errougui, “Solubility in the ternary aqueous systems containing M, Cl^-, NO_3^-, and SO_4^{-2} with M = NH_4^+, Li^+, or Mg^{+2} at T = 298.15 K,” J Chem Eng Data, vol. 54, (2009), doi: 10.1021/je800425z.
[2] X. Ma, B. Hu, W. Li, Y. Dong, Volumetric properties of aqueous $NaCl−MgCl_2−H_2O$ and $KCl−MgCl_2−H_2O$ solutions and their correlation with the Pitzer model, J. Solution Chem. 49 (2020) 1339–1348, doi: 10.1007/s10953-020-01004-z.
[3] M. Claros, M. Taboada, H. Galleguillos, Y. Jimenez, Physicochemical Properties of $CuSO_4$ + PEG4000 + H_2O Solution at Different Temperatures, doi: 10.1007/s10765-016-2089-2.
[4] M Laliberté, A model for calculating the Heat Capacity the Heat Capacity of Aqueous Solutions, with Updated Density and Viscosity Data. Journal of Chemical & Engineering Data, 54(6), (2009), doi: 10.1021/je8008123.

Modeling of the physicochemical properties of the $Li_2SO_4 – LiNO_3 – H_2O$ system

Braian S. Torres[1], Francisca J. Justel[1], Yecid P. Jimenez[2, 3]

[1]*Departamento de Ingeniería Metalúrgica y Materiales, Universidad Técnica Federico Santa María, Valparaíso, Chile.*
[2]*Departamento de Ingeniería Química y Procesos de Minerales, Universidad de Antofagasta, Antofagasta, Chile.*
[3]*Centro de Economía Circular en Procesos Industriales (CECPI), Facultad de Ingeniería, Universidad de Antofagasta, Antofagasta, Chile.*

Corresponding author: E-mail address: braian.torres@sansano.usm.cl

INTRODUCTION

Understanding lithium brine properties is essential for producing lithium salts and valuable by-products. Limited experimental data due to measurement challenges restricts accurate modeling. This study focuses on the impact of concentration and temperature critical for optimizing lithium production. The $Li_2SO_4 – LiNO_3$ system is relevant for producing new batteries due to its high conductivity, with applications in energy storage and generation.

EXPERIMENTAL METHODOLOGY

The experimental design for measuring these physicochemical properties consists of a **mapping of the unsaturated range** of the ternary system below the solubility curve **[1]**.

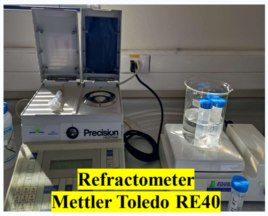

RESULTS

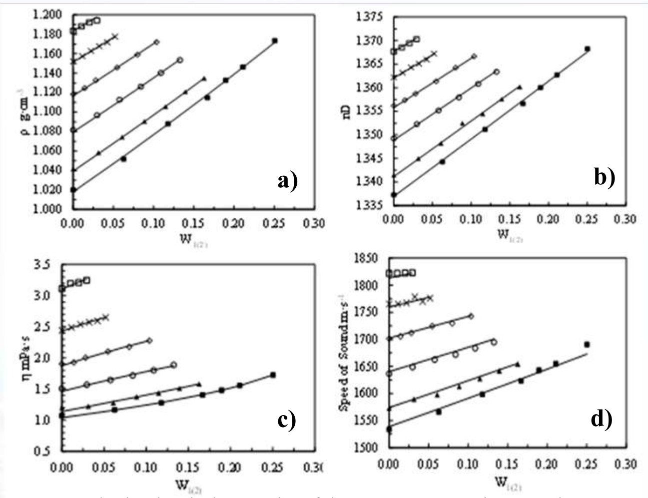

Figure 1. Physicochemical properties of the ternary system $Li_2SO_4 – LiNO_3 – H_2O$ at 298.15 K. (a) Density; (b) Refractive Index; (c) Dynamic Viscosity; (d) Speed of Sound. $W_{1(2)}$: Mass Fraction of Lithium Nitrate. W_1 : Mass Fraction of Lithium Sulphate. (□, W_1 = 0.205; ×, W_1 = 0.1704; ◇, W_1 = 0.132; ○, W_1 = 0.091; ▲, W_1 = 0.047; ■, W_1 = 0.023. This work. – (a) Density Pitzer Model; – (b, d) Othmer´s Rule. – (c) Viscosity (Laliberté et.al).

Density → Pitzer Model [2]

$$\rho = \frac{1000 + \sum_i m_i M_i}{V_\phi \sum_i m_i + 1000/\rho_w} \quad (1)$$

$$V_\phi = \bar{V}^0_{mix} + \left(\frac{R'T}{\sum_i m_i}\right)\left\{\frac{IA_V}{R'T}\frac{\ln(1+bI^{1/2})}{b} + 2\sum_c\sum_a m_c m_a\left(B^V_{ca} + \left(\sum_c m_c z_c\right)C^V_{ca}\right) + \sum_c\sum_{c'} m_c m_{c'}\left(2\theta^V_{cc'} + \sum_a m_a \psi^V_{cc'a}\right) + \sum_a\sum_{a'} m_a m_{a'}\left(2\theta^V_{aa'} + \sum_c m_c \psi^V_{aa'c}\right)\right\} \quad (2)$$

Dynamic Viscosity → Laliberte Model [3]

$$\eta_m = \eta_w^{w_w}\prod \eta_i^{w_i} \quad (3)$$

$$\eta_i = \frac{e^{\left(\frac{v_1(1-w_w)^{v_2}+v_3}{v_4(t°C)+1}\right)}}{v_5(1-w_w)^{v_6}+1} \quad (4)$$

Refractive Index, Sound of Velocity → Othmer's Rule [4]

$$\ln Y_R = \ln\frac{Y}{Y_W} = A + B\ln Y_W = (A_1 w_1 + A_2 w_2) + (B_1 w_1 + B_2 w_2)\ln Y_W \quad (5)$$

Least Squares Method

$$Min \sum_{i=1}^{n}\left(\frac{Y_{exp,i} - Y_{calc,i}}{Y_{exp,i}}\right)^2 \quad (6)$$

ANALYSIS

- Density of the ternary system increases with increasing $LiNO_3$ concentration under constant Li_2SO_4 conditions. Also, density increases under constant $LiNO_3$ conditions, as the Li_2SO_4 concentration increases at 298.15 K.
- A similar evaluation can likewise be applied to refractive index, sound velocity, and dynamic viscosity.
- Density and refractive index decrease with increasing temperature (298.15, 308.15, 318.15 K) across the unsaturated range.
- Dynamic viscosity decreases with rising temperature due to increased ion mobility and transport in the solution.
- Sound velocity increases slightly with temperature.

CONCLUSIONS

- The modeling of the physicochemical properties yielded a good fit, with an average absolute deviation ranging from 0.027% to 0.51%.
- Refraction index and sound of velocity were correlated using Othmer's rule, obtaining a good agreement between experimental and calculated values.
- The dynamic viscosity was modeled using the Laliberté equation, achieving good agreement between experimental and calculated values at different temperatures.

REFERENCES

[1] M. El Guendouzi and A. Errougui, "Solubility in the ternary aqueous systems containing M, Cl^-, NO_3^-, and SO_4^{-2} with M = NH_4^+, Li^+, or Mg^{+2} at T = 298.15 K," J Chem Eng Data, vol. 54, (2009),

[2] X. Ma, B. Hu, W. Li, Y. Dong, Volumetric properties of aqueous $NaCl–MgCl_2–H_2O$ and $KCl–MgCl_2–H_2O$ solutions and their correlation with the Pitzer Model, J. Solution Chem. 49 (2020)

[3] M Laliberté, A model for calculating the Heat Capacity the Heat Capacity of Aqueous Solutions, with Updated Density and Viscosity Data. Journal of Chemical & Engineering Data, 54(6), (2009).

[4] M. Claros, M. Taboada, H. Galleguillos, Y. Jimenez, Physicochemical Properties of $CuSO_4$ + PEG4000 + H_2O Solution at Different Temperatures (2016).

ACKNOWLEDGEMENTS

- ✓ DIRECCIÓN DE POSTGRADO, USM.
- ✓ FONDECYT DE INICIACIÓN N°11220731.
- ✓ DIMM[1]
- ✓ DIQUIMIN[2]

The correlation between surface scaling behavior with solar optical properties of silicon nanowires: An investigation based on fractal concepts

Chandra Kumar[1*], Monika Shrivastava[2], Juan Escrig[3,4], Antonio Zarate[5*]
[1]Escuela de Ingeniería, Facultad de Ciencias, Ingeniería y Tecnología, Universidad Mayor, Santiago 7500994, Chile.
[2]Department of Physics, Malaviya National Institute of Technology (MNIT), Jaipur, India.
[3]Departamento de Física, Universidad de Santiago de Chile (USACH), Avda. Víctor Jara 3493, 9170124 Santiago, Chile.
[4]Center for the Development of Nanoscience and Nanotechnology (CEDENNA), 9170124 Santiago, Chile.
[5]Department of Physics, Faculty of Science, Catholic University of the North (UCN), Avenida Angamos 0610, Casilla, 1280, Antofagasta, Chile

Corresponding authors *: Prof. Antonio Zarate (rzarate@ucn.cl), Dr. Chandra Kumar (chandra.kumar@umayor.cl)

Abstract

The fractal surface of nanostructures has a high impact on their physical properties and the performance of designed opto-electronics devices. Here, we report room temperature grown of silicon nanowires (Si-NWs) through metal assisted chemical etching [1]. The effect of etching time(20 min, 30 min. and 40 min.) and dopant (n-and p-type) on the grown NWs and it's surface scaling, fractal dimension, optical and solar cell parameters are extensively investigated. Autocorrelation and height–height correlation functions were applied to AFM images to extract deep insights about the NWs surfaces. Fractal dimension (D_f) was extracted through the power spectral density (PSD) function[2]. Various scaling exponents, including α, β, and 1/z, of the SiNWs surface were independently observed. The local roughness exponent, α, was approximately 0.87 for etching time of 20 minutes and decreased to 0.81 with higher etching time. The interface width (σ) scales with etching time (Et) as $\sim Et^{\beta}$, [3] with a growth exponent (β) value of 1.37. The lateral correlation length (ξ) follows as[4] $\sim Et^{1/z}$ with a 1/z value of 0.669. Additionally, optical parameters were recorded through UV–Vis. optical spectroscopy, and an attempt was made to correlate them with fractal parameters (D_f & H). Optical absorption (reflection) increased (decreased) with increasing D_f values. The minimum (maximum) reflection (absorption) was observed on the roughest surface ($D_f = 2.11$). The calculated band gap decreased with increasing fractal dimension[5]. This investigation suggests that sputtered surfaces with minimal reflectivity, band gap, and enhanced light-absorbing capacity could potentially be used as active solar layers for advanced optoelectronic devices. On the other hand, field emission properties of SiNWs has been examined through recorded J-E measurements under the Fowler–Nordheim framework. The Si NWs grown showed a minimum turn-on field and also a higher field enhancement factor on rough surface. These investigations suggest that roughens (fractal dimension) influence the field emission parameters of grown NWs, also it was observed that the irregular surfaces are much more favorable for the investigation of field emission properties.

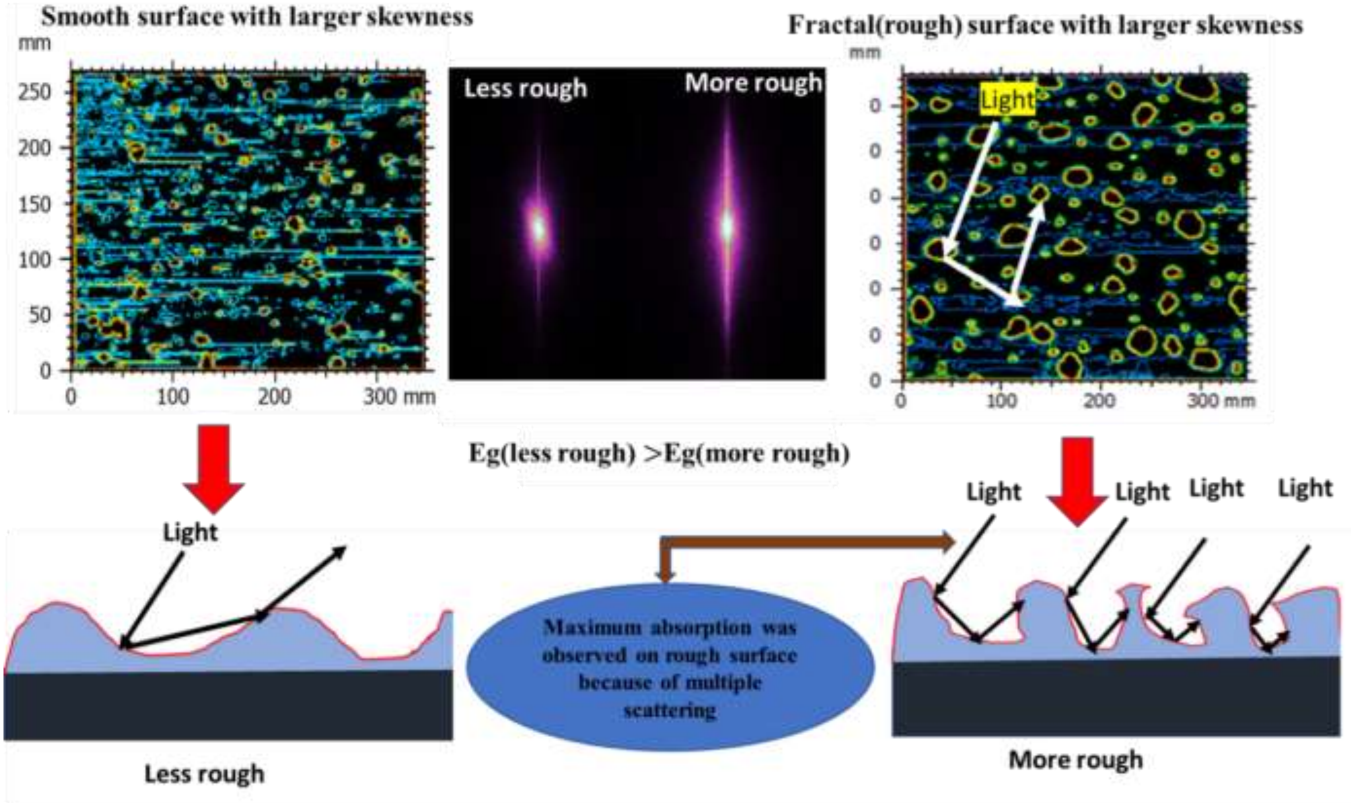

Fig. 1: Light mechanism in smooth and rough surface (maximum absorption take place in rough surface due to multiple scatting) of SiNWs.

Reference

[1] Kumar, C., Kashyap, V., Escrig, J., Shrivastav, M., Kumar, V., Guzman, F., & Saxena, K. (2024). The dopant (n-and p-type)-, band gap-, size-and stress-dependent field electron emission of silicon nanowires. Physical Chemistry Chemical Physics, 26(25), 17609-17621.

[2] Kumar, C., Shrivastav, M., Escrig, J., Campos, L. P., Martinez, A. I., Silva, H., & Zarate, A. (2024). The investigation of thickness-dependent mono-fractal, optical and optoelectronics properties of sputtered silver thin film for silicon solar cell. Vacuum, 225, 113247.

[3] Yadav, R. P., Dwivedi, S., Mittal, A. K., Kumar, M., & Pandey, A. C. (2012). Fractal and multifractal analysis of LiF thin film surface. Applied Surface Science, 261, 547-553.

[4] Yadav, R., Agarwal, D. C., Kumar, M., Rajput, P., Tomar, D. S., Pandey, S. N., ... & Mittal, A. K. (2017). Effect of angle of deposition on the Fractal properties of ZnO thin film surface. Applied Surface Science, 416, 51-58.

[5] Kumar, C., Yadav, R. P., & Singh, B. K. (2024). Surfaces properties correlation with optical parameters of thickness dependent self-affine nanostructured SnS thin films: A study based on scaling law. Colloids and Surfaces A: Physicochemical and Engineering Aspects, 691, 133865.

11th INTERNATIONAL CONFERENCE IN LITHIUM, INDUSTRIAL MINERALS AND ENERGY
November 27-29, Antofagasta, Chile

La correlación entre el concepto de el escalado de la superficie y las propiedades ópticas de los nanocables de silicio: una investigación basada en conceptos fractales

Chandra Kumar[1*], Monika Shrivastava[2], Juan Escrig[3], J.O. Morales-Ferreiro[1], Gerardo Silva-Oelker[1], , Fernando Guzman[4], Antonio Zarate[4]
[1]Escuela de Ingeniería, Facultad de Ciencias, Ingeniería y Tecnología, Universidad Mayor, Santiago 7500994, Chile.
[2]Department of Physics, Malaviya National Institute of Technology (MNIT), Jaipur, India.
[3]Center for the Development of Nanoscience and Nanotechnology (CEDENNA), 9170124 Santiago, Chile.
[4]Departamento de Física, Facultad de Ciencias, Universidad Católica del Norte, Avenida Angamos 0610, Casilla 1280, Antofagasta, Chile.

Universidad Mayor, Santiago

Abstract
La superficie fractal de las nanoestructuras tiene un alto impacto en sus propiedades físicas y el rendimiento de los dispositivos optoelectrónicos diseñados. En este trabajo, informamos sobre el crecimiento a temperatura ambiente de nanocables de silicio (SiNWs) mediante grabado químico asistido por metal. Se investiga en profundidad el efecto del tiempo de grabado (20 min, 30 min y 40 min) y el dopante (tipo n y p) en los NWs cultivados y su escalado superficial, dimensión fractal, emisión de campo y óptica. Se aplicaron funciones de correlación altura-altura a imágenes AFM para extraer información detallada sobre las superficies de los NW. Las propiedades de emisión de campo de los SiNW se examinaron mediante mediciones J-E registradas en el marco de Fowler-Nordheim. Los NWs de Si cultivados mostraron un campo de activación mínimo y también un factor de mejora de campo más alto en los NW de tipo p. La dimensión fractal (Df) se extrajo mediante la función de densidad espectral de potencia (PSD). Se observaron de forma independiente varios exponentes de escala, incluidos α, β y 1/z, de la superficie de SiNWs. El exponente de rugosidad local, α, fue de aproximadamente 0,87 para un tiempo de grabado de 20 minutos y disminuyó a 0,81 con un tiempo de grabado más alto. El ancho de la interfaz (σ) se escala con el tiempo de grabado (Et) como ~ Etβ, con un valor de exponente de crecimiento (β) de 1,17. La longitud de correlación lateral (ξ) sigue como $\sim Et^{1/z}$ con un valor 1/z de 0,703. La reflexión (absorción) mínima (máxima) se observó en la superficie más rugosa (Df = 2,29). El intervalo de banda calculado disminuyó con el aumento de la dimensión fractal. Esta investigación sugiere que las superficies pulverizadas con reflectividad mínima, intervalo de banda y capacidad de absorción de luz mejorada podrían usarse potencialmente como capas solares activas para dispositivos optoelectrónicos avanzados.

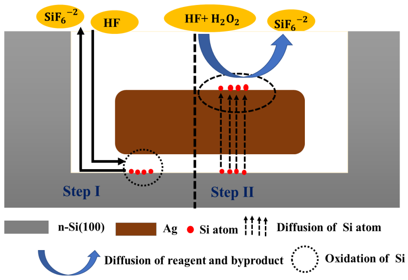

Fig.1 Diagrama esquemático del grabado químico.

Resultado y discusión

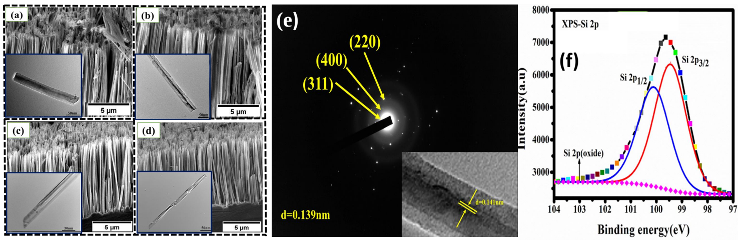

Fig.2 Imagen FESEM de SiNW, (a) n30, (b) p30, (c) p30, (d) p50, (e) HRTEM, (f) XPS de SiNW

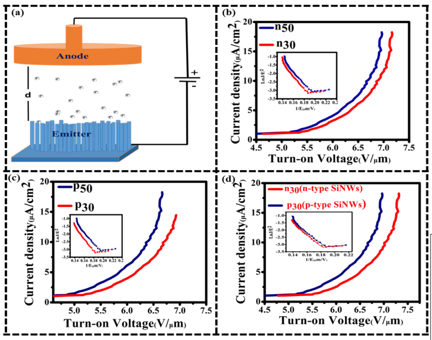

Fig. 4 (a) Diagrama esquemático del experimento de emisión, (b) gráfico J–E para el tipo n, (c) gráfico J–E para el tipo p y (d) comparación entre los gráficos de características J–E de los nanotubos de silicio de tipo n y p

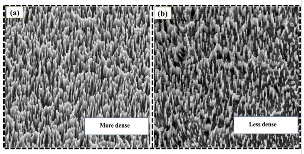

Fig. 3 Imagen FESEM inclinada de 450 grados (que muestra que las muestras de tipo p son menos densas que las muestras de tipo n) de nanocristales de silicio: (a) n30 y (b) p30

Ecuación F-N

$$J = \frac{A_{FN}\beta^2 V^2}{W} \exp\left(-\frac{B_{FN} W^{3/2}}{\beta V}\right)$$

Donde β es el factor de mejora del campo, W es la función de trabajo del emisor

$$\text{PENDIENTE} = -\frac{B_{FN}\, W^{3/2}}{\beta}$$

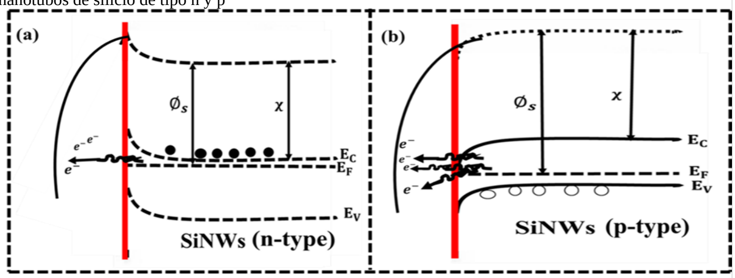

Fig. 5 Diagramas de energía de banda de (a) nanocristales de silicio de tipo n y (b) nanocristales de silicio de tipo p

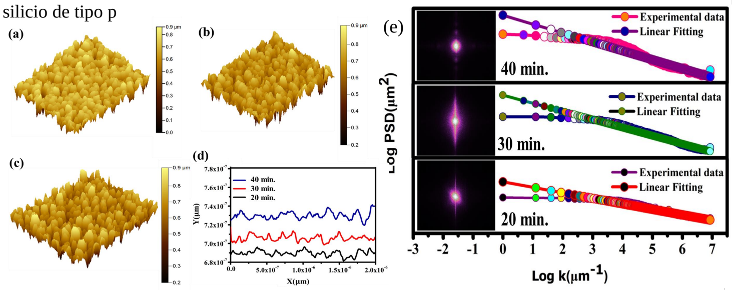

Fig. 6 Imágenes AFM de SiNW en diferentes tiempos de grabado: (a) 30 min., (b) 40 min., (c) 50 min. (d) perfiles de línea, (e) espectros de densidad espectral de potencia

Tabla -1 Parámetros de rugosidad de SiNW

Etching Time(Min.)	Ra(nm)	σ(nm)	σ /R_a	Slope(γ)	D_f	α	ξ(nm)	ρ
30	19.18	23.4	1.22	3.62	2.19	0.844	186.2	0.1047
40	26.0	45.6	1.75	3.54	2.23	0.804	219.3	0.118
50	31.2	59.5	1.90	3.42	2.29	0.796	247.5	0.126

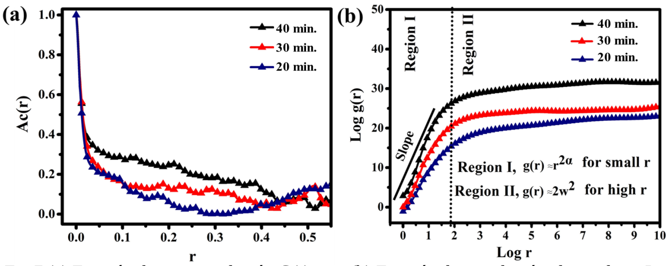

Fig.7 (a) Función de autocorrelación G(r) vs r, (b) Función de correlación altura-altura Log C(r) vs. log r para SiNW.

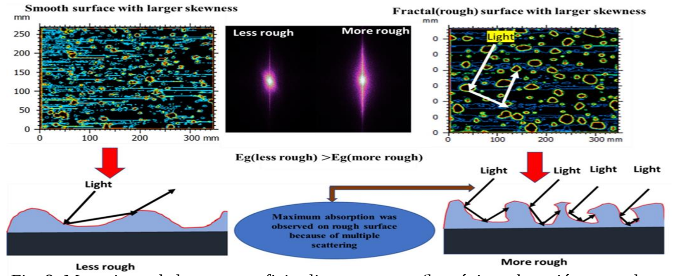

Fig. 8: Mecanismo de luz en superficies lisas y rugosas (la máxima absorción se produce en superficies rugosas debido a la dispersión múltiple) de SiNW

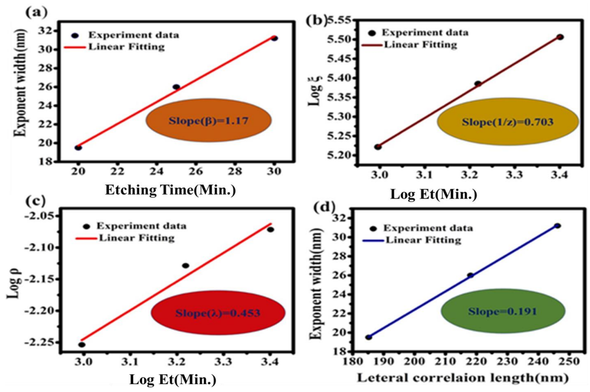

Fig. 9(a): Variación del ancho del exponente con el tiempo de grabado, (b) gráfico del gráfico logarítmico-logarítmico de ξ(t) con Et, (c) variación del gráfico logarítmico-logarítmico de ρ con Et, (d) variación del exponente con la longitud de correlación lateral de SiNW

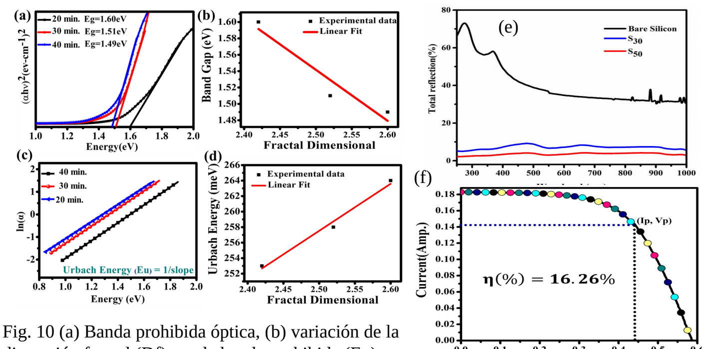

Fig. 10 (a) Banda prohibida óptica, (b) variación de la dimensión fractal (Df) con la banda prohibida (Eg), (c) energía de Urbach, (d) variación de la dimensión fractal (Df) con la energía de Urbach, (e) reflexión, (e) curva IV de la célula solar

Conclusión 1- Los nanocables de silicio se sintetizaron en silicio de tipo n y p.
2-Los resultados mostraron que el silicio tipo p es superior en emisiones.
3-Se calcularon las dimensiones fractales (rugosidad) para nanocables de silicio con un tiempo de grabado de 30 a 50 minutos.
4-Los cálculos de la dimensión fractal fueron 2,24, 2,56 y 2,98 respectivamente.
5-La dimensión fractal aumenta con la disminución de la reflexión, lo que indica que la superficie rugosa es compatible con la aplicación optoelectrónica.

Acknowledgement: Este trabajo fue financiado con el FONDECYT Postdoctoral 3240551

References [1] Kumar, C., Kashyap, V., Escrig, J., Shrivastav, M., Kumar, V., Guzman, F., & Saxena, K. (2024). Physical Chemistry Chemical Physics, 26(25), 17609-17621.
[2]Kumar, C., Shrivastav, M., Escrig, J., Palma, J. L., Yadav, R. P., Silva, H., & Zarate, A. (2024). Ceramics International, 50(21), 41614-41627.

Universidad Mayor, Santiago

Study of Electrodic Reactions to Produce Lithium Hydroxide from Lithium Sulphate by Means of Reactive Electrodialysis

M. Gonzales[1,2], M. Grageda[1,2], A. Quispe[1,2]

[1]*Center for Advanced Research in Lithium and Industrial Minerals, University of Antofagasta, Avenue Universidad de Antofagasta 02800, Antofagasta, Chile.*
[2]*Chemical Engineering Department, University of Antofagasta, Avenue Universidad de Antofagasta 02800, Antofagasta, Chile*

The manufacture of high energy density lithium-ion batteries, such as NMC, NCA and LMO, requires a high-quality precursor material, lithium hydroxide (LiOH) being one of the most suitable for this purpose due to the physical and electrochemical properties it confers to the final material[1]. The conventional method to obtain LiOH from lithium carbonate is complex and consumes large amounts of reagents, equipment, energy, water, causes waste and lithium losses during the process [2][3].
Reactive electrodialysis emerges as an alternative that allows the direct production of high purity LiOH from concentrated LiCl or Li_2SO_4 solutions [4], by migrating lithium and sulphate ions from the dilute to the cathodic and anodic compartment respectively through membranes. The decrease of chloride deposits in Chilean salt flats has increased the sulphate concentration, which makes it necessary to investigate the production of LiOH from Li_2SO_4.

The energy efficiency of this process is highly dependent on efficiency, reaction kinetics and cell potential, with water oxidation being the anodic reaction commonly employed in the electrolysis of Li_2SO_4, whose standard oxidation potential is a critical factor.

$$2H_2O \rightarrow O_2 + 4H^+ + 4\bar{e} \qquad E^{\circ} = 1.229\ V$$

This represents a high energy consumption, as the anodic side of the OER is a four-electron process with slow kinetics, thus requiring a higher cell overpotential. [5]. Thus, it is proposed to replace the anodic reaction with one that involves a lower oxidation potential. Among the options studied were the following species: NH_4OH, KOH y $C_6H_{12}O_6$, because they have a lower oxidation potential than water, they could reduce the energy consumption of the process and generate a high purity by-product with added value.

The study shows that KOH achieves higher limiting current densities at 80°C and 420 ml/min of electrolyte recirculation compared to the other reactions and requires less potential application for this to take place, as shown in Figure 1.

Following these results, catalytic effects were studied for the anodic reaction at 80°C on different types of RuO_2/Ti, Pt/Ti, IrO/Ti, Nickel, Isomolded Graphite and Fully Resin Graphite electrodes. Table 1 shows a summary of the results obtained for the study.

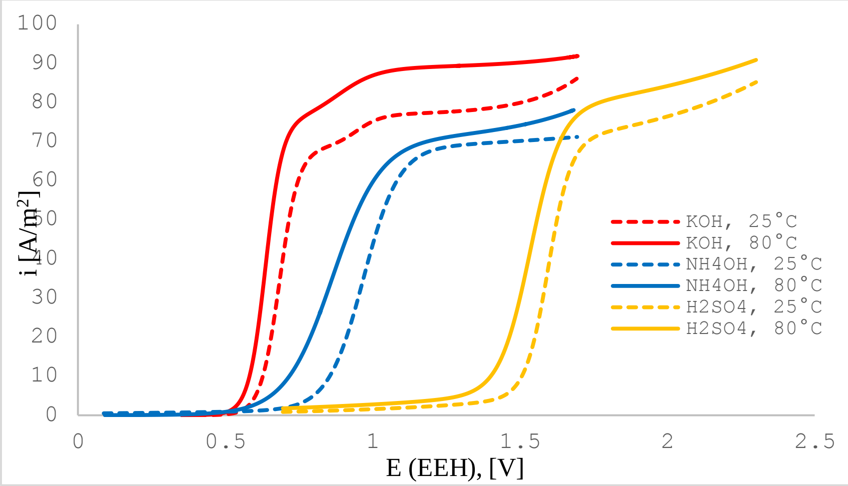

Figure 1: Current density for anodic reactions studied with Pt/Ti electrode

Tabla 1: Limit current density reached at 80°C for the KOH reaction, for different electrodes studied.

Anode species	**KOH**	**KOH**	**KOH**	**KOH**	**KOH**	**KOH**
Electrode material	**IrO_2/Ti**	**RuO_2/Ti**	**Ni/Ti**	**Graphite Isomolded**	**Graphite Fully Resin**	**Pt/Ti**
Limiting current density [A/m^2]	85.18	68.00	70.48	53.66	73.40	74.00

Keywords: electrode reactions, electrodialysis, lithium sulphate, lithium hydroxide.
Acknowledgments: *The authors would like to acknowledge the SQM projects for financial support.*

References:

[1] B. Fitch, M. Yakovleva, and S. Meiere, “Lithium Hydroxide Based Performance Improvements for Nickel Rich Ncm Layered Cathode Material,” *ECS Meet. Abstr.*, vol. MA2016-02, no. 3, pp. 469–469, Sep. 2016, doi: 10.1149/MA2016-02/3/469.

[2] J. M. Dahlkamp, C. Quintero, A. Videla, and R. Rojas, “Production processes for LiOH – A review,” *Hydrometallurgy*, vol. 223, no. October 2023, 2024, doi: 10.1016/j.hydromet.2023.106217.

[3] H. Liu and G. Azimi, “Production of Battery Grade Lithium Hydroxide Monohydrate Using Barium Hydroxide Causticizing Agent,” *Resour. Conserv. Recycl.*, vol. 179, no. December 2021, p. 106115, 2022, doi: 10.1016/j.resconrec.2021.106115.

[4] B. Kang, D. Kang, J. C.-Y. J. Jung, A. Asadi, and P.-C. Sui, “Electrodialysis of a Lithium Sulphate Solution: An Experimental Investigation,” *J. Electrochem. Soc.*, vol. 169, no. 6, p. 063515, 2022, doi: 10.1149/1945-7111/ac76e6.

[5] G. Gao *et al.*, “Recent advances in hydrogen production coupled with alternative oxidation reactions,” *Coord. Chem. Rev.*, vol. 509, no. October 2023, p. 215777, 2024, doi: 10.1016/j.ccr.2024.215777.

11th INTERNATIONAL CONFERENCE IN LITHIUM, INDUSTRIAL MINERALS AND ENERGY

November 27-29, Antofagasta, Chile

Study of Electrodic Reactions for the Production of Lithium Hydroxide from Lithium Sulphate by means of Reactive Electrodialysis

M. Gonzales[1,2], A. Quispe[1,2], M. Grageda [1,2]

[1]Center for Advanced Research in Lithium and Industrial Minerals, University of Antofagasta, Avenue Universidad de Antofagasta 02800, Antofagasta, Chile.

[2]Chemical Engineering Department, University of Antofagasta, Avenue Universidad de Antofagasta 02800, Antofagasta, Chile

INTRODUCTION

Electrodic reactions are heterogeneous processes that take place at the solid-liquid interface and play a crucial role in the production of lithium hydroxide, a compound whose demand is constantly growing due to its importance in the manufacture of high power density batteries. This process uses lithium sulphate, a by-product generated in the evaporation ponds, as a raw material. Electrodialysis to produce LiOH from Li_2SO_4 is based on the oxidation of water as the main anodic reaction. However, this reaction involves a high cell voltage, which would increase the energy consumption of the process. For this reason, in this work it was proposed to study the oxidation of other species with lower oxidation potential to replace the water oxidation reaction.

The aim of the work was to find the species with the highest limiting current density, the most suitable electrocatalytic material for the reaction and the best operating conditions.

.MATERIAL AND METHODS

Linear sweep voltammetry tests were performed in a three-compartment cell with three electrodes. Cationic and anionic Nafion 117 and Neosepta membranes were used, respectively. The species proposed for the oxidation study were: NH_4OH, KOH, $C_6H_{12}O_6$ and H_2SO_4. The following materials were used as working electrodes: Pt/Ti, RuO_2/Ti, IrO_2/Ti, Nickel, Isomolded Graphite and Resin Fully Graphite. Temperatures of 25°C and 80°C, electrolyte flow rates of 240, 330 and 420 ml/min were used.

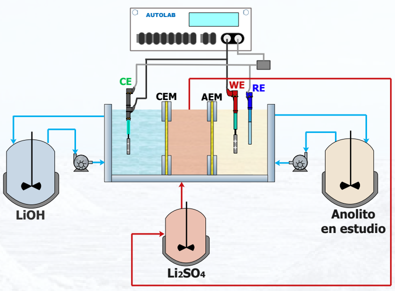

Figure 1: Experimental setup for electrodialysis study

Understanding the kinetic phenomenology of a redox process is important to propose the kinetic controls to which reactions develop during tests. In this way, the following mathematical model was proposed to quantify all the anodic reactions (main and secondary) by determining their kinetic parameters.

$$i_{Theor-Tot}^{anodic} = \frac{i_{oNH_4OH}\, i_{L,NH_4OH}}{i_{oNH_4OH} + i_{L,NH_4OH} \exp\left(\frac{\alpha_A n F \eta_{NH_4OH}}{R\,T}\right)} + i_{oH_2O} \exp\left(\frac{\alpha_A n F \eta_{H_2O}}{R\,T}\right) \quad (1)$$

$$i_{Theor-Tot}^{anodic} = \frac{i_{oKOH}\, i_{LKOH}}{i_{oKOH} + i_{LKOH} \exp\left(\frac{\alpha_A n F \eta_{KOH}}{R\,T}\right)} + i_{oH_2O} \exp\left(\frac{\alpha_A n F \eta_{H_2O}}{R\,T}\right) \quad (2)$$

$$i_{Theor-Tot}^{anodic} = \frac{i_{oH_2SO_4}\, i_{LH_2SO_4}}{i_{oH_2SO_4} + i_{LH_2SO_4} \exp\left(\frac{\alpha_A n F \eta_{H_2SO_4}}{R\,T}\right)} + i_{oH_2O} \exp\left(\frac{\alpha_A n F \eta_{H_2O}}{R\,T}\right) \quad (3)$$

In a first stage, the most suitable anode species was identified by evaluating its performance as a function of the limiting current density. Subsequently, in a second stage, the optimal electrocatalytic material for the system was selected and the most favourable experimental conditions were designed to maximize the efficiency of the system.

RESULTS AND DISCUSSION

Figure 2a shows the modeled anodic reactions and is possible to observe that the calculated theoretical current curve has good agreement with the experimental current curve, 2b shows a comparison with H_2SO_4 at different temperatures.

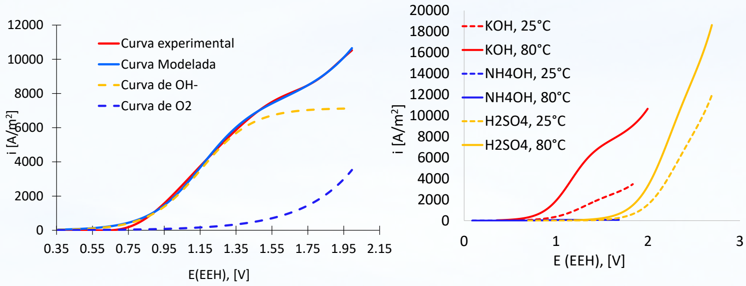

Figure 2: a) LSV for KOH to 420 ml/min and 80°C, b) Different anolytes and temperatures as a function of limiting current density.

The results shown in Table 1 reveal that the species with the highest limiting current density is KOH, reaching a value of 7145 A/m² at 420 ml/min and 80°C. The limit current density increases with increasing temperature and recirculation, as shown in Figure 3 a) and 3 b).

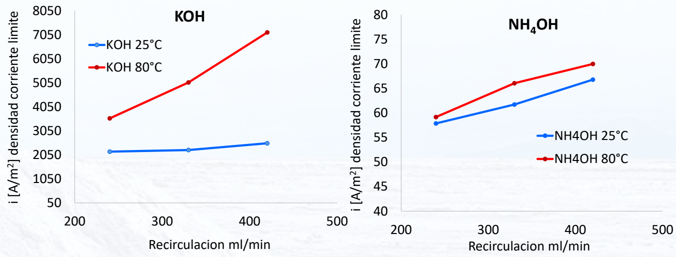

Figure 3: Limit current density as a function of temperature and recirculation a) KOH, b) NH_4OH

Table 1: Limiting current density at different conditions and analytes

ANOLITO	240 ml/min		330 ml/min		420 ml/min	
	25°C	80°C	25°C	80°C	25°C	80°C
	i [A/m²]	i [A/m²]	i [A/m²]	i [A/m²]	i [A/m²]	i [A/m²]
NH_4OH	57.9	59.2	61.7	66.1	66.8	70.0
KOH	2183.8	3567.9	2250.5	5063.7	2532.3	7144.9
H_2SO_4					8295.5	12933.1

H_2SO_4 achieves a higher limiting current density, but it needs a higher cell voltage to achieve this, compared to KOH, as a show Figure 2b).

CONCLUSIONS

- KOH as an anodic species, presents the highest current densities.
- The increase in temperature and electrolyte flow rate increases the current density in the anodic reactions.
- IrO_2/Ti presented the most suitable electrocatalytic properties for the process.

ACKNOWLEDGMENTS: The authors would like to acknowledge the SQM projects for the financial support

Performance Evaluation of Li-O_2 Cells with Fe_2O_3-Modified Cathodes Using Atomic Layer Deposition

P. Márquez[1], J. Amici[2], D. Aburquenque[3] and J. Escrig[4].

[1]*Universidad Central de Chile, Facultad de Ingeniería, Santa Isabel 1186, Santiago, Chile.*

[2]*Department of Applied Science and Technology (DISAT), Politecnico di Torino, C.so Duca degli Abruzzi 24, 10129, Torino, Italy*

[3]*Centro de Nanotecnología Aplicada, Facultad de Ciencias, Ingeniería y Tecnología, Universidad Mayor, Camino La Pirámide 5750, Huechuraba, Santiago, Chile*

[4]*Physics Department, Universidad de Santiago de Chile (USACH), 917-0124 Santiago, Chile*

Lithium-oxygen batteries (LOB) offer an innovative solution to meet the increasing demand for energy storage in applications such as electric vehicles and portable electronic devices. LOBs have a high theoretical energy density, surpassing lithium-ion batteries and even approaching that of gasoline. However, they face challenges such as poor cycle stability, low power capacity, and large polarizations in both the oxygen reduction reaction (ORR) and oxygen evolution reaction (OER). Various strategies are being explored, including the development of bifunctional catalysts for cathodes, which could significantly improve the overall performance of these batteries [1].

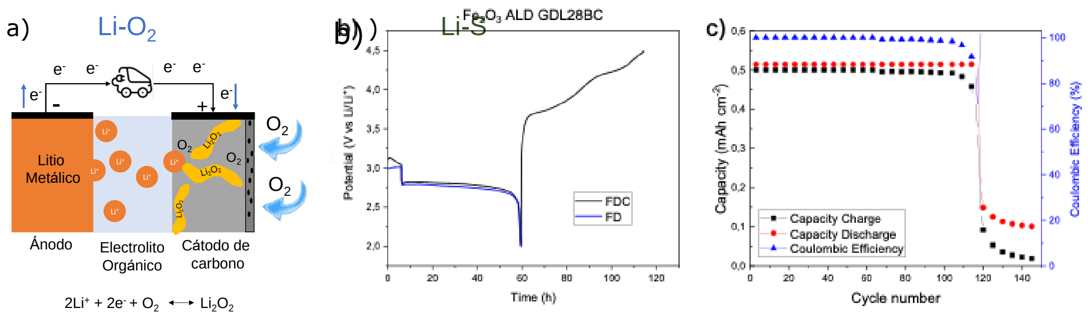

Figure 1. (a) Schematic of a Li-O_2 cell. (b) Full discharge and Discharge-charge response of a Li-O_2 cell with a commercial cathode (GDL28BC) modified with 2000 ALD cycles of Fe_2O_3. (c) Cell performance during discharge/charge cycles. Density current of 0.1 mA cm^{-2}.

The atomic layer deposition (ALD) technique is an atomic-scale manufacturing method that allows for precise control of thickness, uniformity, and conformity in the deposition of ultrathin films. This technique is particularly interesting for the synthesis of nanometric-thickness catalysts on membranes used as cathode substrates [2]. In this study, the galvanostatic response of cathodes modified with different thicknesses of hematite; Fe_2O_3, using ALD, is presented. The performance is evaluated in terms of Full discharge and Full Discharge-Charge (FD and FDC) studies, as well as cycling stability. Also, post-mortem analyses were conducted using X-ray diffraction (XRD) and field emission scanning electron microscopy (FESEM) to identify the products formed during electrochemical cycling.

In Figure 1(a), a schematic is shown representing the components and operation of a $Li\text{-}O_2$ cell. In (b), the response of a Full discharge and Full discharge-charge process of a $Li\text{-}O_2$ cell with a commercial cathode (GDL28BC) modified with 2000 ALD/cycles of Fe_2O_3 is presented. The electrolyte is a solution of 0.5 M LiTFSI in DMSO on a glass fiber separator, and the anode is a Li metal disc at a current density of 0.1 mA cm^{-2}. Fig. 1(c) shows the cell performance during discharge/charge cycles. The cell exhibits a specific capacity of 5.3 mAh cm^{-2}, maintaining stability over approximately 110 discharge/charge cycles. When comparing the specific capacity of the electrode with and without hematite, no significant difference is observed, with both reaching a specific capacity of 5.0 mAh cm^{-2}. However, in terms of cycling performance, the Fe_2O_3/GDL28BC cathode exhibits significantly higher cyclability (110 vs. 10 cycles for Fe_2O_3/GDL28BC and GDL28BC, respectively). Based on this data, the key advantage of modifying the cathode surface with this material lies in its ability to enhance performance over multiple cycles, addressing one of the main issues associated with the use of these batteries.
Finally, these results will be compared with the responses of cathodes modified with 500 and 1000 ALD/Cycles.

Keywords: Lithium-oxygen batteries ($Li\text{-}O_2$), atomic layer deposition (ALD), hematite Fe_2O_3 , Oxygen reduction reaction (ORR) and Oxygen evolution reaction (OER).

Acknowledgments:
Subvención a Instalación en la Academia 2021, SIA77210080 (PM), Fondecyt Iniciación 11230889 (D.A.)

References:

[1] P. Aduama, et al., Energies, 16 (2023).
[2] Y. Zhou, et al. ACS Nano, 18, 16489−16504 (2024)

Performance evaluation of Li-O₂ Cells with Fe₂O₃-Modified cathodes using Atomic Layer Deposition

Universidad Central

P. Márquez[1], J. Amici[2], D. Aburquenque[3] and J. Escrig[4].

[1]Universidad Central de Chile, Facultad de Ingeniería, Santa Isabel 1186, Santiago, Chile.
[2]Department of Applied Science and Technology (DISAT), Politecnico di Torino, C.so Duca degli Abruzzi 24, Torino, Italy
[3]Facultad de Ciencias, Ingeniería y Tecnología, Universidad Mayor, Camino La Pirámide 5750, Huechuraba, Santiago, Chile
[4]Physics Department, Universidad de Santiago de Chile (USACH), 917-0124 Santiago, Chile

paulina.marquez@ucentral.cl

Politecnico di Torino

1. Introduction

Lithium-oxygen batteries (LOB) offer an innovative solution to meet the increasing demand for energy storage in applications such as electric vehicles and portable electronic devices. LOBs have a high theoretical energy density, surpassing lithium-ion batteries and even approaching that of gasoline. However, they face challenges such as poor cycle stability, low power capacity, and large polarizations in both the oxygen reduction reaction (ORR) and oxygen evolution reaction (OER). Various strategies are being explored, including the development of bifunctional catalysts for cathodes, which could significantly improve the overall performance of these batteries [1]. The atomic layer deposition (ALD) technique is an atomic-scale manufacturing method that allows for precise control of thickness, uniformity, and conformity in the deposition of ultrathin films. This technique is particularly interesting for the synthesis of nanometric-thickness catalysts on membranes used as cathode substrates [2]. In this study, the galvanostatic response of cathodes modified with different thicknesses of hematite; Fe_2O_3, using ALD, is presented.

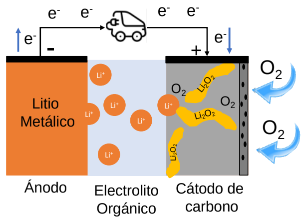

2. Materials and Methods

a) Fe_2O_3-Cathode preparation with ALD

The deposition was performed in a Savannah S100 ALD reactor at 200 °C using $FeCp_2$ and O_3 as precursors. Ferrocene was heated to 80 °C, and ozone (10% concentration) was generated with an Ol80W/FM100V. Pulse times were 2 s ($FeCp_2$) and 0.2 s (O_3), with 5 s exposure and 15 s pump times. A constant nitrogen flow of 20 sccm was maintained.

Savannah S100 ALD reactor

Cathode: GDL28BC

b) Performance of Li-O_2

Li-O_2 Cell: GDL-24BC is used as cathode, Li disc as anode, and glass fiber as separator.
Electrolyte: 0.5 M LiTFSI in DMSO. The cell used was a ECC-Air cell design (EL-Cell, GmbH).
Testing was conducted via galvanostatic discharge/charge at a current density of 0.1 mA cm^{-2} within a voltage range of 2.25–4.4 V (vs. Li/Li$^+$), using an Arbin BT-2000 battery tester. Pure O_2 was continuously supplied at a flow rate of 3.0 mL min^{-1} during the measurements.

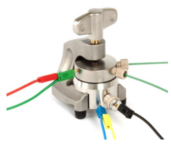

3. Results

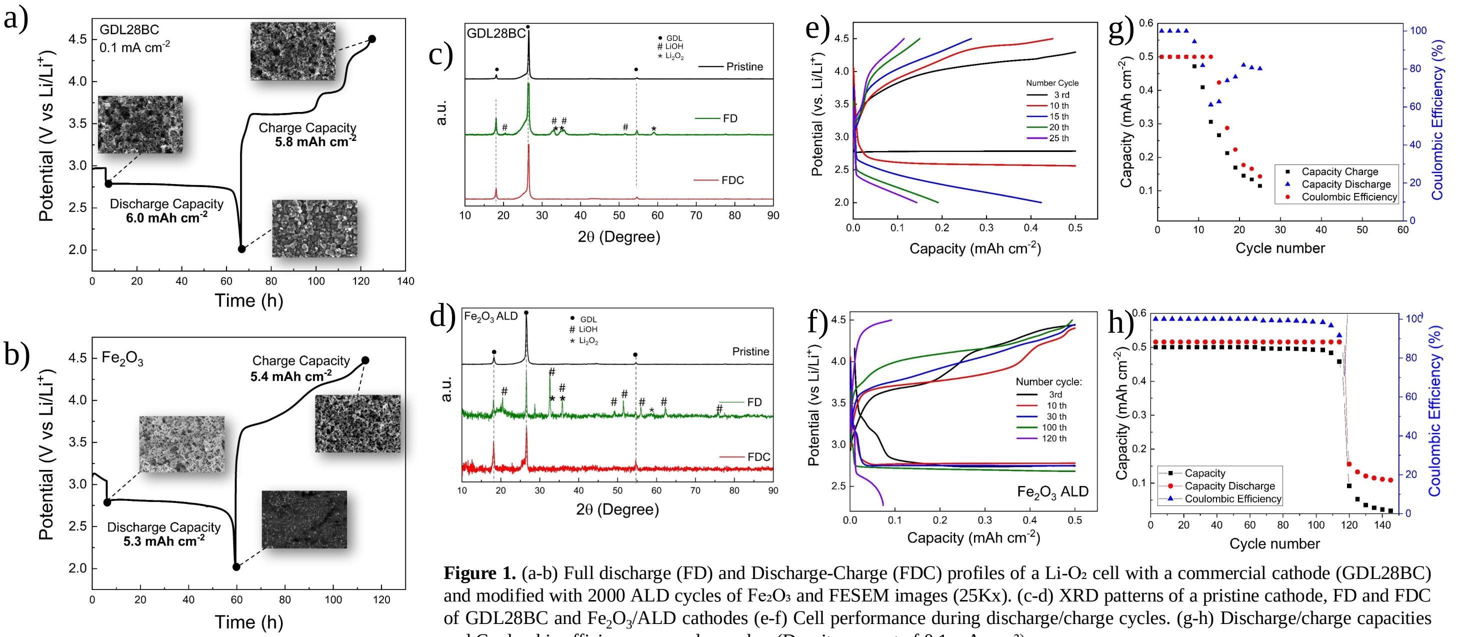

Figure 1. (a-b) Full discharge (FD) and Discharge-Charge (FDC) profiles of a Li-O_2 cell with a commercial cathode (GDL28BC) and modified with 2000 ALD cycles of Fe_2O_3 and FESEM images (25Kx). (c-d) XRD patterns of a pristine cathode, FD and FDC of GDL28BC and Fe_2O_3/ALD cathodes (e-f) Cell performance during discharge/charge cycles. (g-h) Discharge/charge capacities and Coulombic efficiency vs. cycle number (Density current of 0.1 mA cm^{-2})

4. Conclusions

When comparing the specific capacity of the electrode with and without hematite, no significant difference is observed, with both reaching a specific capacity of 5.0 mAh cm^{-2}. However, in terms of cycling performance, the Fe_2O_3/ALD cathode exhibits significantly higher cyclability (120 vs. 25 cycles for Fe_2O_3/ALD and GDL28BC, respectively). Based on this preliminary data, the key advantage of modifying the cathode surface with this material lies in its ability to enhance performance over multiple cycles, addressing one of the main issues associated with the use of these batteries.

Acknowledgements

Proyecto de Investigación, ANID, Subvención a la Instalación en la Academia 2021 (SIA77210080)

References

[1] P. Aduama, et al., Energies, 16 (2023).
[2] Y. Zhou, et al. ACS Nano, 18, 16489 (2024)

Modeling and Simulation of the Co-precipitation Synthesis Process of the Janus nanoparticles in batch Reactor

S. Pablo[1,2], Svetlana Ushak.[1,2]

[1]Center for Advanced Research in Lithium and Industrial Minerals, University of Antofagasta, Avenue Universidad de Antofagasta 02800, Antofagasta, Chile.

[2]Chemical Engineering Department, University of Antofagasta, Avenue Universidad de Antofagasta 02800, Antofagasta, Chile

Janus nanoparticles (JNPs) are anisotropic particles that have a different chemical structure and morphology [1], and can have spherical, rod-shaped, raspberry, snowman and dumbbell structures [2]. Among dumbbells there are three categories: polymeric double spheres, polymeric-inorganic double spheres and double spheres of inorganic materials [3]. In particular, there is interest in dumbbell-type JNPs based on inorganic materials due to their excellent performance. Due to their amphiphilic characteristic, these particles are potential stabilizers of emulsion phase change materials applied to heat transfer fluids [4].

SiO_2-based dumbbell-type Janus nanoparticles have one SiO_2 sphere hydrophobically modified and the other hydrophilically modified and both are coupled by an amino group and an epoxy group. Figure 1 details the procedure for obtaining JNPs, in which the SiO_2 nanosphere is modified with hydrophobic molecules (e.g. hexamethyldisiloxane), together with the animo group, which in most syntheses is 3-(aminopropyl) triethoxysilane (APTES), and another sphere is modified with hydrophilic molecules such as an epoxysilane and then coupled to form the dumbbell. As can be seen, the inorganic material used to obtain the JNPs is SiO_2 and this component is obtained from the reaction of Tetraethylorthosilicate (TEOS) with water in alcoholic medium with ammonia as catalyst, this method was developed by Stoeber et al 1989 [5]. Therefore, in this work the modelling and simulation of SiO_2 production is carried out in order to establish the operating parameters of a co-precipitation reactor.

For the simulations, a batch reactor with a capacity of 2 litres and a temperature of 30 °C was considered. The reaction mechanism and the reaction rate equation developed by Herbert Giesche 1994 (equation 1) were used, where the concentrations of TEOS, H_2O and NH_3 were varied between the ranges of 0.01 to 10 mol/L, the simulations were performed in Matlab software version R2020a.

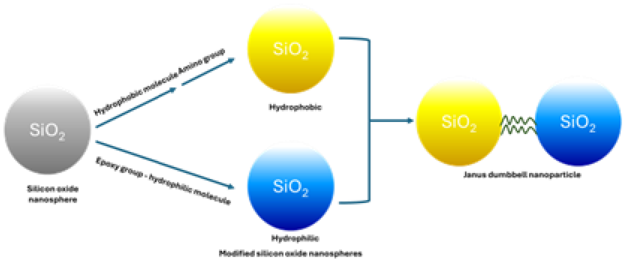

Figure 1. Schematic of the production of dumbbell-type Janus nanoparticles

$$Si(OC_2H_5)_4 + 4H_2O \rightarrow Si(OH)_4 + 4C_2H_5OH \qquad \text{Hydrolysis}$$
$$Si(OH)_4 \rightarrow SiO_2 + 2H_2O \qquad \text{Condensation}$$

$$NH_3 + H_2O \leftrightarrow NH_4^+ + OH^- \quad \text{Catalyst}$$

$$Si(OC_2H_5)_4 + 3H_2O + NH_3 \rightarrow SiO_2 + 4C_2H_5OH + NH_4OH$$

$$r_{SiO_2} = k\, exp\left\{\frac{-3256}{T}\right\} C_{H_2O}^{1,18}\, C_{NH_3}^{0,97}\, C_{TEOS} \quad (1)$$

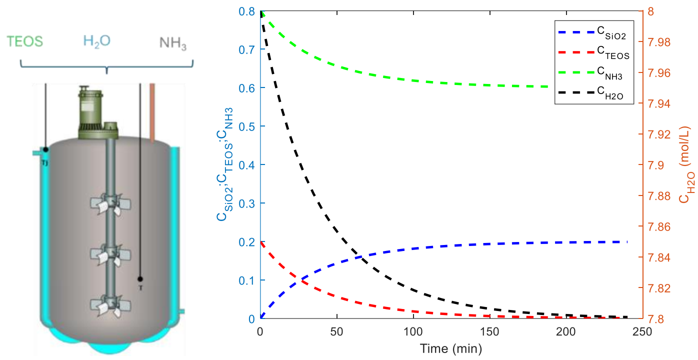

Figure 2. Batch reactor (left) and reaction kinetics result to obtain SiO_2 precursor (right).

The simulation results indicated that the optimal concentrations are 0.2 mol TEOS ($Si(O_2C_2H_5)_4$), 8 mol/L H_2O and 0.8 mol/L NH_3. Figure 2 details the reaction kinetics, where the consumption of the reactants and the formation of SiO_2 over time can be observed, it can be seen that TEOS is totally converted into SiO_2 and NH_3 is the excess reactant.
Therefore it is concluded that the simulation gives us parameters of initial concentrations to obtain SiO_2 for the Janus nanoparticles.

Keywords: Janus nanoparticles; Stoeber Method; SiO_2; amphiphilic; emulsion phase change materials

Acknowledgments: *The authors gratefully acknowledge the funding of the project ANID/FONDECYT REGULAR/1231721*

References:

[1] Meiying He, Pingmei Wang, Peiwen Xiao, Xinli Jia, Jianhui Luo, Bo Jiang y Bo Xiao, «Synthesis of amphiphilic dumbbell-like Janus nanoparticles through one-step coupling,» *Nanocomposites,* pp. 175-183, 2022.

[2] Wu Z, Li L, Liao T, Chen X, Jiang W, Luo W, Yang J y Sun Z, «Janus nanoarchitectures: From structural design to catalytic applications,» *Nanotoday,* vol. 22, pp. 62-82, 2018.

[3] Jin-Gyu Park, Jason D. Forster y Eric R. Dufresne, «High-Yield Synthesis of Monodisperse Dumbbell-Shaped Polymer Nanoparticles,» *Journal of the American Chemical Society,* vol. 132, p. 17, 2010.

[4] D. Cabaleiro, F. Agresti, L. Fedele, S. Barison, C. Hermida-Merino, S. Losada-Barreiro, S. Bobbo y M.M. Piñeiro, «Review on phase change material emulsions for advanced thermal management: Design, characterization and thermal performance,» *Renewable and Sustainable Energy Reviews,* vol. 159, 2022

2024 IWLiME
11th INTERNATIONAL CONFERENCE IN LITHIUM, INDUSTRIAL MINERALS AND ENERGY
November 27-29, Antofagasta, Chile

Modeling and Simulation of the Co-precipitation Synthesis Process of the Janus nanoparticles in batch Reactor

S.Pablo[1,2], Svetlana Ushak1[1,2]

[1]Center for Advanced Research in Lithium and Industrial Minerals, University of Antofagasta, Avenue Universidad de Antofagasta 02800, Antofagasta, Chile.

[2]Chemical Engineering Department, University of Antofagasta, Avenue Universidad de Antofagasta 02800, Antofagasta, Chile

1. Introduction

Janus nanoparticles (JNPs) are anisotropic particles that have a different chemical structure and morphology, and can have spherical, rod-shaped, raspberry, snowman and dumbbell structures. Among dumbbells there are three categories: polymeric double spheres, polymeric-inorganic double spheres and double spheres of inorganic materials. In particular, there is interest in dumbbell-type JNPs based on inorganic materials due to their excellent performance. Due to their amphiphilic characteristic, these particles are potential stabilizers of emulsion phase change materials applied to heat transfer fluids.

SiO_2-based dumbbell-type Janus nanoparticles have one SiO_2 sphere hydrophobically modified and the other hydrophilically modified and both are coupled by an amino group and an epoxy group. The inorganic material used to obtain the JNPs is SiO_2 and this component is obtained from the reaction of Tetraethylorthosilicate (TEOS) with water in alcoholic medium with ammonia as catalyst, this method was developed by Stoeber et al 1989. Therefore, in this work the modelling and simulation of SiO_2 production is carried out in order to establish the operating parameters of a co-precipitation reactor.

2. Methodology

For the simulations, a batch reactor with a capacity of 2 litres and a temperature of 30 °C was considered. The reaction mechanism and the reaction rate equation developed by Herbert Giesche 1994 (equation 1) were used, where the concentrations of TEOS, H_2O and NH_3 were varied between the ranges of 0.01 to 10 mol/L, the simulations were performed in Matlab software version R2020a.

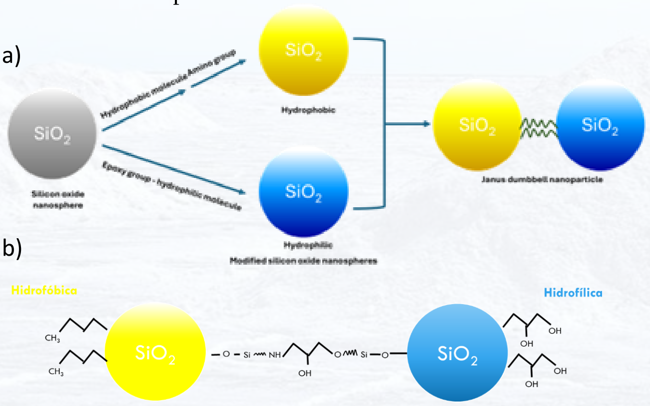

Figure 1. a) Schematic of the production of dumbbell-type Janus nanoparticles; b) dumbbell-type janus nanoparticles

Reaction mechanism of SiO_2 production:

$$Si(OC_2H_5)_4 + 4H_2O \rightarrow Si(OH)_4 + 4C_2H_5OH$$

$$Si(OH)_4 \rightarrow SiO_2 + 2H_2O$$

$$NH_3 + H_2O \leftrightarrow NH_4^+ + OH^-$$

$$Si(OC_2H_5)_4 + 3H_2O + NH_3 \rightarrow SiO_2 + 4C_2H_5OH + NH_4^+ + OH^-$$

$$r_{SiO_2} = k\, exp\left\{\frac{-3256}{T}\right\} C_{H_2O}^{1,18}\, C_{NH_3}^{0,97}\, C_{TEOS}$$

3. Results

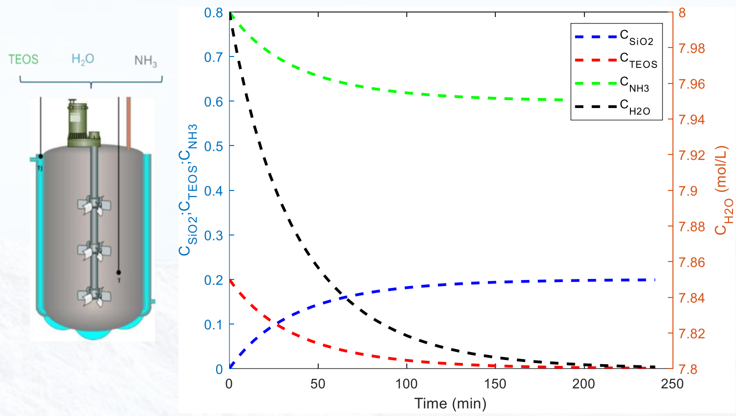

Figure 2. Batch reactor (left) and reaction kinetics result to obtain SiO_2 precursor (right).

The simulation results indicated that the optimal concentrations are 0.2 mol TEOS ($Si(O_2C_2H_5)_4$), 8 mol/L H_2O and 0.8 mol/L NH_3. Figure 2 details the reaction kinetics, where the consumption of the reactants and the formation of SiO_2 over time can be observed, it can be seen that TEOS is totally converted into SiO_2 and NH_3 is the excess reactant.

4. Conclusions

Therefore it is concluded that the simulation gives us parameters of initial concentrations to obtain SiO_2 for the Janus nanoparticles.

Acknowledgments:
The authors gratefully acknowledge the funding of the project ANID/FONDECYR REGULAR/1231721

Synthesis and characterization of a nickel and lithium ferrite for electrochemical applications

Lucas Humanez*, Jaime Llanos, Jonathan Cisterna, Alifhers Mestra
[a]Departamento de química, Facultad de Ciencias, Universidad Católica del Norte, Angamos 0610, Antofagasta
Email: lucas.humanez@alumnos.ucn.cl

Long life, low-cost and safe electrochemical energy storage systems are crucial for the sustainable development of human society . However, these devices have some drawbacks related to the poor stability of the materials used. Several materials undergo phase changes, exhibit low charge capacities, and experience volume expansions during operation cycles. For this reason, the development of materials with good chemical and thermal stability and high charge capacities, among other properties still poses a grand challenge in materials chemistry . In this work, we present preliminary results on the synthesis and chemical/electrochemical characterization of a new material derived from the compound $Li_2NiFe_2O_4$. This material can be a promising electroactive material for Lithium-ion batteries, since exhibit moderate electrical potential, good thermal and chemical stability, and high electrical and ionic conductivities. The $Li_2NiFe_2O_4$ oxide was synthesized by the solid-state method using metal oxide precursors. Structural, morphological, and surface characterizations were performed using conventional techniques, which allowed us to identify a micrometric, macroporous, pure, and homogeneous cubic spinel phase with a $Fd\bar{3}m$ space group. Electrochemical properties were also evaluated through voltammometric analysis, galvanostatic tests, and electrochemical impedance spectroscopy. According to our results, the compound behaves as a conversion material, dominated by diffusion-controlled processes (88.32%) with capacitive contributions (11.68%), allowing it to achieve a storage capacity of 980 mAh/g. These structural and electrochemical characterizations demonstrate the viability of using $Li_2NiFe_2O_4$ as an active material in energy storage applications.

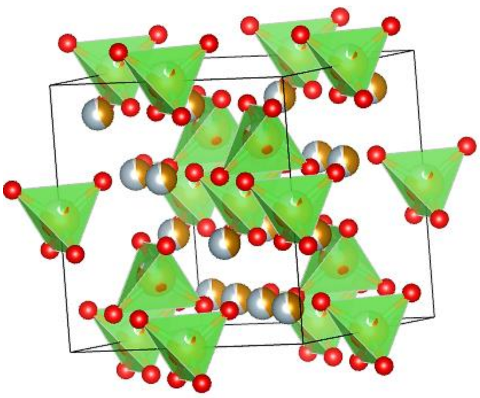

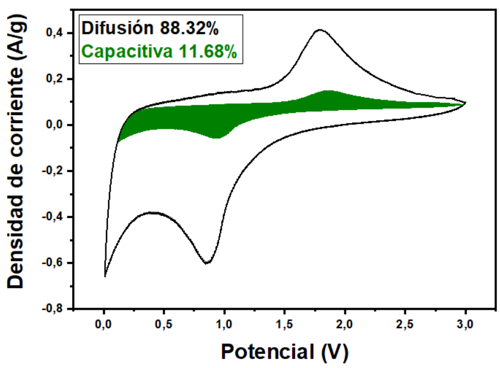

Figure 1. Structure of $Li_2NiFe_2O_4$ and Separation of Diffusional and Capacitive Contributions.

Keywords: *Lithium-ion batteries, Solid-state synthesis, Energy storage*

Acknowledgments: *Center of Universidad Católica del Norte, the MAINI Scientific Equipment Unit, the Lithium I+D+i.UCN*

References:

[1] M. R. Palacín, “Recent advances in rechargeable battery materials: a chemist’s perspective”, Chem Soc Rev, vol. 38, nº9, p. 2565, (2009).
[2] H. Zhang, J. Zhang, X. Gao, L. Wen, W. Li, y D. Zhao, “Advances in materials and structures of supercapacitors”, Ionics (Kiel), vol. 28, nº2, pp. 515–531, feb. (2022).
[3] Nabi, Ghulam, et al. "Role of cerium-doping in CoFe2O4 electrodes for high performance supercapacitors." Journal of Energy Storage 29 (2020).
[4] C. Cherpin, D. Lister, F. Dacquait, y L. Liu, “Study of the Solid-State Synthesis of Nickel Ferrite ($NiFe_2O_4$) by X-ray Diffraction (XRD), Scanning Electron Microscopy (SEM) and Raman Spectroscopy”, Materials, vol. 14, nº10, p. 2557, may (2021).

11th INTERNATIONAL CONFERENCE IN LITHIUM, INDUSTRIAL MINERALS AND ENERGY
November 27-29, Antofagasta, Chile
IWLiME 2024

Synthesis and characterization of a nickel and lithium ferrite for electrochemical applications

L. Humanez[1,2], J. Llanos[1,2], J. Cisterna[1,2], A. Mestra[1,2]

[1]Departamento de Química, Facultad de Ciencias, Universidad de Católica del Norte, Sede Casa Central, Av. Angamos 0610, Antofagasta, Chile
[2]Centro Lithium I+D+i, Universidad Católica del Norte, Avenida Angamos 0610, 1270709, Antofagasta, Chile

ABSTRACT: Long life, low-cost and safe electrochemical energy storage systems are crucial for the sustainable development of human society . However, these devices have some drawbacks related to the poor stability of the materials used. Several materials undergo phase changes, exhibit low charge capacities, and experience volume expansions during operation cycles[1,2]. For this reason, the development of materials with good chemical and thermal stability and high charge capacities, among other properties still poses a grand challenge in materials chemistry. In this work, we present preliminary results on the synthesis and chemical/electrochemical characterization of a new material derived from the compound $Li_2NiFe_2O_4$. This material can be a promising electroactive material for Lithium-ion batteries, since exhibit moderate electrical potential, good thermal and chemical stability, and high electrical and ionic conductivities[3,4]. The $Li_2NiFe_2O_4$ oxide was synthesized by the solid-state method using metal oxide precursors. Structural, morphological, and surface characterizations were performed using conventional techniques, which allowed us to identify a micrometric, macroporous, pure, and homogeneous cubic spinel phase with a $Fd\overline{3}m$ space group. Electrochemical properties were also evaluated through voltammometric analysis, galvanostatic tests, and electrochemical impedance spectroscopy. According to our results, the compound behaves as a conversion material, dominated by diffusion-controlled processes (88.32%) with capacitive contributions (11.68%), allowing it to achieve a storage capacity of 980 mAh/g. These structural and electrochemical characterizations demonstrate the viability of using $Li_2NiFe_2O_4$ as an active material in energy storage applications.

METHODOLOGY

Li_2O
Lithium (300˚C) 24 h
Oxigen atmosphere

Fe_2O_3
Iron (800˚C) 24 h

$Li_2NiFe_2O_4$
Ni, Li_2O, Fe_2O_3 1:1:1
Argon atmosphere
900˚C 72 h

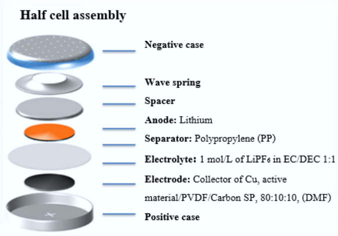

Voltammetric Analysis → Galvanostatic Analysis → Impedance

STRUCTURAL CHARACTERIZATION

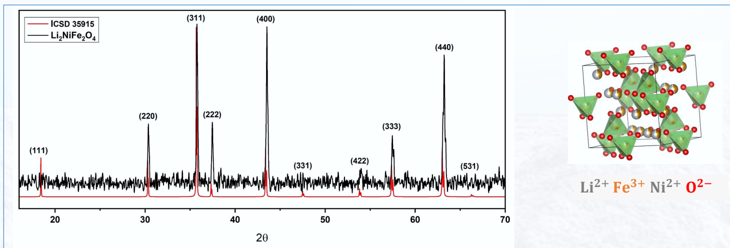

Figure 1: $Li_2NiFe_2O_4$ phase diffractogram compared with the of a cubic spinel pattern (ICSD 35915).

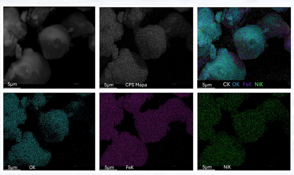

Figure 2: Elemental mapping images by EDS.

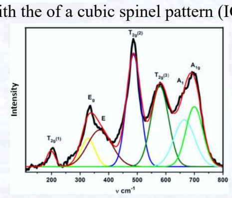

Figure 3: Raman Spectroscopy

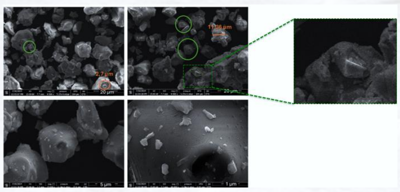

Figure 4: Scanning Electron Microscopy.

ELECTROCHEMICAL CHARACTERIZATION

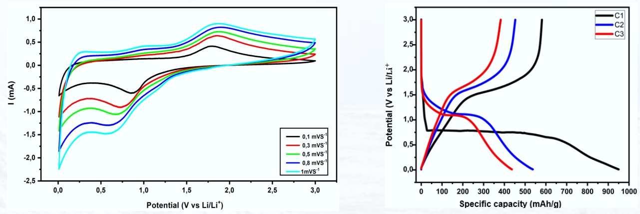

Figure 5: Cyclic voltammetry at different scan rates and galvanostatic charge-discharge curves.

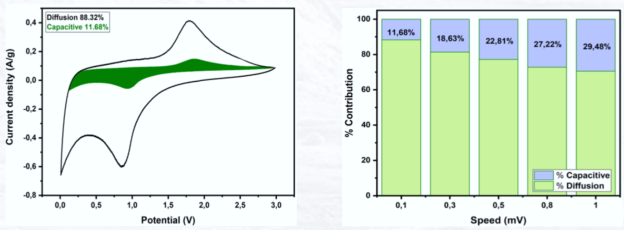

Figure 6: Separation of the current into capacitive and diffusive contributions.

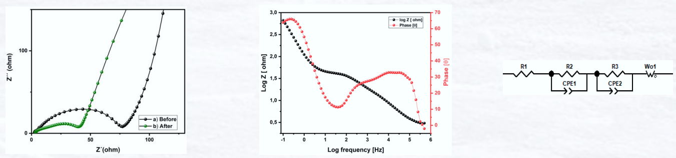

Figure 7: Nyquist plots before and after voltammetric analyses and Bode plot.

CONCLUSIONS: The oxide was succesful synthesized using the solid-state methods, and its structure and morphology were confirmed by powder X-ray diffraction, raman and SEM characterizations, which is micrometric, porous, and crystalline. Regarding electrochemical properties, the material exhibited quasi-reversible redox behavior as an anode within a 0 to 3 V range, with mixed Faradaic/Capacitive processes. Charge-discharge curves indicated a charge retention is 92.43%.

REFERENCES:
[1] Palacín, M. R. *Chemical Society Reviews* 2009, vol. 38, no. 9, p. 2565.
[2] Zhang, H., et al. *Ionics (Kiel)*, 2022, vol. 28, no. 2, pp. 515–531.
[3] Nabi, G., *Energy Storage* 202,0 vol.29, p.101452.
[4] Cherpin, C., Liset al. ter D., Dacquait, F., & Liu, L. *Materials* 2021, vol. 14, nº10, p. 2557.

ACKNOWLEDGMENTS: lithium I+D+i UCN, Química UCN, MAINI Unidad de Equipamiento Científico

Organized by: UA Universidad de Antofagasta, celimin, Universidad Católica del Norte, lithium I+D+i UCN, SQM Soluciones para el desarrollo humano, Somos Litio... Somos Futuro, SERC Chile Solar Energy Research Center

Sponsors: SQM Soluciones para el desarrollo humano, Somos Litio... Somos Futuro, CROMTEK, Merck, SAGU, Watson Marlow Fluid Technology Solutions, MACCOR

Purification of LiCl brines from EDL through electrochemical alkalinization

G. Choque[1,2], A. Gonzalez[1,2], M. Grágeda[1,2]

[1]*Center for Advanced Research in Lithium and Industrial Minerals, University of Antofagasta, Avenue Universidad de Antofagasta 02800, Antofagasta, Chile.*

[2]*Chemical Engineering Department, University of Antofagasta, Avenue Universidad de Antofagasta 02800, Antofagasta, Chile*

Lithium is key to the global energy transition, positioning Chile as a world leader with 24% of the production from brines. However, the conventional lithium extraction method using evaporation ponds consumes around 2000 tons of water for each ton of LCE produced, generates chemical waste, and impacts ecosystems. In response, companies like SQM and Albemarle are testing direct lithium extraction (DLE) technologies, which offer a more environmentally friendly lithium production process but still face challenges in removing impurities and require equally sustainable secondary purification processes.

The work focused on developing an electrochemical process for purifying real LiCl brines obtained after the DLE process [1]. The goal was to produce a purified LiCl solution, free from impurities, suitable for later integration into a membrane electrolysis process for the direct production of LiOH. Two initial compositions were evaluated: one from laboratory-scale tests and another from pilot-scale DLE tests, both with varying concentrations of Ca, Mg, Na, K, and Li.

An electrodialysis process was implemented using a three-compartment electrolyzer [2] [3], separated by an anionic membrane (AMX) and a cationic membrane (AMX). This configuration allows for the simultaneous separation of Ca and Mg impurities from lithium brines, while alkalinizing the LiCl solution and removing the Mg and Ca impurities through the formation of $Mg(OH)_2$ and $Ca(OH)_2$.

Specific energy consumption, impurity removal percentages, and lithium recovery were determined under different current conditions and concentrations. The best results were achieved in concentrated pilot-scale solutions, with 99% removal of Mg and 98% removal of Ca, and a lithium recovery of 96%. Specific energy consumption ranged from 32.4 to 27.3 kWh/kg of treated Li, with lower consumption when operating at a lower current density.

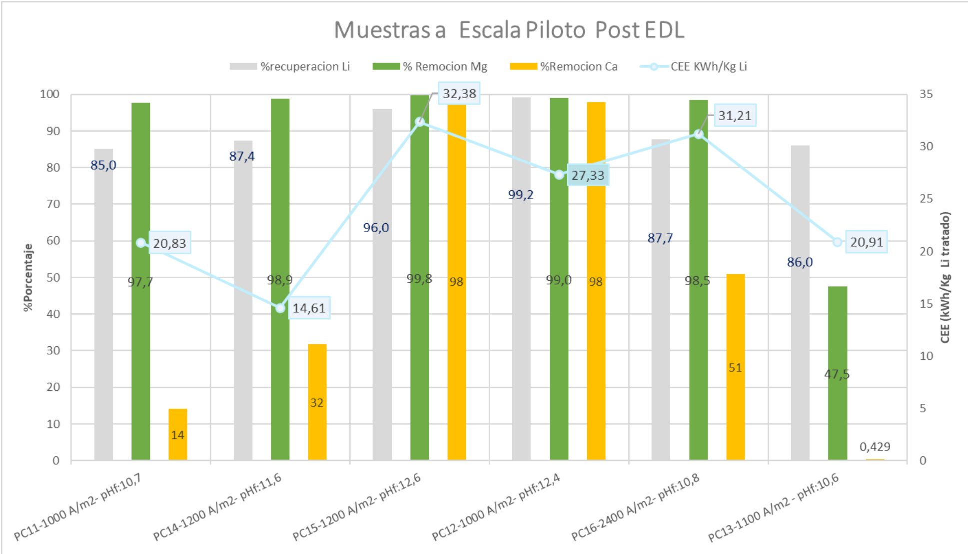

Figure 1. Results of Current Density Effect for EDL Solutions PC1-Concentrated Pilot

This study demonstrates the feasibility of the electrodialysis process as a more sustainable alternative for reducing the concentration of Mg and Ca in a post-EDL solution. This configuration eliminates the need for chemical reagents, which not only minimizes environmental impact but also prevents the generation of Cl_2.

Keywords: Technology EDL, LiCl brine, Electrodialysis, Precipitation of Ca-Mg

Acknowledgments: *Authors thank to the "Plataforma para la producción de materiales avanzados sustentables y manufactura de baterías de litio" SQM-CELIMIN Project for the financial support*

References:

[1] M. L. Vera, W. R. Torres, C. I. Galli, A. Chagnes and V. Flexer, "Environmental impact of direct lithium extraction from brines," *Nature Reviews. Earth and Environment,* pp. 149-165, 2023.

[2] C. H. Díaz Nieto, J. A. Kortsarz, M. L. Vera and V. Flexer, "Effect of temperature, current density and mass transport during the electrolytic removal of magnesium ions from lithium rich brines," *Elsevier,* vol. 529, no. 115652, 2022.

[3] C. H. Díaz Nieto, N. A. Palacios, K. Verbeeck, A. Prévoteau, K. Rabaey and V. Flexer, "Membrane electrolysis for the removal of Mg2+ and Ca2+ from lithium rich brines," *Water Research*, vol. 154, pp. 117-124, 2019.

IWLiME 2024

11th INTERNATIONAL CONFERENCE IN LITHIUM, INDUSTRIAL MINERALS AND ENERGY

November 27-29, Antofagasta, Chile

Purification of LiCl brines from DLE through electrochemical alkalinization

G.Choque[1,2], A. González[1,2], M. Grágeda[1,2]

[1]Center for Advanced Research in Lithium and Industrial Minerals, University of Antofagasta, Avenue Universidad de Antofagasta 02800, Antofagasta, Chile.

[2]Chemical Engineering Department, University of Antofagasta, Avenue Universidad de Antofagasta 02800, Antofagasta, Chile

geovanna.choque.guisbert@ua.cl; alonso.gonzalez@uantof.cl; mario.grageda@uantof.cl

Introduction

The conventional method of lithium extraction using evaporation pools consumes 2000 tons of water per ton of LCE and generates chemical waste, which has prompted companies such as SQM and Albemarle to test Direct Lithium Extraction (DLE) technologies at the pilot level, suggesting future implementation at industrial scale. These technologies produce LiCl solutions with a lower environmental impact, but their direct use in the production of Li_2CO_3 or LiOH presents limitations due to the low lithium concentration, acid pH and the high presence of impurities such as Na, K, Mg and Ca. These difficulties are motivation to to anticipate future challenges by developing more sustainable purification processes using electromembrane technologies to purify post-DLE LiCl solutions.

Materials and Method

This work proposes a three-compartment electrolyzer with ion exchange membranes (AMX and CMX) to purify post-DLE lithium brines, removing Ca and Mg. The acidic character of LiCl solutions allows OH- to be generated at the cathode by the reduction of water, raising the pH and causing the precipitation of Mg^{2+} and Ca^{2+} as $Mg(OH)_2$ and $Ca(OH)_2$ due to their low solubility.

$$2H_2O + 2e \rightarrow H_2 + 2\,OH^- \qquad E^o = -0.8277\ V$$

$$Mg^{2+}_{(ac)} + 2OH^-_{(ac)} \leftrightarrow Mg(OH)_{2\,(s)} \qquad K_{ps} = 5.61 \cdot 10^{-12}$$

$$Ca^{2+}_{(ac)} + 2OH^-_{(ac)} \leftrightarrow Ca(OH)_{2\,(s)} \qquad K_{ps} = 5.02 \cdot 10^{-6}$$

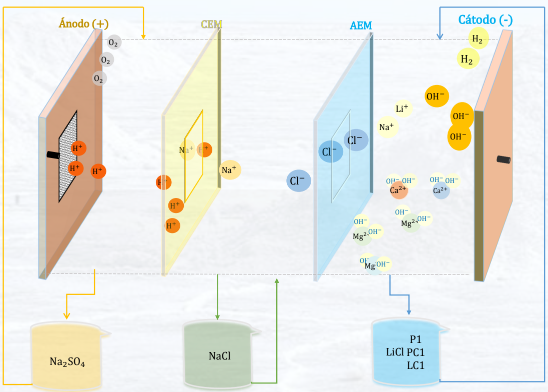

Fig. 1. Experimental scheme of electrochemical alkalinization

Results and discussion

Specific energy consumption (CEE), Ca and Mg impurity removal and Li recovery were evaluated under different current densities and concentrations. Although the electrolyzer was not designed for such a configuration and it was not certain whether it was suitable for internal precipitation, the best results were obtained in concentrated solutions with Mg and Ca removals of 99.8% and 98.0%, respectively. And lithium recovery ranged from 96% to 99%. The specific energy consumptions varied between 32.4 and 27.3 KWh/Kg Li treated in solution, being lower when working with a current density of 1000 A/m2.

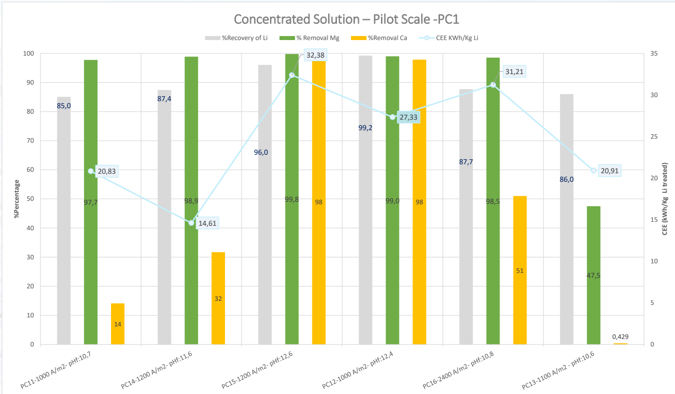

Fig. 2. Percentage of Mg and Ca removal, lithium recovery and CEE in concentrated LiCl solution Post EDL

Conclusions

Best results are obtained in concentrated LiCl Post DEL solutions, this design allows efficient removal of Mg and Ca without the use of additional reagents. In addition, it avoids the formation of toxic gas such as Cl2, and generates valuable by-products such as H_2SO_4, H_2 and O_2, which do not represent environmental risks. As a next step, it is proposed to optimize the specific energy consumption (CEE) to increase the efficiency of the system.

Acknowledgments

Authors thanks to the“Plataforma para la producción de materiales avanzados sustentables y manufactura de baterías de litio” SQM-CELIMIN Project for the financial support.

SIMULATION OF THE PROCESS FOR OBTAINING POTASSIUM SULFATE FROM REGIONAL RAW MATERIALS

M. Ticona[1], E. Barrientos[2], P. Vargas[1]

[1]*Center for Advanced Research in Lithium and Industrial Minerals*
Phase Diagram Lab, University of Antofagasta, Avenue Universidad de Antofagasta 02800, Antofagasta, Chile.
[2]*Chemical Engineering Department, University of Antofagasta, Avenue Universidad de Antofagasta 02800, Antofagasta, Chile*

Potassium sulfate (K_2SO_4) can be produced in several ways from compounds that supply the sulfate ion. In this context, the present study aims to design processes for obtaining K_2SO_4 from mirabilite ($Na_2SO_4.10H_2O$), and sylvite minerals with the use of quaternary diagrams that consist of two chemical conversion reactions, both at a temperature of 25 °C, which is presented in figure 1. The first chemical reaction occurs by mixing mirabilite ($Na_2SO_4.10H_2O$), potassium chloride and water, producing glaserite ($Na_2SO_4.3K_2SO_4$) in equilibrium with saturated solution. The second reaction uses the glaserite ($Na_2SO_4.3K_2SO_4$) obtained in the previous stage, which decomposes when mixed with potassium chloride and water, generating a saturated solution of chloride ions and a solid (K_2SO_4). The results obtained were variable according to the different cases. The optimal result was obtained by using pure raw materials until equilibrium is reached consisting of a saturated solution of three phases: sylvite, glaserite and thenardite (Na_2SO_4), for the first reaction and subsequent second reaction in addition to the recirculation of the saturated solutions obtaining a potassium yield equal to 86.82% it is present in the table 1.

The simulation using the OLI software of the process without recycling was compared with the theoretical results obtained based on the quaternary diagrams and which showed the existence of minimal significant deviations, on the other hand, in the processes with recycling there were important deviations attributed to the thermodynamic basis of OLI specifically in the concentrations of the sulfate anion for this reason an experimental verification was carried out in the laboratory of the invariant points reported bibliographically of system Na_2Cl_2-K_2Cl_2-Na_2SO_4-K_2SO_4 – H_2O at the temperature of 25 °C. Reporting congruence between them and therefore, the validation of the process designs for obtaining potassium sulfate using the use of quaternary diagrams.

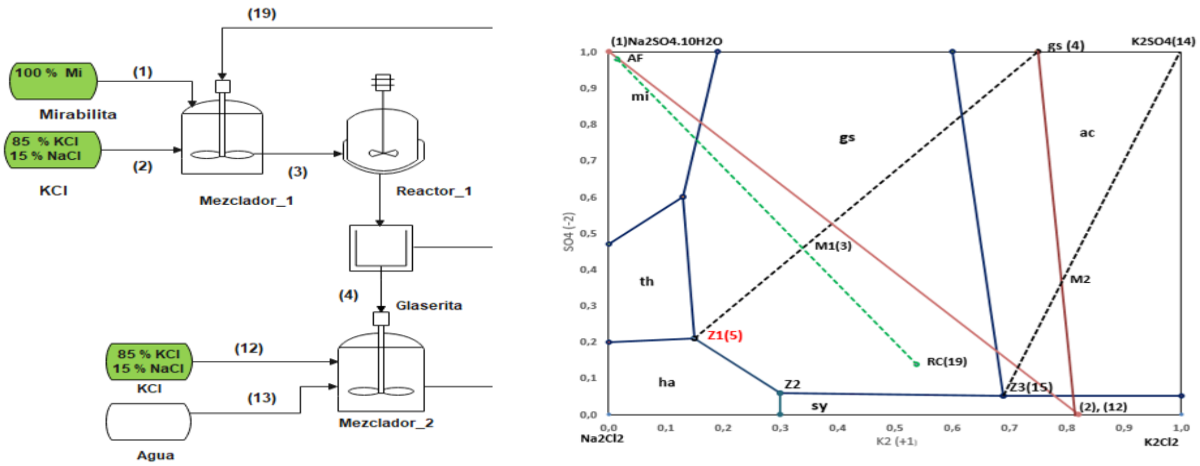

Figure 1. Description of the process for obtaining K_2SO_4, according to reciprocal quaternary diagrams, case 1.2

Parameters	Units	Case 1.1		Case 1.2		Case 1.3		Case 1.4		Case 2.1	
		DF	**OLI**	DF	**OLI**	DF	**OLI**	DF	**OLI**	DF	**OLI**
Potassium Yield[I]	% p/p	74,28	**64,92**	72,00	**53,54**	71,19	**64,44**	63,13	**53,59**	56,65	**51,53**
Potassium Yield [II]	% p/p	63,51	**58,69**	41,69	**31,53**	63,51	**59,85**	42,20	**38,52**	57,82	**53,64**
Global Potassium Yield	% p/p	86,82	**74,56**	62,72	**43,55**	80,82	**78,84**	63,20	**57,35**	67,39	**59,95**

Table 1. Results of yields and raw material consumption in the process of obtaining K_2SO_4 using DF and OLI with recycling

Keywords: Quaternary diagrams, potassium sulfate and invariant points.

Acknowledgments:
First, I would like to thank GOD enormously for accompanying me, protecting me, guiding me and being the light on my path and for giving me the wisdom to carry out this work and to be able to carry it out.
To my tutors, Dr. Pedro Vargas and MSc. Einar Barrientos
To the company SQM and especially to the team of the Innovation and Development Management.

References:

[1] Blaslade. (1918). Separation of chlorides, sulphates, Na, K. The journal of industrial and engineering chemistry.10,344-347.
[2] Bromley, L.A. (1973). Thermodynamic Properties of Strong Electrolytes in Aqueous Solutions. AIChE J.19, 313.
[3] Cisternas L. A. (2009). Phase diagram and its application. Spain: Reverte. S.A

11th INTERNATIONAL CONFERENCE IN LITHIUM, INDUSTRIAL MINERALS AND ENERGY

November 27-29, Antofagasta, Chile

IWLiME 2024

SIMULATION OF THE PROCESS FOR OBTAINING POSTASSIUM SULFATE FROM REGIONAL RAW MATERIALS

M. Ticona[1], E. Barrientos[2] , P. Vargas[2]

[1]*Center for Advanced Research in Lithium and Industrial Minerals, University of Antofagasta, Avenue Universidad de Antofagasta 02800, Antofagasta, Chile.*
[2]*Chemical Engineering Department, University of Antofagasta, Avenue Universidad de Antofagasta 02800, Antofagasta, Chile*

1. INTRODUCTION

The Atacama salt flat, located in northern Chile, is home to vast reserves of salts such as mirabilite and sylvite, which are essential to produce potassium sulphate (K_2SO_4), a highly valued fertilizer for its potassium and sulfur content, ideal for chlorine-sensitive crops. This work focuses on the design of an innovative process for obtaining K_2SO_4 using quaternary phase diagrams of the Na^+, K^+, Cl^-, SO_4^{2-} system at 25 °C and simulation with OLI Systems software. Using high- and low-grade mirabilite and sylvite, critical variables in crystallization are analyzed and process yields are evaluated, guaranteeing its technical, economic and environmental viability. This approach allows raw materials with impurities to be converted into high-value products, minimizing environmental impacts and optimizing available resources.

2. METODOLOGY

The research of the different authors Garrett (1996), Fabrik et al. (2017), Ogedengbe, et al. (2020), in obtaining K_2SO_4 an illustrative sequence of the steps for the process design was developed.
Another important collection was the solubility data in the K_2-Na_2-Cl_2-SO_4-H_2O system at different temperatures for the construction of reciprocal quaternary phase diagrams and with them to be able to design new processes with different unit operations.
The conversion process occurs in two stages according to the phase diagram of the reciprocal salt pair and described by the pair of equations:

$$4\ Na_2SO_4.10H_2O + 3\ K_2Cl_2 \rightarrow Na_2SO_4.3K_2SO_4 + 3\ Na_2Cl_2 + 40\ H_2O$$

$$Na_2SO_4.3K_2SO_4 + K_2Cl_2 \rightarrow 4\ K_2SO_4 + Na_2Cl_2$$

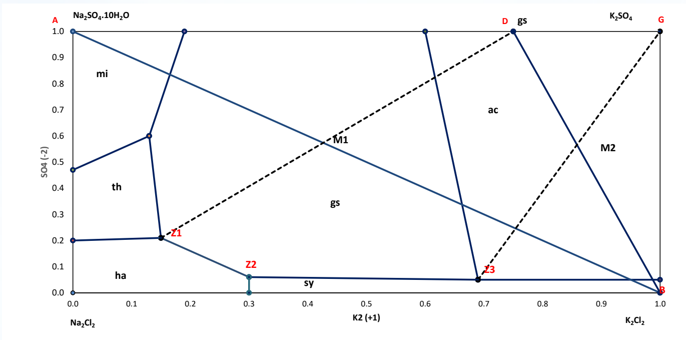

Figure 1. Description of obtaining K_2SO_4 with the invariant point Z1

3. RESULTS AND DISCUSSION

In obtaining potassium sulphate using quaternary diagrams, from the case studies presented in Table 1. The generation of a design was obtained, the industrial process covering the unit operations, which are presented in Figure 2.

Table 2. Description of case studies the potassium sulphate production process with and without recycling

N.°	Case description	Invariant solution	Description of raw materials	
			Mirabilite [%]	Sylvinite [%]
1	1.1	Z1	100	100
2	1.2	Z1	100	85
3	1.3	Z1	90	100
4	1.4	Z1	90	85
5	2.1	Z2	100	100

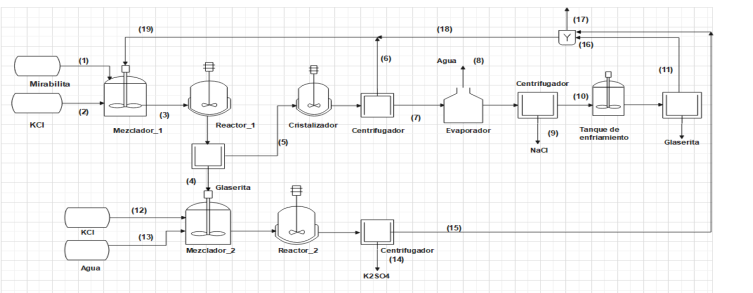

Figure 2. Process for obtaining potassium sulfate with recycling case 1.1 mirabilite and pure sylvite

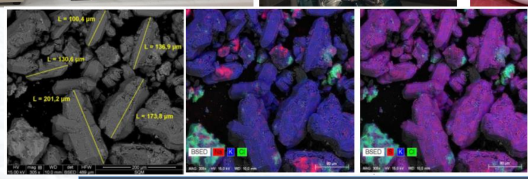

Figure. 3. SEM micrograph with EDS analysis

Evidently, the recirculation of the invariant solutions were important, since they generated increases in the overall yields of potassium and sulfate in the five cases studied compared to the processes without recycle.
There was a decrease in the consumption of raw materials in the glaserite conversion processes.

Table 3. Results of yields and raw material consumption in the process of obtaining K2SO4 using DF and OLI with recycling

Parameters	Units	Case 1.1		Case 1.2		Case 1.3		Case 1.4		Case 2.1	
		DF	OLI	DF	OLI	DF	OLI	DF	OLI	DF	OLI
Potassium Yield[I]	% p/p	74,28	64,92	72,00	53,54	71,19	64,44	63,13	53,59	56,65	51,53
Potassium Yield [II]	% p/p	63,51	58,69	41,69	31,53	63,51	59,85	42,20	38,52	57,82	53,64
Global Potassium Yield	% p/p	86,82	74,56	62,72	43,55	80,82	78,84	63,20	57,35	67,39	59,95

Acknowledgments:
To my tutors, Dr. Pedro Vargas and MSc. Einar Barrientos
To the company SQM and especially to the team of the Innovation and Development

4. CONCLUSIONS

A graphical approach based on solubility diagrams of the Na^+, K^+, Cl^-, SO_4^{2-} system was developed to design potassium sulphate production processes. Simulation and experimental validation demonstrated a potassium yield of 57.03%, increased to 86.82% with recirculation. Impurities and operating conditions affected the results.
The design for obtaining potassium sulphate from high and low grade mirabilite and sylvite was achieved.
The simulations of the case studies were important in the OLI thermodynamic software, we managed to obtain a consistent and reliable description of the equilibrium.

5. REFERENCE

1. Fabrik, M., A. Echeveria, P. Kindermann, and H. Ibrahim. (2017). An integrated process for producing potassium sulfate from potash mining wastes. *Journal of waste Management and Environmental. 1,* 1-9.
2. Garrett, D. (1996). Potash, Processing, Properties and Uses. (1 ªed.). California, USA: Saline Processors, Inc

Synthesis and Characterization of $LiNi_{0.5}Mn_{1.5}O_4$: A Comparative Study of the effect of Lithium Sources

L. Rojas[1], M. Grageda[1,2], M. Arratia[1]

[1]*Center for Advanced Research in Lithium and Industrial Minerals, University of Antofagasta, Avenue Universidad de Antofagasta 02800, Antofagasta, Chile.*

[2]*Chemical Engineering Department, University of Antofagasta, Avenue Universidad de Antofagasta 02800, Antofagasta, Chile*

The development of high-performance cathode materials is critical for advancing lithium-ion battery technology. This study focuses on the synthesis of $LiNi_{0.5}Mn_{1.5}O_4$ (LNMO), a promising cathode material known for its high operating voltage (~4.7 V vs Li/Li^+), excellent energy density, and thermal stability [1]. Different lithium precursors were used for the synthesis of LNMO: Lithium Carbonate (Li_2CO_3), Lithium Hydroxide Monohydrate ($LiOH \cdot H_2O$), and Lithium Sulfate Monohydrate ($Li_2SO_4 \cdot H_2O$). Prior to synthesis, a $Ni_{0.25}Mn_{0.75}CO_3$ precursor was prepared via coprecipitation, ensuring uniform cation distribution and controlled morphology. The LNMO material was obtained through a subsequent high-temperature calcination process.

By SEM and XRD measurements, it is observed that the morphology and crystallinity of $LiNi_{0.5}Mn_{1.5}O_4$ materials depend on the lithium precursor used. LNMO-LC and LNMO-LOH exhibit quasi-spherical secondary particles (~4-5 µm) and primary octahedra (~250-500 nm and ~150-300 nm, respectively). LNMO-LS shows irregular morphology (~0.5-2 µm) and impure phases (NiMn2O4, principal phase) according to XRD, attributable to its higher melting point [2] (LS=845°C), in contrast to the other precursors (LC=720°C and LOH=460°C), evidencing its incomplete decomposition. Materials synthesized with Li_2CO_3 and $LiOH \cdot H_2O$ are pure and crystalline, indexed to the fd-3m space group (LNMO). LNMO-LOH, with smaller particle size and higher uniformity, is projected as the material with better electrochemical performance.

The choice of lithium precursor also significantly influenced its electrochemical performance. Among the synthesized samples, those derived from $LiOH \cdot H_2O$ exhibited superior electrochemical behavior due to improved lithium-ion diffusion pathways and a well-ordered spinel structure. Electrochemical testing demonstrated that LNMO synthesized with $LiOH \cdot H_2O$ delivered a high initial discharge capacity (95.56 mAh/g), and stable cycling performance (99.85% capacity retention after 25 cycles at C/5), making it suitable for high-power applications.

This study highlights the advantages of LNMO, such as its cobalt-free composition, cost-effectiveness, and high-voltage operation, which align with the demand for sustainable and efficient energy storage systems [3]. The methodology employed also emphasizes the importance of precursor selection and processing conditions in tailoring material properties. The findings contribute to the ongoing development of advanced cathode materials, positioning LNMO as a key candidate for next-generation lithium-ion batteries, particularly in electric vehicles and grid energy storage applications.

Keywords: $LiNi_{0.5}Mn_{1.5}O_4$ synthesis, Lithium source, high-voltage cathode, lithium-ion batteries

Acknowledgments: *Project "Platform for the production of advanced sustainable materials and manufacturing of lithium batteries",*

References:

[1] X. Zhu, X. Zhu, A. Huang, I. Martens, N. Vostrov, Y. Sun, M.-I. Richard, T. Schülli, and L. Wang., High-Voltage Spinel Cathode Materials: Navigating the Structural Evolution for Lithium-Ion Batteries, *Advanced Materials*, 36 (2024), doi: 10.1002/adma.202403482.I

[2] Y. Liu, J. Li, M. Zeng, Y. Huang, X. Xu, M. Yan, J. Guo, J. Deng, J. Yang., Octahedral nano-particles constructed LiNi0.5Mn1.5O4 microspheres as high-voltage cathode materials for long-life lithium-ion batteries, *Ceramics International*, 44 (2018), doi: 10.1016/j.ceramint.2018.07.278.

[3] R. Amin, N. Muralidharan, R. Petla, H. Ben, S. Jassim, R. Essehli, C. Daniel, M. Khaleel, I. Belharouak, Research advances on cobalt-free cathodes for Li-ion batteries - The high voltage LiMn1.5Ni0.5O4 as an example, *Journal of Power Sources*, 467 (2020), doi: 10.1016/j.jpowsour.2020.228318.

2024 IWLiME

11th INTERNATIONAL CONFERENCE IN LITHIUM, INDUSTRIAL MINERALS AND ENERGY

November 27-29, Antofagasta, Chile

UA Universidad de Antofagasta

Synthesis and Characterization of $LiNi_{0.5}Mn_{1.5}O_4$: A Comparative Study of the effect of Lithium Sources

celimin CENTER FOR ADVANCED RESEARCH ON LITHIUM AND INDUSTRIAL MINERALS

L. Rojas[1], M. Grageda[1,2], M. Arratia[1]

[1]*Center for Advanced Research in Lithium and Industrial Minerals, University of Antofagasta, Avenue Universidad de Antofagasta 02800, Antofagasta, Chile.*

[2]*Chemical Engineering Department, University of Antofagasta, Avenue Universidad de Antofagasta 02800, Antofagasta, Chile*

Introduction

The growing demand for efficient lithium-ion batteries drives the search for advanced cathode materials. $LiNi_{0.5}Mn_{1.5}O_4$ (LNMO) stands out for its high voltage (~4.7 V), high energy density and thermal stability, being a sustainable alternative to cobalt. This work focuses on the synthesis of LNMO from three industrially produced lithium sources in Chile (Li_2CO_3, $LiOH{\cdot}H_2O$ and $Li_2SO_4{\cdot}H_2O$) by heat treatment, preceded by coprecipitation of a $Ni_{0.25}Mn_{0.75}CO_3$ precursor, exploring the impact of the precursors on the physical and electrochemical properties of the material.

Experimental methodology

Stage I: Coprecipitation

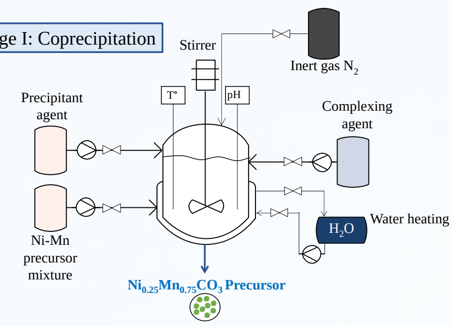

$$M^{2+} + xNH_4OH(aq) \rightarrow M(NH_3)_n^{2+}(aq) + xH_2O \quad (1)$$

$$M(NH_3)_n^{2+}(aq) + yCO_3^{-} \leftrightarrow MCO_3(s) + nNH_3 \quad (2)$$

Stage II: Solid state reaction

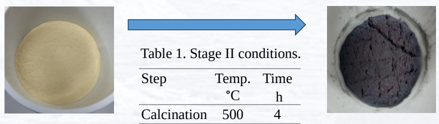

Table 1. Stage II conditions.

Step	Temp. °C	Time h
Calcination	500	4
Sintering 1	850	14
Sintering 2	600	4

- $Ni_{0.25}Mn_{0.75}CO_3$ precursor was obtained by controlled coprecipitation of nickel and manganese salts with a complexing and precipitating agent (Eq. 1 and 2, respectively).
- Subsequently, the precursor was mixed with three different lithium sources (Li_2CO_3, $LiOH{\cdot}H_2O$ and $Li_2SO_4{\cdot}H_2O$) in stoichiometric proportions. The mixtures were subjected to heat treatment for the formation of the cathodic material.
- The LNMO were characterized by techniques such as XRD, SEM and electrochemical tests to evaluate its performance in coin cell.

Table 2. Lithium sources.

Li source	Material identification
Li_2CO_3	LNMO-LC
$LiOH{\cdot}H_2O$	LNMO-LOH
$Li_2SO_4{\cdot}H_2O$	LNMO-LS

Table 3. Coin cell cycling conditions.

Description	Detail
Voltage range, V	3.5 – 4.9
Constant C-rate	C/5
Cycles number	25
Anode	Li metal

Acknowledgments

Project: "Platform for the production of advanced sustainable materials and manufacturing of lithium batteries",

Results and discussions

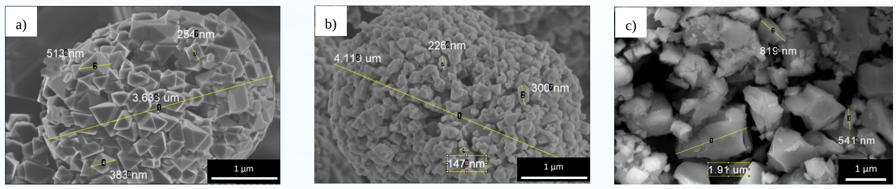

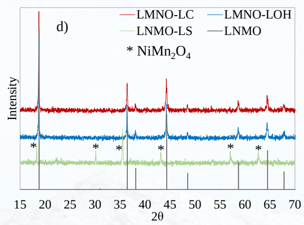

SEM images of each synthesized material are shown in Fig. 1. It is observed that the morphology and crystallinity of $LiNi_{0.5}Mn_{1.5}O_4$ materials depend on the lithium precursor used. LNMO-LC and LNMO-LOH (Fig. 1a-b, respectively) exhibit quasi-spherical secondary particles (~4-5 µm) and primary octahedra (~250-500 nm and ~150-300 nm, respectively). LNMO-LS shows irregular morphology (~0.5-2 µm) and impure phases ($NiMn_2O_4$, principal phase *) according to XRD (Fig. 1d), attributable to its higher melting point (LS=845°C), in contrast to the other precursors (LC=720°C and LOH=460°C), evidencing its incomplete decomposition. Materials synthesized with Li_2CO_3 and $LiOH{\cdot}H_2O$ are pure and crystalline, indexed to the fd-3m space group (LNMO). LNMO-LOH, with smaller particle size and higher uniformity, is projected as the material with better electrochemical performance.

Fig. 1. SEM images of a) LNMO-LC; b) LNMO-LOH; and c) LNMO-LS, respectively; and d) XRD patterns of the three materials and its reference (LNMO).

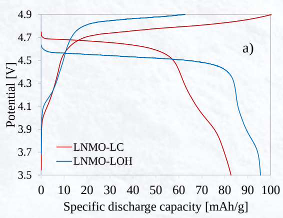

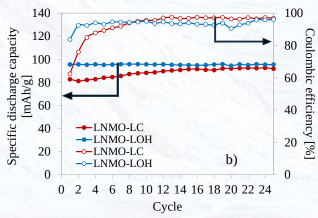

Table 4. Results of coin cell cycling.

Description	LMNO-LC	LMNO-LOH
C-rate	C/5	
Initial discharge cap., mAh/g	82.72	95.56
Final discharge cap., mAh/g	91.84	95.43
Average coulombic efficiency, %	92.83	93.81
Capacity retention, %	111.02	99.86

Fig. 2. a) First cycle charge/discharge voltage profile; and b) cycling performance and coulombic efficiency of LNMO-LC and LNMO-LOH respectively.

The electrochemical characterization is presented in Fig. 2. It was not performed with the LNMO-LS material due to the impurity found and is under optimization. The electrochemical results show significant differences between LNMO-LC and LNMO-LOH after 25 cycles. LNMO-LC exhibited an increase in specific discharge capacity, from 82.72 to 91.84 mAh/g, with a capacity retention of 111.02%. This increase is associated with an initial activation process, where the porosity of the material improves accessibility to active sites for Li ions and inter-particle interaction. In the other hand, LNMO-LOH demonstrated greater stability, with capacities of 95.56 and 95.43 mAh/g at the beginning and end of the test, respectively, and a retention of 99.85%. The coulombic efficiency achieved for each material (LC and LOH) was 92.83 and 93.81%, respectively, achieving a slightly higher stability between charge and discharge for LNMO-LOH. Its smaller particle size and greater structural uniformity for efficient reaction kinetics and lower resistance to charge transfer, standing out as the most stable material.

Conclusions

- The type of lithium precursor significantly influences the morphology, crystallinity and electrochemical performance of $LiNi_{0.5}Mn_{1.5}O_4$ (LNMO).
- LNMO-LOH and LNMO-LC exhibit more homogeneous particles and better crystallization, while LNMO-LS contains impure phases.
- LNMO-LOH demonstrated higher stability and electrochemical efficiency.
- The use of $Li_2SO_4{\cdot}H_2O$ as a precursor requires adjustments in the synthesis conditions to improve the purity and yield of the cathode material.

Experimental evaluation of nitrate mixtures as PCMs in thermal energy storage for industrial applications

Franklin R. Martinez Alcocer[1,2], Svetlana Ushak[2], Emiliano Borri[1], Saranprabhu Mani Kala[1], Luisa F. Cabeza[1,*]
[1]*GREiA Research Group, University of Lleida, Pere de Cabrera 3, 25001-Lleida, Spain,*
[2]*Center for Advanced Research in Lithium and Industrial Minerals, University of Antofagasta, Avenue Universidad de Antofagasta 02800, Antofagasta, Chile*
**e-mail: luisaf.cabeza@udl.cat*

According to the International Energy Agency (IEA) [1], in 2022, industry was responsible for 25% of the CO_2 emissions of the global energy system, reflecting the need in this sector to optimize its processes by implementing cleaner technologies. Thermal energy storage (TES) with phase change materials (PCM) has been applied as useful engineering solution to reduce the gap between energy supply and demand in cooling or heating applications by storing extra energy generated during peak collection hours and dispatching it during off-peak hours [2]. However, to implement this technology, it is essential to have an adequate selection of suitable storage materials to ensure the performance of the TES system. Nitrates are an attractive option to be considered as PCMs mainly because they have good thermal stability up to 400 ºC (mass loss is not observed), they have high enthalpy, they are not expensive, and they are less corrosive than other inorganic salts such as chlorides. In addition, large quantities of nitrates are produced in Salar de Atacama (North of Chile) for various applications [3]. In this study, three eutectic mixtures of nitrate and one single nitrate salt were fully characterized by thermogravimetric analysis (TGA), differential scanning calorimetry (DSC), and hot disk. The results of comprehensive characterization were compared with the results reported in the literature to identify discrepancies. Table 1 Summary of characterization results summarizes the values found experimentally. The main differences identified in this study were decomposition temperature and thermal conductivity.

Table 1 Summary of characterization results

PCM	Literature values				Experimental values						
	T_m (ºC)	**ΔH_m (J/g)**	**T_{deg} (ºC)**	**k (W/m·K)**	**T_m (ºC)**	**ΔH_m (J/g)**	**Var (%)**	**T_{onset} (ºC)**	**T_{mid} (ºC)**	**k (W/m·K)**	**Var (%)**
$LiNO_3$-$NaNO_3$-KNO_3 (20-28-52wt.%)	150 [4]	n.a.	n.a.	n.a.	187.03	169.08	-	>400	>400	0.6906	-
$LiNO_3$-$NaNO_3$ (49-51wt.%)	194 [5]	265 [5]	n.a.	n.a.	185.72	107.5	-65.23	>400	>400	0.5608	-
$NaNO_3$–KNO_3	227 [2]	109 [6]	624 [2]	0.24 [6]	225.27	125.27	+14.93	>400	>400	0.8793	+266

(60–40wt.%)											
$LiNO_3$	250 [7]	370 [7]	470 [3]	1.7 [3]	253.83	452.51	+22.30	>400	>400	0.8405	-50.56

Keywords: Phase change materials, thermal energy storage, industrial application

Acknowledgments: *This project was funded by the European Union's Horizon Europe Research and Innovation Programme under grant agreement 101103552 (SUSHEAT). Views and opinions expressed are however those of the author(s) only and do not necessarily reflect those of the European Union or CINEA. Neither the European Union nor the granting authority can be held responsible for them. This work was partially funded by the Ministerio de Ciencia e Innovación - Agencia Estatal de Investigación (AEI) (PID2021-123511OB-C31 - MCIN/AEI/10.13039/501100011033/FEDER, UE), and Ministerio de Ciencia e Innovación - Agencia Estatal de Investigación (AEI) (RED2022-134219-T). The authors would like to thank the Catalan Government for the quality accreditation given to their research group (2021 SGR 01615. GREiA is certified agent TECNIO in the category of technology developers from the Government of Catalonia. S. Ushak acknowledges to ANID/ PUENTE Nº 1523A0006 and ANID/FONDECYT REGULAR Nº 1231721 projects.*

References:

[1] [IEA] - International Energy Agency, IEA Policies database, (n.d.). https://www.iea.org/policies?qs=ger&technology=Appliances&region=Middle East (accessed March 2, 2022).

[2] C. Prieto, A. Lopez-Roman, L.F. Cabeza, Experimental evaluation of the thermal degradation of solar salt under different gas covers, J Energy Storage 72 (2023). https://doi.org/10.1016/j.est.2023.108412.

[3] Y.E. Milián, N. Reinaga, M. Grágeda, S. Ushak, Development of new inorganic shape stabilized phase change materials with LiNO3 and LiCl salts by sol-gel method, J Solgel Sci Technol 94 (2020) 22–33. https://doi.org/10.1007/s10971-019-05090-4.

[4] R.I. Olivares, W. Edwards, LiNO3–NaNO3–KNO3 salt for thermal energy storage: Thermal stability evaluation in different atmospheres, Thermochim Acta 560 (2013) 34–42. https://doi.org/10.1016/j.tca.2013.02.029.

[5] M.M. Kenisarin, High-temperature phase change materials for thermal energy storage, Renewable and Sustainable Energy Reviews 14 (2010) 955–970. https://doi.org/10.1016/j.rser.2009.11.011.

[6] A. Svobodova-Sedlackova, A. Palacios, Z. Jiang, A.I.F. Renna, Y. Ding, H. Navarro, C. Barreneche, Thermal stability and durability of solar salt-based nanofluids in concentrated solar power thermal energy storage: An approach from the effect of diverse metal alloys corrosion, J Energy Storage 75 (2024) 109715. https://doi.org/10.1016/j.est.2023.109715.

[7] G. Alva, L. Liu, X. Huang, G. Fang, Thermal energy storage materials and systems for solar energy applications, Renewable and Sustainable Energy Reviews 68 (2017) 693–706. https://doi.org/10.1016/j.rser.2016.10.021.

IWLiME 2024
11th INTERNATIONAL CONFERENCE IN LITHIUM, INDUSTRIAL MINERALS AND ENERGY
November 27-29, Antofagasta, Chile

Experimental evaluation of nitrate mixtures as PCMs in thermal energy storage for industrial applications

Franklin R. Martinez Alcocer[1,2], Svetlana Ushak[2], Emiliano Borri[1], Saranprabhu Mani Kala[1], Luisa F. Cabeza[1*]
[1]GREiA Research Group, University of Lleida, Pere de Cabrera 3, 25001-Lleida, Spain,
[2]Center for Advanced Research in Lithium and Industrial Minerals, University of Antofagasta, Avenue Universidad de Antofagasta 02800, Antofagasta, Chile
*e-mail: luisaf.cabeza@udl.cat

Introduction

- The EU funded project SUSHEAT aims to develop an efficient heat upgrade system to store thermal energy for intensive factory processing needs.
- The SUSHEAT system is based on two latent heat thermal energy storage (LHTES) tanks using phase change materials in two ranges of temperature: 60-80 ºC and 150-250 ºC
- Nitrates are considered optimal for this aim thanks to their high energy storage density, their good thermal stability and their less corrosiveness
- In this study, three mixtures of nitrates and one single salt were fully characterized by TGA-DSC and hot disk to evaluate them as potential PCMs

DSC and TGA analysis

- Heating/cooling rate: 1K/min
- Sapphire crucibles
- Temperature ranges TGA/DSC: 25 ºC to 400 ºC
- Temperature range DSC: 50 ºC below and above the melting point

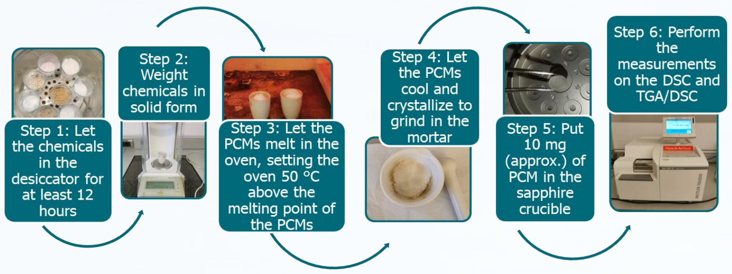

Figure 1. DSC and TGA/DSC measurements procedure

Hot disk analysis

- Sensor Kapton 5506 F2
- Room temperature
- Transient plane source method
- Compact and flat solid block of PCMs

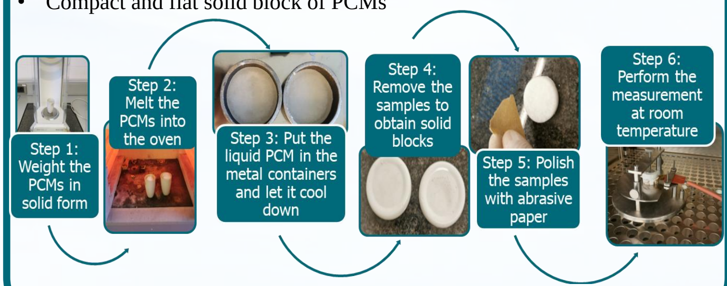

Figure 2. Thermal conductivity measurements procedure

Characterization results

Characterization results are summarized in the following table. The values of enthalpy and melting temperature in DSC are an average of the second and third cycles, because during the first cycle, the initial sample is a powder and is not distributed in the same way as in the subsequent cycles (recrystallised sample), and therefore its behaviour may be a little different.

Summary of characterization results

PCM	Literature values				Experimental values									
					DSC			TGA/DSC					Hot disk	
	T_m (ºC)	ΔH_m (J/g)	T_{deg} (ºC)	k (W/m·K)	T_m (ºC)	ΔH_m (J/g)	Var (%)	T_m (ºC)	ΔH_m (J/g)	Var (%)	T_{onset} (ºC)	T_{mid} (ºC)	k (W/m·K)	Var (%)
$LiNO_3$-$NaNO_3$-KNO_3 (20-28-52wt.%)	150.0 [1]	n.a.	n.a.	n.a.	175.9	103.7	n.a.	187.0	169.1	-	>400.0	>400.0	0.69	-
$LiNO_3$-$NaNO_3$ (49-51wt.%)	194.0 [2]	265.0 [2]	n.a.	n.a.	176.9	66.7	-74.8	185.7	107.5	-65.2	>400.0	>400.0	0.56	-
$NaNO_3$–KNO_3 (60–40wt.%)	227.0 [3]	109.0 [4]	624.0 [3]	0.24 [4]	223.2	85.8	-21.3	225.3	125.3	+14.9	>400.0	>400.0	0.88	+266.0
$LiNO_3$	250.0 [5]	370.0 [5]	470.0 [6]	1.70 [6]	249.6	276.9	-25.2	253.8	452.5	+22.3	>400.0	>400.0	0.84	-50.6

Conclusions

- Experimental TGA-DSC results show that nitrate mixtures have good thermal stability up to 400 ºC (mass loss was not observed)
- The melting enthalpy values obtained with both DSC and TGA/DSC were high, showing that nitrates are a good option to be applied as PCM
- The values of thermal conductivity obtained with the hot disk at room temperature were also good, they are in the range of 0.6 and 0.9 W/m·K

Acknowledgment

This project was funded by the European Union’s Horizon Europe Research and Innovation Programme under grant agreement 101103552 (SUSHEAT). Views and opinions expressed are however those of the author(s) only and do not necessarily reflect those of the European Union or CINEA. Neither the European Union nor the granting authority can be held responsible for them. This work was partially funded by the Ministerio de Ciencia e Innovación - Agencia Estatal de Investigación (AEI) (PID2021-123511OB-C31 - MCIN/AEI/10.13039/501100011033/FEDER, UE), and Ministerio de Ciencia e Innovación - Agencia Estatal de Investigación (AEI) (RED2022-134219-T). The authors would like to thank the Catalan Government for the quality accreditation given to their research group (2021 SGR 01615. GREiA is certified agent TECNIO in the category of technology developers from the Government of Catalonia. S. Ushak acknowledges to ANID/ PUENTE Nº 1523A0006 and ANID/FONDECYT REGULAR Nº 1231721 projects.

Organized by:

Sponsors:

Industrial process Steam Supply – Demonstration of an ultra-dynamic thermal energy storage

Saranprabhu Mani Kala[1], Emiliano Borri[1], Franklin R. Martinez Alcocer[1,2], Cristina Prieto[3,4], Luisa F. Cabeza[1]*

[1]GREiA Research Group, University of Lleida, Pere de Cabrera 3, 25001-Lleida, Spain,
[2]Center for Advanced Research in Lithium and Industrial Minerals, University of Antofagasta, Avenue Universidad de Antofagasta 02800, Antofagasta, Chile
[3]University of Seville, Department of Energy Engineering, Camino de los Descubrimientos s/n, 41092, Seville, Spain
[4]Build to Zero S.L., Camino de los Descubrimientos s/n, 41092, Seville, Spain
**e-mail: luisaf.cabeza@udl.cat*

Heat is the most beneficial form of final energy for producing steam for industrial purposes. Fossil fuels being the main energy sources for the industrial sectors for steam production, also contribute to an increase in CO2 emissions [1]. Furthermore, a shift in energy sources is required in the industrial sector of Europe, as 62% of the heat generated on the continent comes from the burning of fossil fuels [2]. It will be ideal to use renewable energy sources for industrial process steam applications [3] to minimize CO_2 emissions related to the burning of fossil fuels.

A vital technological advancement that made the energy and heat transition possible is the thermal energy storage (TES) technology. Owing to phase change material (PCM) high energy storage density (lower storage mass) [4] and its ability to deliver heat at constant temperature, the latent heat thermal energy storage systems were found to be more favourable among TES systems. However, there is still a lack of technically advanced thermal energy storage systems for high-temperature ranges. This CETparnership project ISSDEMO, aims to develop a modular, highly efficient latent heat thermal energy storage technology for industrial steam production based on molten metal alloy as PCM. As an energy storage medium, a molten metal alloy was chosen because of its superior thermal conductivity over both organic and inorganic PCMs. This storage system employs $ZnAl_6$, a metal alloy PCM with a phase transition enthalpy of 110 kJ/kg [5] and a melting point of 381 ºC, as its energy storage medium [5]. Other potential metal alloy PCMs were also being explored to be used as an energy storage medium. Their thermal properties such as latent heat capacity, specific heat and thermal conductivity were evaluated via a differential scanning calorimeter (DSC) and hot disk (thermal conductivity). In the project, a demo scale TES will be developed, and tests will be performed to assess its charging, discharging behaviour and efficiency. The system will be operated for at least 300 cycles and its performance will be evaluated to speed up the independence from fossil fuel in industrial process steam applications.

Keywords: Thermal energy storage**,** Phase change materials, Metal alloy, Process steam

Acknowledgments: *This research was funded by CETPartnership, the Clean Energy Transition Partnership is a transnational joint programming initiative to boost and accelerate the energy transition, building upon regional and national RDI funding programmes. The initiative is* *receiving funding from the European Union's research and innovation programme "Horizon Europe" under grant agreement No 101069750. This study receives funding from the Ministerio de Ciencia e Innovación - Agencia Estatal de Investigación (MCIN/AEI/10.13039/501100011033) through the PCI2023-145964-2 project and the European Union "NextGenerationEU"/PRTR. This work was also partially funded by Ministerio de Ciencia e Innovación - Agencia Estatal de Investigación (AEI) (PID2021-123511OB-C31 - MCIN/AEI/10.13039/501100011033/FEDER, UE), and by Ministerio de Ciencia e Innovación - Agencia Estatal de Investigación (AEI) (RED2022-134219-T). Also, this work is partially supported by ICREA under the ICREA Academia programme. The authors would like to thank the Departament de Recerca i Universitats of the Catalan Government for the quality accreditation given to their research group (2021 SGR 01615). GREiA is certified agent TECNIO in the category of technology developers from the Government of Catalonia*

References:

[1] L.J.R. Nunes, The Rising Threat of Atmospheric CO2: A Review on the Causes, Impacts, and Mitigation Strategies, *Environments* 10 (2023). https://doi.org/10.3390/environments10040066.

[2] EU energy in figures – Statistical pocketbook 2022, *Publications Office of the European Union*, 2022.

[3] R.-H. Hechelmann, J.-P. Seevers, A. Otte, J. Sponer, M. Stark, Renewable Energy Integration for Steam Supply of Industrial Processes—A Food Processing Case Study, *Energies (Basel)* 13 (2020) https://doi.org/10.3390/en13102532.

[4] C. Suresh, R.P. Saini, Thermal performance of sensible and latent heat thermal energy storage systems, *Int J Energy Res* 44 (2020) https://doi.org/10.1002/er.5255.

[5] S. Heim, L. Komogowski, Analysis of Technology Potential of a Metal-based Latent Heat Storage for Backup Process Steam Supply, *Chemie Ingenieur Technik* 93 (2021) https://doi.org/10.1002/cite.202000169.

11th INTERNATIONAL CONFERENCE IN LITHIUM, INDUSTRIAL MINERALS AND ENERGY

IWLiME 2024

November 27-29, Antofagasta, Chile

Industrial process Steam Supply – Demonstration of an ultra-dynamic thermal energy storage

Saranprabhu Mani Kala[1], Emiliano Borri[1], Franklin R. Martinez Alcocer[1,2], Cristina Prieto[3,4], Luisa F. Cabeza[1]*

[1]GREiA Research Group, University of Lleida, Pere de Cabrera 3, 25001-Lleida, Spain,
[2]Center for Advanced Research in Lithium and Industrial Minerals, University of Antofagasta, Avenue Universidad de Antofagasta 02800, Antofagasta, Chile
[3]University of Seville, Department of Energy Engineering, Camino de los Descubrimientos s/n, 41092, Seville, Spain
[4]Build to Zero S.L., Camino de los Descubrimientos s/n, 41092, Seville, Spain
**e-mail: luisaf.cabeza@udl.cat*

Universitat de Lleida

research group GREiA

Introduction

- By 2020, 62% of the total heat generation in Europe was generated from fossil fuels and so a heat transition in Europe industry is needed.
- Energy storage is an important technology needed to make a heat transition and an energy transition, possible.
- CETparnership funded project ISSDEMO, aims to develop a modular, highly efficient latent heat thermal energy storage technology for industrial steam production based on molten metal alloy as PCM
- In the developed concept, molten metal alloy was chosen because of its superior thermal conductivity over both organic and inorganic PCMs

Objectives of ISSDEMO

- To demonstrate the efficiency and functionality of a thermal energy storage system for high-temperature applications (250 °C – 500 °C) and the production of process steam for various industrial applications.
- To implement and demonstrate the technology in an industrial process steam application with a capacity of about 1 MWh.

Energy consumption of Europe

2018

- Industry sector: 3,100 TWh
- Chemical and petrochemical industry: 611 TWh
- Paper, pulp and printing sector: 393 TWh
- Food and beverages and tobacco sector: 354 TWh

2020

- 62% of heat generation from fossil fuels

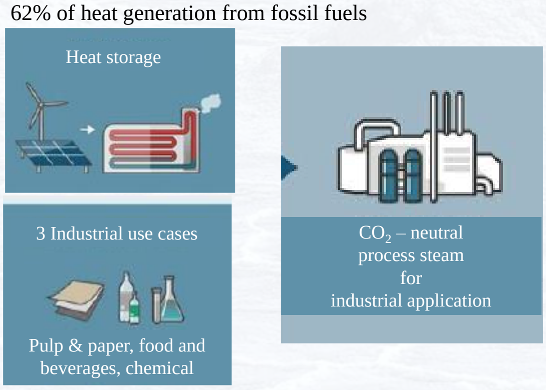

Potential PCMs

Metal alloy	Melting temperature (°C)	Enthalpy (kJ/kg)	Thermal conductivity (W/m·K)
PbSb11.1	252	40	34
ZnMg46.3	340	122	141
ZnAl6	381	110	140
AlMg35.8	450	383	210
AlCu33	548	339	286

Expected outcomes

- Development and demonstration of a new, innovative high-temperature storage technology in an industrial application.
- Optimizing efficient charging strategies and technologies or investigating the interaction with other technologies for heat or steam generation such as heat pumps or biomass boilers.
- The technology can have significant impact on the CO_2 reduction of the focused industries.

Acknowledgment

This research was funded by CETPartnership, the Clean Energy Transition Partnership is a transnational joint programming initiative to boost and accelerate the energy transition, building upon regional and national RDI funding programmes. The initiative is receiving funding from the European Union's research and innovation programme "Horizon Europe" under grant agreement No 101069750. This study receives funding from the Ministerio de Ciencia e Innovación - Agencia Estatal de Investigación (MCIN/AEI/10.13039/501100011033) through the PCI2023-145964-2 project and the European Union "NextGenerationEU"/PRTR. This work was also partially funded by Ministerio de Ciencia e Innovación - Agencia Estatal de Investigación (AEI) (PID2021-123511OB-C31 - MCIN/AEI/10.13039/501100011033/FEDER, UE), and by Ministerio de Ciencia e Innovación - Agencia Estatal de Investigación (AEI) (RED2022-134219-T). Also, this work is partially supported by ICREA under the ICREA Academia programme. The authors would like to thank the Departament de Recerca i Universitats of the Catalan Government for the quality accreditation given to their research group (2021 SGR 01615). GREiA is certified agent TECNIO in the category of technology developers from the Government of Catalonia

Organized by:

Sponsors:

Cellular Automaton Model for Corrosion Simulation and Oxide Ion Influence in Thermal Storage Systems with Molten Salts

Juan C. Reinoso-Burrows [1]*, Marcelo Cortés Carmona [1], Carlos Durán Mora [1], Carlos Soto Soto [1], Felipe Galleguillos Madrid [1], Mauro Henríquez [2]

[1] Centro de Desarrollo Energético de Antofagasta, Universidad de Antofagasta, Av. Universidad de Antofagasta 02800, Antofagasta 1271155, Chile.

[2] Centro Ibérico de Investigación en Almacenamiento de Energía, Polígono 13, Parcela 31, "El Cuartillo",10004 Cáceres, España.

*Correspondence: Juan C. Reinoso-Burrows, juan.reinoso.burrows@ua.cl

1. Instroduction

The constant increase in demand for electrical energy and environmental care has driven the development of sustainable solutions. Concentrated Solar Power (CSP) plants with Thermal Energy Storage (TES) systems are a promising alternative. However, thermal energy storage at high temperatures poses a significant challenge, such as corrosion of materials used mainly in TES systems [1].

Although there are techniques for studying corrosion, they are often limited in their capabilities, extensive in time, and economically resource intensive [2]. In this context, mathematical and computational models emerge as a solution to this problem. The Cellular Automaton (CA) model appears as a solution that allows estimating and predicting the degree of corrosion of steels used in CSP plants [3]. Cellular automata simulate corrosion behavior at the mesoscopic scale, capturing intricate interactions between electrochemical reactions, materials, and environmental factors [4],[5].

2. Procedure

The CA developed in this study simulated the corrosion process of a 347H steel exposed to solar salt (60% $NaNO_3$ and 40% KNO_3) melted at 400°C. Experimental tests were conducted at the molten salt thermal storage pilot plant at the University of Antofagasta, which has a 1m3 capacity tank.

Corrosion rate was calculated using gravimetry at 500h and 1000h of exposure, and complementary tests (SEM and DRX) were conducted to obtain the morphology of the cross-section and corrosion products, respectively.

2. Results

Existing results shown in Fig 1 indicate that the computational algorithm projects the growth of a corrosion layer over time, estimating corrosion rates and corrosion products generated at times longer than those normally studied experimentally, projecting the moment when the steel is completely corroded.

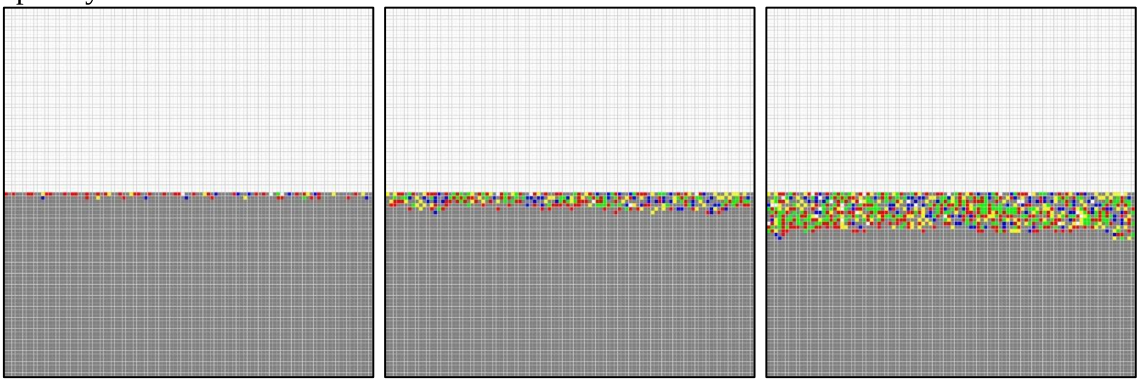

Fig 1: Screenshot capture of the evolution over time of the corrosion layer using the CA model.

Acknowledgement

The authors would like to acknowledge the financial support provided by CONICYT / FONDAP 1523A0006 "Solar Energy Research Center" SERC-Chile, FIC-R 30413089 – 30488809 funded by Antofagasta Government. Engineering Project 2030 Code 16ENl2-71940 of Corfo. VIU21P0051 Project National Research and Development Agency, Government of Chile. PhD Program in Solar Energy, University of Antofagasta.

References

[1] M. Walczak, F. Pineda, Á. G. Fernández, C. Mata-torres, and R. A. Escobar, "Materials corrosion for thermal energy storage systems in concentrated solar power plants," *Renew. Sustain. Energy Rev.*, vol. 86, no. January, pp. 22–44, 2018, doi: 10.1016/j.rser.2018.01.010.

[2] V. Encinas-Sánchez, M. T. de Miguel, M. I. Lasanta, G. García-Martín, and F. J. Pérez, "Electrochemical impedance spectroscopy (EIS): An efficient technique for monitoring corrosion processes in molten salt environments in CSP applications," *Sol. Energy Mater. Sol. Cells*, vol. 191, no. November 2018, pp. 157–163, 2019, doi: 10.1016/j.solmat.2018.11.007.

[3] B. Chopard and M. Droz, *Cellular Automata Modeling of Physical Systems*. Cambridge: Cambridge University Press, 1998.

[4] W. Wang, B. Guan, X. Wei, J. Lu, and J. Ding, "Cellular automata simulation on the corrosion behavior of Ni-base alloy in chloride molten salt," *Sol. Energy Mater. Sol. Cells*, vol. 203, no. September, p. 110170, 2019, doi: 10.1016/j.solmat.2019.110170.

[5] Z. Xu, X. Wei, J. Lu, J. Ding, and W. Wang, "Simulation of corrosion behavior of Fe–Cr–Ni alloy in binary NaCl–CaCl2 molten salt using a cellular automata method," *Sol. Energy Mater. Sol. Cells*, vol. 231, no. February, p. 111301, 2021, doi: 10.1016/j.solmat.2021.111301.

2024 IWLiME
11th INTERNATIONAL CONFERENCE IN LITHIUM, INDUSTRIAL MINERALS AND ENERGY
November 27-29, Antofagasta, Chile

Cellular Automaton Model for Corrosion Simulation and Oxide Ion Influence in Thermal Storage Systems with Molten Salts

Juan C. Reinoso-Burrows[1*], Marcelo Cortés Carmona[1], Carlos Durán Mora[1], Carlos Soto Soto[1], Felipe Galleguillos Madrid[1], Mauro Henríquez Heimpeller[2]

[1]Centro de Desarrollo Energético de Antofagasta, Universidad de Antofagasta, Av. Universidad de Antofagasta 02800, Antofagasta 1271155, Chile.
[2]CenCentro Ibérico de Investigación en Almacenamiento de Energía, Polígono 13, Parcela 31, "El Cuartillo",10004 Cáceres, España.
* Correspondence: Juan C. Reinoso-Burrows, juan.reinoso.burrows@ua.cl

INTRODUCTION

Thermal Energy Storage (TES) systems face challenges like material corrosion, but the Cellular Automaton (CA) model offers a solution by simulating corrosion behavior of steels used in CSP plants at the mesoscopic scale, capturing key interactions between electrochemical reactions and environmental factors [1]-[5].

BACKGROUND

The CA model consists of a grid of cells, each with a defined local state. The cells evolve over time based on rules that depend on the states of their neighboring cells. These simple rules allow for the simulation of complex system behaviors [6], [7].

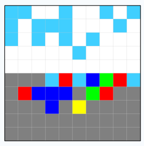

Fig. 1: Cellular automaton lattice.

PROCEDURE

The corrosion study was conducted at the molten salts pilot plant of the University of Antofagasta. A 347H stainless steel sample was exposed to 60% $NaNO_3$ + 40% KNO_3 at 400°C for durations ranging from 168h to 1635h. SEM/EDS analyses were performed on the 168h sample to validate the model. The model was adjusted based on the 168h EDS results.

Fig. 2: Procedure for placing and removing samples in a pilot plant.

SIMULATED CORROSION MECHANISM

The corrosion mechanism to be simulated is given by the dissociation of nitrate, $NaNO_3$, into Na^+ and NO_3^-. The nitrate dissociates into O^{2-} and NO^{2-}. The O^{2-} generates reactions *i.* to *iv.*, which are considered in the model. The model does not take into account intermediate reactions and focuses on long-term behavior [8], [9].

i. $3Fe + 4O^{2-} \leftrightarrow Fe_3O_4$

ii. $2Fe_3O_4 + O^{2-} \leftrightarrow 3Fe_2O_3$

iii. $2Cr + 3O^{2-} \leftrightarrow Cr_2O_3$

iv. $Ni + O^{2-} \leftrightarrow NiO$

RESULTS

The results shown in Fig. 3 and Fig. 4 indicate that the 2D cellular automaton model, implemented through a computational algorithm, projects the growth of a corrosion layer on AISI 347H steel exposed to solar salt at 400°C over time. The algorithm estimates both the corrosion rates and the products generated at different stages of the process. After 60.000 steps, the model predicted a corrosion layer with a depth of 4.25 µm, with a mean squared error of 2% compared to experimental data obtained via SEM/EDS. Furthermore, this computational approach projects the corrosion of the steel over longer periods than can typically be studied experimentally, allowing the prediction of when the steel will be completely corroded. These results suggest that the simulation is an effective tool for predicting the steel's lifespan in thermal energy storage systems in CSP plants, forecasting long-term degradation under extreme operational conditions.

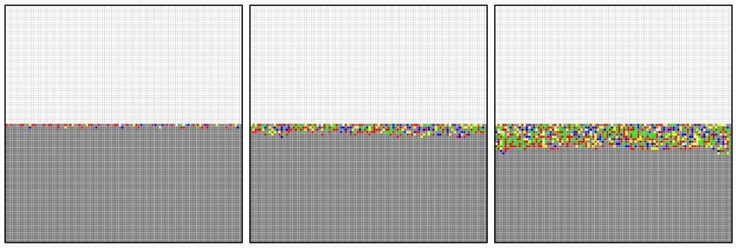

Fig. 3: Corrosion layer growth at 10,000, 30,000 and 60,000 steps.

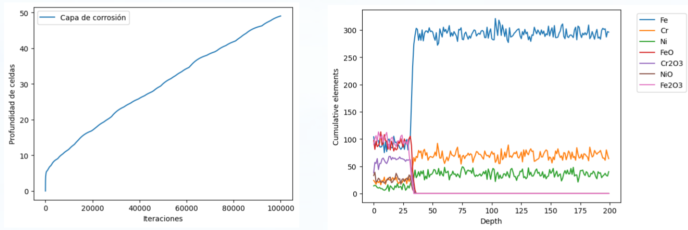

Fig. 4: Corrosion layer growth and product formation at 60,000 steps.

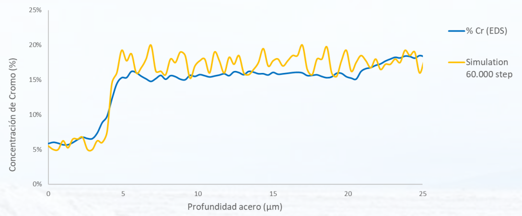

Fig. 5: Simulated chromium vs EDS chromium

CONCLUSION

The adjusted cellular automaton model could help estimate long-term corrosion behavior, overcoming the limitations of short-term experimental studies. This could allow the projection of failure points in AISI 347H steel and optimization of maintenance in CSP plants. The model could be an effective tool for predicting corrosion and steel lifespan in thermal storage systems, improving planning and failure prevention under extreme operational conditions.

ACKNOWLEDGEMENTS

The authors would like to acknowledge the financial support provided by CONICYT / FONDAP 1523A0006 "Solar Energy Research Center" SERC-Chile, FIC-R 30413089 – 30488809 funded by Antofagasta Government. Engineering Project 2030 Code 16ENI2-71940 of Corfo. VIU21P0051 Project National Research and Development Agency, Government of Chile. Doctoral Program in Solar Energy Universidad de Antofagasta, Chile.

REFERENCES

[1] M. Walczak, F. Pineda, Á. G. Fernández, C. Mata-torres, and R. A. Escobar, "Materials corrosion for thermal energy storage systems in concentrated solar power plants," Renew. Sustain. Energy Rev., vol. 86, no. January, pp. 22–44, 2018, doi: 10.1016/j.rser.2018.01.010.
[2] V. Encinas-Sánchez, M. T. de Miguel, M. I. Lasanta, G. García-Martín, and F. J. Pérez, "Electrochemical impedance spectroscopy (EIS): An efficient technique for monitoring corrosion processes in molten salt environments in CSP applications," Sol. Energy Mater. Sol. Cells, vol. 191, no. November 2018, pp. 157–163, 2019, doi: 10.1016/j.solmat.2018.11.007.
[3] B. Chopard and M. Droz, Cellular Automata Modeling of Physical Systems. Cambridge: Cambridge University Press, 1998.
[4] W. Wang, B. Guan, X. Wei, J. Lu, and J. Ding, "Cellular automata simulation on the corrosion behavior of Ni-base alloy in chloride molten salt," Sol. Energy Mater. Sol. Cells, vol. 203, no. September, p. 110170, 2019, doi: 10.1016/j.solmat.2019.110170.
[5] Z. Xu, X. Wei, J. Lu, J. Ding, and W. Wang, "Simulation of corrosion behavior of Fe–Cr–Ni alloy in binary NaCl–CaCl2 molten salt using a cellular automata method," Sol. Energy Mater. Sol. Cells, vol. 231, no. February, p. 111301, 2021, doi: 10.1016/j.solmat.2021.111301.
[6] J. T. Schwartz, J. von Neumann, and A. W. Burks, "Theory of Self-Reproducing Automata," Mathematics of Computation, vol. 21, no. 100. p. 745, 1967.
[7] B. Chopard and M. Droz, Cellular Automata Modeling of Physical Systems. Cambridge: Cambridge University Press, 1998.
[8] A. S. Dorcheh, R. N. Durham, and M. C. Galetz, "High temperature corrosion in molten solar salt: The role of chloride impurities," Mater. Corros., vol. 68, no. 9, pp. 943–951, 2017.
[9] S. Bell, T. Steinberg, and G. Will, "Corrosion mechanisms in molten salt thermal energy storage for concentrating solar power," Renew. Sustain. Energy Rev., vol. 114, no. November 2018, p. 109328, 2019

Study and Evaluation of the Thermal Behavior in the Synthesis of the Cathode Material Na_xMnO_2 by the Solid-State Method

Heidy Huanca R.[1,2,3], Edgar Bautista Q.[1], Boris Parraga A.[3]

[1]*Cathode Materials Pilot Plant, Yacimientos de Litio Bolivianos, La Palca - Potosí, Bolivia*

[2]*Chemical Engineering Career, Faculty of Engineering, Universidad Mayor de San Andrés, La Paz, Bolivia*

[3]*Institute for Research and Development of Chemical Processes (IIDEPROQ), Universidad Mayor de San Andrés, La Paz, Bolivia.*

Sodium-based cathode materials have emerged as intercalation materials for energy storage systems since the 1970s[1]. Although lithium-based materials achieved commercial maturity due to their higher volumetric energy density, the need for more abundant and cost-effective alternatives has renewed interest in sodium-based materials[2]. Unlike lithium compounds, sodium materials exhibit different crystalline structures, including layered structures of particular interest. Sodium manganese oxide, Na_xMnO_2, displays various crystalline phases depending on the value of x, such as monoclinic, orthorhombic, hexagonal and trigonal [3]. In this study, thermogravimetric analysis and differential scanning calorimetry (TGA-DSC) are employed to monitor the thermal changes during the synthesis of Na_xMnO_2 using Na_2CO_3 and $MnCO_3$ as precursors [4],[5]. In a first stage, TGA curves for both precursors were obtained separately as shown in Figure 1.

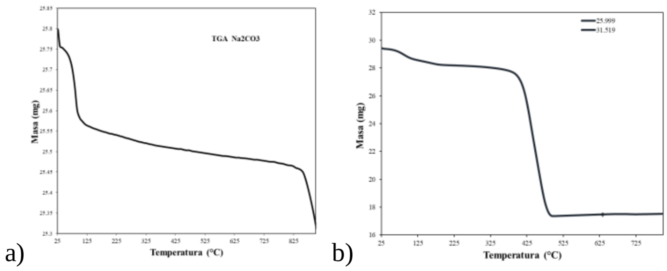

Figure 1. Sodium carbonate decomposition and Manganese carbonate decomposition TGA results. ; this study a) Sodium carbonate decomposition, T = 900°C at 5°C/min; b) Manganese carbonate decomposition, T = 800°C 5°C/min, into a nitrogen environment.

In Figure 2, the TGA curve for the synthesis of Na_xMnO_2 is shown aiming to provide insights into the thermal behavior of this material during synthesis at different molar relation and decomposition rates, shown in Table 1, revealing a deeper understanding of its formation and subsequent stages of material characterization.

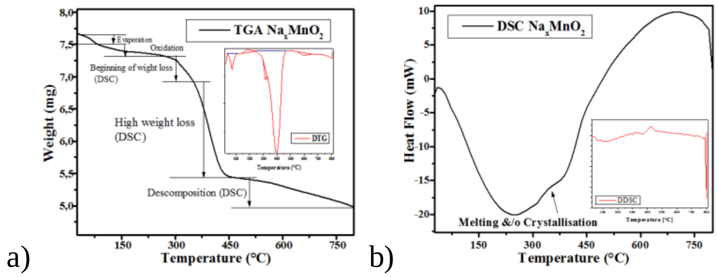

Figure 2. Sodium Manganese oxides, dinamic decomposition at T = 800°C and 5°C/min ; a), TGA – DTG loss weight b) DSC – DDSC curve decomposition

Table 1 Parameters in Different TGA analyses

Code	Na:Mn	T°C	Rate °C/min
003	1:1	800°C	5°C
005	1:1	800°C	15°C
006	1:1	800°C	30°C
007	0,33:1	800°C	5°C
008	0,66:1	800°C	5°C

Additionally, the study will include the electrochemical characterization of the material and the evaluation of particle morphology through scanning electron microscopy (SEM) and the characterization of crystal structures through X-ray diffraction (XRD).

Keywords: Sodium Manganese oxide, Solid-State Synthesis, TGA.

Acknowledgments: *Thanks to Yacimientos de Litio Bolivianos for their support in carrying out this project.*

References:

[1] C. Delmas, D. Carlier, y M. Guignard, «The Layered Oxides in Lithium and Sodium-Ion Batteries: A Solid-State Chemistry Approach», *Adv. Energy Mater.*, vol. 11, n.º 2, p. 2001201, 2021, doi: 10.1002/aenm.202001201.
[2] P.-F. Wang, Y. You, Y.-X. Yin, y Y.-G. Guo, «Layered Oxide Cathodes for Sodium-Ion Batteries: Phase Transition, Air Stability, and Performance», *Adv. Energy Mater.*, vol. 8, n.º 8, p. 1701912, mar. 2018, doi: 10.1002/aenm.201701912.
[3] Tianyuan Ma, «Manganese based layered oxides as cathode material for sodium-ion batteries», 2017, Acceded on June: 30th 2024. [on line]. Available in: https://urresearch.rochester.edu/institutionalPublicationPublicView.action?institutionalItemId=32883
[4] L. Biernacki y S. Pokrzywnicki, «The Thermal Decomposition of Manganese Carbonate Thermogravimetry and Exoemission of Electrons», *J. Therm. Anal. Calorim.*, vol. 55, n.º 1, pp. 227-232, ene. 1999, doi: 10.1023/A:1010165029080.
[5] J.-W. Kim y H.-G. Lee, «Thermal and carbothermic decomposition of Na2CO3 and Li2CO3», *Metall. Mater. Trans. B*, vol. 32, n.º 1, pp. 17-24, feb. 2001, doi: 10.1007/s11663-001-0003-0.

11th INTERNATIONAL CONFERENCE IN LITHIUM, INDUSTRIAL MINERALS AND ENERGY

IWLiME 2024

November 27-29, Antofagasta, Chile

Study and Evaluation of the Thermal Behavior in the Synthesis of the Cathode Material NaxMnO2 by the Solid-State Method

Heidy J. Huanca R.[1,2] , Boris Parraga A [2].

[1]Chemical Engineering Career, Faculty of Engineering, Universidad Mayor de San Andrés, La Paz, Bolivia
[2]Institude for Research and Development of Chemical Processes (IIDEPROQ), Universidad Mayor de San Andrés, La Paz, Bolivia.

1 Introduction

Sodium-based cathode materials have emerged as intercalation materials for energy storage systems since the 1970s [1]. Sodium manganese oxide, Na_xMnO_2, exhibits various crystalline phases depending on the x value, such as monoclinic, orthorhombic, hexagonal, and trigonal in two environments [3]. In this study, thermogravimetric analysis and differential scanning calorimetry (TGA-DSC) are used to monitor thermal changes during the synthesis of Na_xMnO_2 from Na_2CO_3 and $MnCO_3$ precursors [4],[5], and their decomposition (Figure 1a). The analysis reveals key processes such as manganese carbonate oxidation and Na_xMnO_2 formation. This research aims to provide insights into the thermal behavior of Na_xMnO_2 during synthesis at different molar ratios and decomposition rates, offering a deeper understanding of its formation and subsequent material characterization stages.

2 Methology

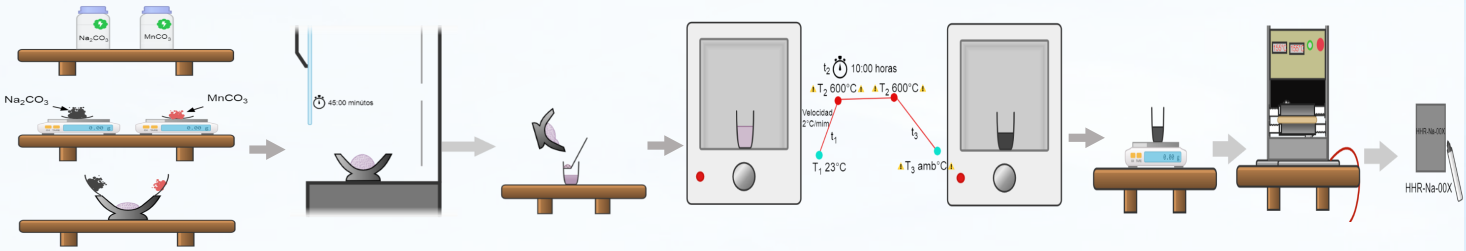

3 Results and Analysis

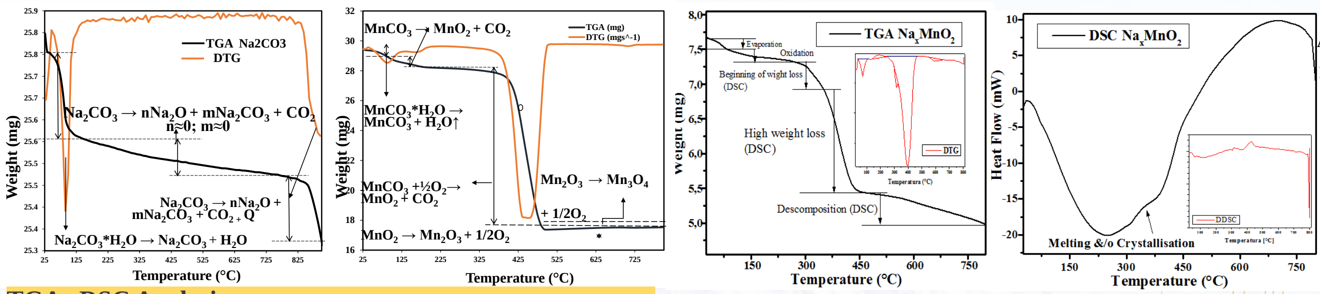

Figure 1: Thermic Analysis of a) Na_2CO_3, b) $MnCO_3$, c) TGA of Na_xMnO_2 and d) DSC of Na_xMnO_2

TGA –DSC Analysis

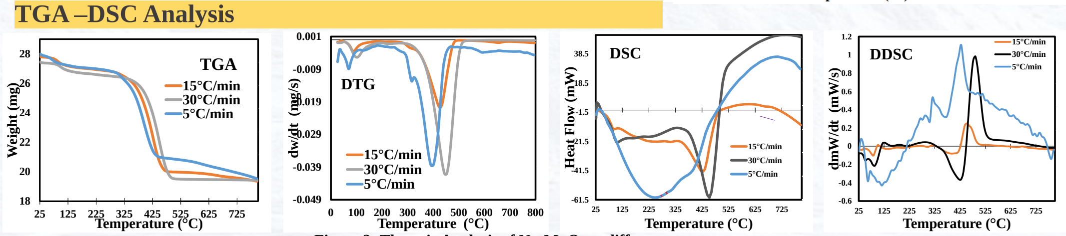

Figure 2: Thermal Analysis of Na_xMnO_2 to different rates

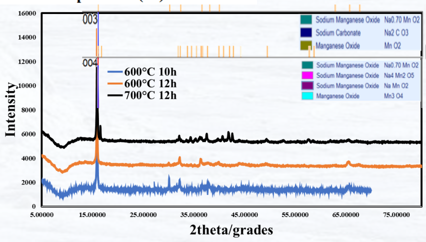

Figure 3: X-Ray Diffraction at different temperatures of calcination

Characterization

The precursors and the resulting mixture were analyzed by simultaneous thermogravimetric analysis and differential scanning calorimetry (TGA-DSC 3+, Mettler Toledo) in a nitrogen atmosphere. The crystalline structure of Na_xMnO_2 was characterized by X-ray diffraction (XRD, BRUKER D8 ADVANCE and RIGAKU), while the microstructure and morphology were examined by scanning electron microscopy (SEM, TESCAN Vega 3XMU) with a gold coating to prevent electrostatic charging.

	Theoric	Real	
	$NaMnO_2$	Na_xMnO_2	x
001	15,00g	17,60	0,87
002	15,00g	17,50g	0,89
003	6,21g	7,90g	0,8
004	6,83g	7,50g	0,96
009	20g	20,5g	0,99

Table 1: Correct value of x

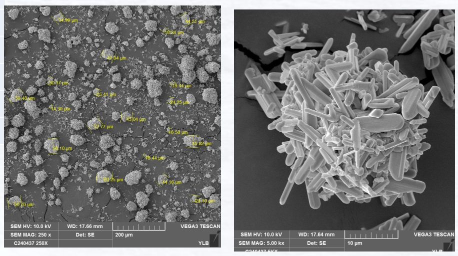

Figure 4: Scanning Electron Microscopy SEM at 900°C of calcination

4 Conclusions

The increase in heat flow revealed a formation process starting at 270 °C, followed by a melting phase. During this process, thermal events such as the conversion of manganese carbonate to MnO_2 and its subsequent reduction to Mn_2O_3 were observed. Although the formation of Na_xMnO_2 is barely noticeable in the DSC analysis due to the solid-state nature of the reaction, the changes are more evident in the DTG and DDSC derivatives, which allow for precise identification of the thermal peaks associated with the sample transformations.

Acknowledgments

Thank the National Strategic Public Company of Lithium Deposits of Bolivia (YLB) for their support and Dr. Edgar Bautista to carry out this project.

References:

[1] C. Delmas et al., "The Layered Oxides in Lithium and Sodium-Ion Batteries," *Adv. Energy Mater.*, vol. 11, no. 2, p. 2001201, 2021.
[2] P.-F. Wang et al., "Layered Oxide Cathodes for Sodium-Ion Batteries," *Adv. Energy Mater.*, vol. 8, no. 8, p. 1701912, 2018.
[3] T. Ma, "Manganese Based Layered Oxides as Cathode Material for Sodium-Ion Batteries," University of Rochester, 2017. Available at: https://urresearch.rochester.edu.
[4] L. Biernacki y S. Pokrzywnicki, "Thermal Decomposition of Manganese Carbonate," *J. Therm. Anal. Calorim.*, vol. 55, no. 1, pp. 227-232, 1999.
[5] J.-W. Kim y H.-G. Lee, "Thermal and Carbothermic Decomposition of Na2CO3 and Li2CO3," *Metall. Mater. Trans. B*, vol. 32, no. 1, pp. 17-24, 2001.

Assessment of Dust Deposition Effects on Photovoltaic Modules Using an Accelerated Soiling Chamber Simulating Atacama Desert Environmental Conditions

J. Montoya[1], J. Rakotoniaina[4], A. Marzo[2,3], L. Conde[2], J. Aimé[4], E. Pilat[4], V. Del Campo[2,5], E. Fuentealba[1,2], And D. Olivares[1,2]

[1]*Centro de Desarrollo Energético Antofagasta (CDEA), Universidad de Antofagasta, Avenue Universidad de Antofagasta 02800, Antofagasta, Chile.*
[2]*Solar Energy Research Center, Universidad de Chile, Tupper 2007, 8370451 Santiago, Chile.*
[3]*Departamento de Óptica, Universidad de Granada, Spain.*
[4] *CEA-INES, LSPV (Systems Laboratory), France*
[5] *Departamento de Física, Universidad Técnica Federico Santa María, España 1680, Valparaíso, Chile*

Dust accumulation on photovoltaic (PV) modules poses a significant challenge for operation and maintenance, particularly in arid environments such as the Atacama Desert. This phenomenon reduces the amount of light reaching the solar cells, thereby affecting current generation and overall performance (Bessa et al., 2021). Additionally, dust alters the optical properties of the module by increasing reflectance and light scattering, which in turn elevates operation and maintenance costs. In response to this issue, soiling chambers emerge as a viable option for conducting accelerated soiling studies, allowing researchers to save time when investigating phenomena that typically require extended periods to observe.

To evaluate the impact of dust on the performance of PV modules, soil samples from the Atacama Desert, recognized for their cementation capacity, were employed in combination with an accelerated soiling chamber (Figure 1.a). Two types of experiments were designed and conducted. The first corresponds to the electrical analysis, where electrical losses due to soiling were evaluated using a reference cell to measure the IV curves with a solar simulator. From these curves, the short-circuit current was extracted as the main indicator of the PV module's performance. The second corresponds to the analysis of optical properties, in which transmittance was examined using a spectrophotometer. The accelerated soiling chamber was configured to replicate a complete day-night cycle, promoting dust cementation on the PV modules. The process was developed in three sequential stages: dust deposition, moisture condensation (camanchaca), and finally cementation. These three conditions were applied sequentially to the samples.

In Figure 1(b), the short-circuit current (Isc) measurements are presented. The graph exhibits a decreasing trend, indicating that as the dust density on the module surface increases, the short-circuit current decreases. An average reduction of 5% is observed compared to the clean reference cell with each deposition, while the dust density increases to 1.2 mg/cm². In the optical tests, decreases in transmittance and increases in diffuse and specular reflectance were observed in the spectral ranges of 350 to 1200 nm, with average transmittance losses of up to 50% in samples with the highest dust density, as shown in Figure 1(c). Additionally, an increase in diffuse reflectance of 17% and in specular reflectance of 23% was observed. This study also encompasses Scanning Electron Microscopy (SEM) and reflectance analysis to comprehensively characterize dust deposition on photovoltaic (PV) modules. SEM was employed to investigate the morphology and distribution of dust particles on the module surfaces, providing detailed insights into the cementation process. These analyses were not included in this instance as this is a summary, but they are planned for the final version.

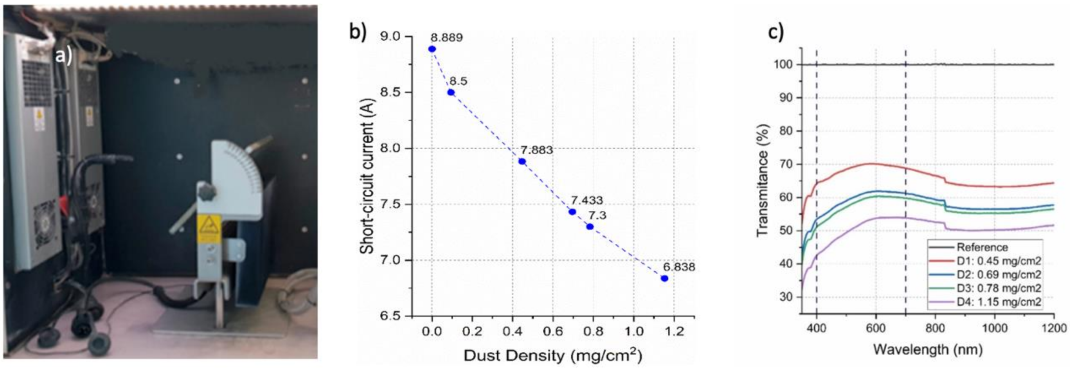

Figure 1. **a)** Soiling chamber, **b)** Short-circuit current losses relative to dust density, **c)** Transmittance losses with respect to increasing dust density in each deposition.

The results indicate that the methodology employed with the soiling chamber successfully replicates the characteristic environmental conditions of the Atacama Desert, thereby facilitating the cementation process in a controlled environment. Compared to previous studies conducted under outdoor conditions, the observed relationship between dust density and transmittance reduction demonstrates high concordance (Olivares et al., 2021), suggesting that the methodology enables effective simulation of soiling behavior under natural conditions. This tool facilitates the acceleration of studies in controlled settings, optimizing the time required to obtain results and contributing to enhanced performance analysis of solar technologies deployed in desert regions.

Keywords: *Soiling in PV modules; Accelerated soiling chamber; Dust impact on photovoltaic technologies; Atacama Desert; Dust deposition.*

Acknowledgments:
The authors express gratitude to the projects:
-ANID/FONDAP/1523A00006 "Solar Energy Research Center"- SERC-Chile and the project ATAMOSTEC with the contract no. 17PTECES-75830.
-ECOS-ANID "Graphene as transparent current spreading electrode in silicon heterojunction solar cells" #ECOS210038.

References:
Bessa, J.G., Micheli, L., Almonacid, F., Fern´andez, E.F., 2021. Monitoring photovoltaic soiling: assessment, challenges, and perspectives of current and potential strategies. iScience 24. https://doi.org/10.1016/j.isci.2021.102165.
Olivares, D., Ferrada, E., Escobar, R., Soto, C., Pino, A., y Cortés, A., 2021. Characterization of Changes in the Soiling Properties and Deposition Rates Because of Groundworks Near a PV Plant in the Atacama Desert. *ISES Conference Proceedings*.

2024 IWLiME

11th INTERNATIONAL CONFERENCE IN LITHIUM, INDUSTRIAL MINERALS AND ENERGY

November 27-29, Antofagasta, Chile

Assessment of Dust Deposition Effects on Photovoltaic Modules Using an Accelerated Soiling Chamber Simulating Atacama Desert Environmental Conditions

J. Montoya[1], J. P Rakotoniaina[4], A. Marzo[2,3], L. Conde[2], J. Aimé [4], E. Pilat[4], I. Tsanakas[4], V. Del Campo[2,5], E. Fuentealba[1,2] And D. Olivares [1,2]

[1] Centro de Desarrollo Energético Antofagasta (CDEA), Universidad de Antofagasta, Avenue Universidad de Antofagasta 02800, Antofagasta, Chile.
[2]Solar Energy Research Center, Universidad de Chile, Tupper 2007, 8370451 Santiago, Chile.
[3]Departamento de Óptica, Universidad de Granada, Spain.
[4] CEA, Liten, Campus INES, 73375 Le Bourget du Lac, France
[5]Departamento de Física, Universidad Técnica Federico Santa María, España 1680, Valparaiso, Chile

INTRODUCTION

The phenomenon of soiling represents a challenge in the maintenance of photovoltaic plants, especially in desert regions. The accumulation of dust on photovoltaic modules reduces the incident light, affecting their optical properties, decreasing energy generation, causing economic losses, and, in some cases, compromising the profitability of these installations (Bessa et al., 2021). Due to the difficulty of evaluating these effects in outdoor studies, which require long periods to observe soiling effects, response times are limited. To address this issue, soiling chambers are proposed as a viable solution for conducting accelerated soiling studies. This paper describes the use of a soiling chamber to simulate the dust deposition characteristic of the Atacama Desert, with emphasis on the evaluation of optical and electrical losses associated with soiling.

MATERIALS AND METHOD

This study focuses on evaluating the effect of an accelerated soiling chamber under indoor conditions, simulating the environmental characteristics of the Atacama Desert. Soil samples from this desert, known for their cementation capacity, with a particle size of 38 microns, were used to replicate soiling conditions.

The soiling chamber was configured to replicate a complete day-night cycle in a controlled environment, promoting the cementation of dust on photovoltaic modules. This indoor process was developed in three sequential stages: (1) dust deposition (Figure 2.b), (2) simulated humidity condensation (Figure 2.c), and (3) final cementation (Figure 2.d). These conditions were sequentially applied to the samples, allowing for the analysis of accelerated soiling effects under strict control in a laboratory environment.

Two main experiments were conducted. The first experiment focused on analyzing the optical properties of the glass, specifically transmittance (%), measured with a spectrophotometer. The second was an electrical analysis designed to evaluate the efficiency losses caused by soiling. A reference cell was used to measure IV curves using a solar simulator.

***Figure 1.** CEA-INES Soiling chamber replicating the Atacama Desert conditions*

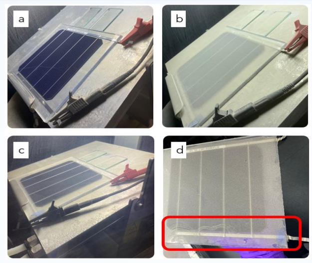

***Figure 2.** a) Samples in normal condicions. b) Samples with dust deposition. c) Samples with moisture condensation. d) Samples with cementation.*

RESULTS AND DISSCUSION

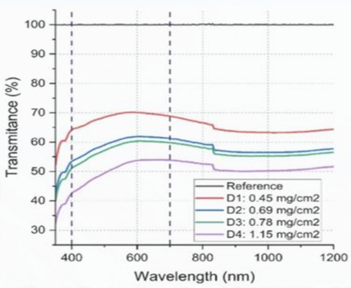

***Figure 3.** Transmittance losses (%) with respect to increasing surface dust density (mg/cm²) in each deposition.*

Surface dust density (mg/cm2)	Transmitance (%)
0,000	100,0
0,447	65,7
0,695	57,8
0,783	56,3
1,153	50,2

***Table 1.** Transmittance losses (%) in each deposition.*

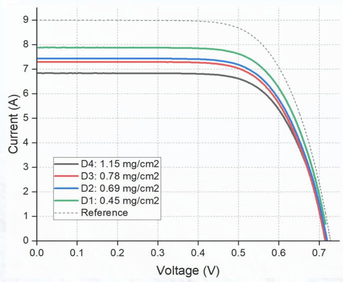

***Figure 5.** IV curves performance in each deposition*

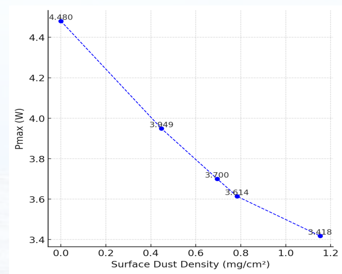

***Figure 6.** Pmax of the cell (W) on the electrical measurement of every cicle of deposition*

- The results of this study demonstrate that soiling accumulation on the surface of photovoltaic mini modules reduces light transmittance (Figure 3), directly impacting the energy available for conversion into electricity, results congruent with those reported in the literature (Figure 5, 6). As soiling density increases, transmittance losses can reach up to 50,2% (Table 1), leading to a corresponding reduction of 23,7% on maximum power (Pmax). Even at lower soiling densities of around 0.4 mg/cm², optical losses of up to 34.3% and Pmax reductions of up to 11,9% were observed.
- These findings align with those reported by Olivares et al. (2021) who conducted outdoor exposure studies at the Plataforma Solar del Desierto de Atacama (PSDA) and observed similar losses at comparable dust densities. **This consistency validates the ability of the soiling chamber to effectively simulate outdoor conditions**, even for extreme variable conditions such as those present in the Atacama Desert.
- The study simulated higher soiling densities than those found in the Atacama Desert. Densities of 1,153 mg/cm2 generate losses of up to 50,2% in transmittance generating 23,7% power losses, to assess the potential impact of extreme soiling scenarios on the optical and electrical properties of photovoltaic modules.

CONCLUSIONS

The results of this study confirm that the soiling chamber effectively replicates the optical losses observed in outdoor conditions, as evidenced by the consistency with findings from previous outdoor experiments conducted at the Plataforma Solar del Desierto de Atacama (Olivares et al., 2021). This demonstrates the reliability of the soiling chamber as a tool for simulating natural conditions under controlled indoor environments. Moreover, the soiling chamber significantly reduces the time required for experimental studies on soiling, achieving equivalent results in just one and a half days compared to the approximately one month needed for outdoor experimentation. These advantages highlight the soiling chamber as a valuable methodology for accelerating research on the effects of soiling.

Acknowledgments:

The authors express gratitude to the projects:

-ANID/FONDAP/1523A0006 "Solar Energy Research Center"- SERC-Chile and the project ATAMOSTEC with the contract no. 17PTECES-75830.

-ECOS-ANID "Graphene as transparent current spreading electrode in silicon heterojunction solar cells" #ECOS210038.

-Contrato RYC2021-031958-I finaciado por MCIN/AEI/10.13039/501100011033 y NextGenerationEU/PRTR

- CACTUS project funded by HORIZON-INFRA-2023-DEV-01-06 program (Ref.: 101132182)

References:

-Bessa, J.G., Micheli, L., Almonacid, F., Fernandez, E.F., 2021. Monitoring photovoltaic soiling: assessment, challenges, and perspectives of current and potential strategies. iScience 24. https://doi.org/10.1016/j.isci.2021.102165.

-Olivares, D., Ferrada, E., Escobar, R., Soto, C., Pino, A., y Cortés, A., 2021. Characterization of Changes in the Soiling Properties and Deposition Rates Because of Groundworks Near a PV Plant in the Atacama Desert. ISES Conference Proceedings.

Organized by:

Sponsors:

Volumetric properties modelling in unsaturated solution of Li–Na–K–Cl–H_2O system from 288.15 to 323.15 K using the Pitzer equations

José D. Arriagada[1], Aldo N. Fuentes[2], Yecid P. Jimenez[2,3], Jesús M. Casas[1], Francisca J. Justel[1]
[1]*Departamento de Ingeniería Metalúrgica y Materiales, Universidad Técnica Federico Santa María, Av. España 1680, Valparaíso, Chile*
[2]*Departamento de Ingeniería Química y Procesos de Minerales, Facultad de Ingeniería, Universidad de Antofagasta, Av. Angamos 601, Antofagasta, Chile*
[3]*Centro de Economía Circular en Procesos Industriales (CECPI), Facultad de Ingeniería, Universidad de Antofagasta, Av. Angamos 601, Antofagasta 1240000, Chile*

In recent times, lithium has gained significant importance due to its diverse applications in pharmacology, ceramics, glass, lubricants, greases, casting powders, coolants, polymers, and aluminum alloys. However, it is in lithium–ion batteries where its importance has increased notably, demonstrating sustained growth in demand in recent years, with prospects for even greater increases in the future [1].

Chile currently holds the third-largest reserve of lithium in brine and stands as the world's second–largest producer [2], where various lithium compounds are manufactured, including lithium carbonate, lithium hydroxide, and lithium chloride. This process is primarily carried out through precipitation in solar evaporation ponds of highly concentrated brines extracted from natural salt flats followed by purification and crystallization.

An accurate understanding of the impact of solute concentration and temperature on the density of these brines is essential for optimizing and designing lithium compound production processes. In this context, modeling this property is an extremely useful tool, as it is directly related to the apparent molar volume. This, in turn, is influenced by the excess thermodynamic property primarily caused by electrostatic interactions between dissolved species, resulting in a deviation from ideal solution behavior.

There are several modeling developments aimed at understanding thermodynamics in highly concentrated saline solutions [3]. Based on the original work of Debye–Hückel [4], whose equations are valid for low molalities, the semi–empirical Pitzer model [5] has been widely adopted due to its extensive applicability. This model can accurately represent excess thermodynamic properties in electrolytic solutions up to very high concentrations (typically up to 6 $mol \cdot kg^{-1}$), as it considers binary and ternary interactions among charged and uncharged species, as well as the effects of ionic strength [5].

In this study, modeling of density was carried out for unsaturated solutions in the quaternary system Li–Na–K–Cl–H_2O from 288.15 to 323.15 K. For this purpose, the volumetric Pitzer ionic interaction model was employed, using experimental density data. The electrolytic system under investigation contains the solutes of interest in the lithium industry; sodium and potassium, which are the major components among the cations present in brines extracted from the Salar de Atacama [6], additionally, chloride is the main anion in these brines.

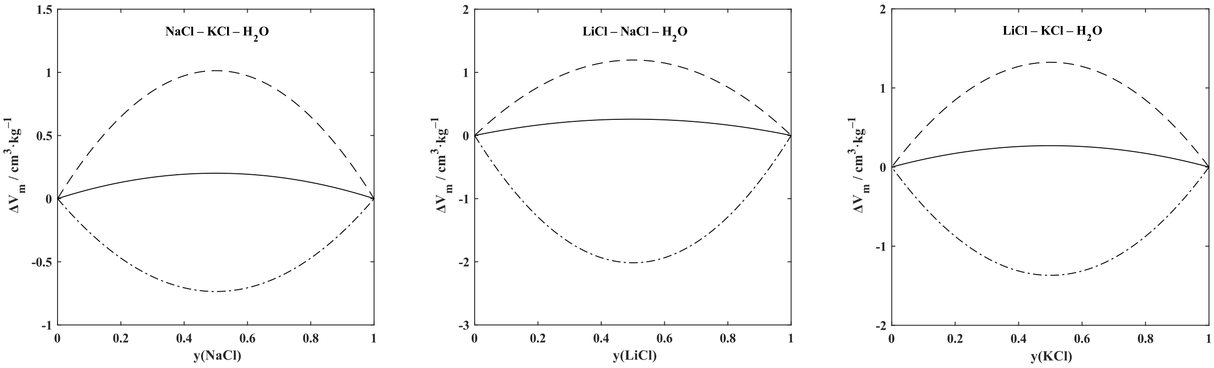

Figure 1. Calculated volume of mixing of ternary systems NaCl – KCl – H_2O, LiCl – NaCl – H_2O, and LiCl – KCl – H_2O at different ionic strengths, 298.15 K and 101.3 kPa, and as a function of ionic strength fraction y, with $y = I_1/(I_1 + I_2)$. (—) I = 1 mol·kg^{-1}; (– –) I = 3 mol·kg^{-1}; (– · –) I = 6 mol·kg^{-1}.

The volume of mixing values (ΔV_m) were calculated at different ionic strengths at 298.15 K in each constituent ternary system of the quaternary system studied (see Figure 1). The ΔV_m values can be negative or positive depending on whether the two binary solutes have the same or different structural abilities to orient water molecules, respectively [7]. In all ternary systems studied at low to medium ionic strength, the solutes exhibit different structural abilities. However, at high ionic strength (I = 6 mol·kg^{-1}), a solute may shift to being a structure breaker of water (KCl in the NaCl – KCl – H_2O and LiCl – KCl – H_2O systems, and LiCl in the LiCl – NaCl – H_2O system).

Keywords: Volumetric Pitzer model, lithium, density, apparent molar volume, volume of mixing, brines.

Acknowledgment: *This work was funded by ANID through the Fondecyt Project N°11220731. A.N. Fuentes thanks grant ANID-Subdirección de Capital Humano/Doctorado Nacional/2023-21230277.*

References

[1] D. Calisaya-Azpilcueta, S. Herrera-Leon, L.A. Cisternas, Current and future global lithium production till 2025, *Open Chem. Eng. J.*, 14 (2020) dx.doi.org/10.2174/1874123102014010036.

[2] U.S. Geological Survey, Mineral commodity summaries 2024, *U.S. Geological Survey*, (2024) dx.doi.org/10.3133/mcs2024.

[3] A.N. Fuentes, F.J. Justel, Y.P. Jimenez, J.M. Casas, Speciation and thermochemical modeling of the ternary system $CuSO_4$ – H_2SO_4 – H_2O in the temperature range 273.15–373.15 K, *J. Mol. Liq.*, 391B (2023) dx.doi.org/10.1016/j.molliq.2023.123377.

[4] P. Debye, E. Hückel, Zur theorie der elektrolyte. I. Gefrierpunktserniedrigung und verwandte erscheinungen, *Phys. Z.*, 24 (1923).

[5] K.S. Pitzer, Activity coefficients in electrolyte solutions, 2nd Edition, CRC Press, (1991).

[6] T. Tran, V.T. Luong, Chapter 3—Lithium Production Processes, in: A. Chagnes, J. Światowska (Eds.), Lithium Process Chemistry, Elsevier, Amsterdam, (2015).

[7] J.E. Desnoyers, M. Arel, G. Perron, C. Jolicoeur, Apparent molal volumes of alkali halides in water at 25 °C. Influence of structural hydration interactions on the concentration dependence, *J. Phys. Chem.*, 73 (1969) dx.doi.org/10.1021/j100844a032.

2024 IWLiME

11th INTERNATIONAL CONFERENCE IN LITHIUM, INDUSTRIAL MINERALS AND ENERGY

November 27-29, Antofagasta, Chile

Volumetric properties modelling in unsaturated solutions of Li–Na–K–Cl–H_2O system from 288.15 to 323.15 K using the Pitzer equations

José D. Arriagada[1], Aldo N. Fuentes[2], Yecid P. Jimenez[2,3], Jesús M. Casas[1], Francisca J. Justel[1]

[1] Departamento de Ingeniería Metalúrgica y Materiales, Universidad Técnica Federico Santa María, Av. España 1680, Valparaíso, Chile
[2] Departamento de Ingeniería Química y Procesos de Minerales, Facultad de Ingeniería, Universidad de Antofagasta, Av. Angamos 601, Antofagasta, Chile
[3] Centro de Economía Circular en Procesos Industriales (CECPI), Facultad de Ingeniería, Universidad de Antofagasta, Av. Angamos 601, Antofagasta 1240000, Chile

ABSTRACT

In this work, an experimental study and a thermodynamic model have been developed to describe the volumetric properties in unsaturated solutions of the quaternary system Li–Na–K–Cl–H_2O from 288.15 to 323.15 K and at 101.3 kPa. For this, the volumetric Pitzer ionic interaction model was employed, whose calibrations were carried out based on our own density measurements as a function of electrolyte concentration and temperature. The model achieved fitting standard deviations of 0.08%, 0.19%, and 0.07% in the ternary systems NaCl – KCl – H_2O, LiCl – NaCl – H_2O, and LiCl – KCl – H_2O, respectively. The ΔV_m calculated at different ionic strengths at 298.15 K showed that in all ternary systems studied at low to medium ionic strength, the solutes exhibit different structural abilities; however, at high ionic strength (I = 6 mol·kg^{-1}), a solute may shift to being a structure breaker of water (KCl in the NaCl – KCl – H_2O and LiCl – KCl – H_2O systems, and LiCl in the LiCl – NaCl – H_2O system).

INTRODUCTION

- ✓ The quaternary system Li–Na–K–Cl–H_2O is a key component of the electrolyte system representing brines extracted from the Salar de Atacama in Chile, which are used for the production of lithium compounds.
- ✓ Understanding the impact of salt concentrations and temperature on solution density is crucial, as inaccuracies in this knowledge can affect the precision of mass balances and the proper sizing of equipment in production processes.
- ✓ In this study, density modeling was performed for unsaturated solutions in the quaternary system Li–Na–K–Cl–H_2O from 288.15 to 323.15 K and at 101.3 kPa, utilizing the Pitzer equations.

METHODOLOGY

Experimental work

Solution densities were determined for the systems LiCl – H_2O, NaCl – H_2O, KCl – H_2O, NaCl – KCl – H_2O, LiCl – NaCl – H_2O, and LiCl – KCl – H_2O from 288.15 to 323.15 K

Volumetric Pitzer Model [1–3]

$$V_\phi = \overline{V}^0_{\text{mix}} + \left(\frac{R'T}{\sum_i m_i}\right)\left\{\frac{IA_V}{R'T}\frac{\ln\left(1+bI^{1/2}\right)}{b} + 2\sum_c\sum_a m_c m_a\left(B^V_{ca} + \left(\sum_c m_c z_c\right)C^V_{ca}\right) + \sum_c\sum_{c'} m_c m_{c'}\left(2\theta^V_{cc'} + \sum_a m_a \psi^V_{cc'a}\right) + \sum_a\sum_{a'} m_a m_{a'}\left(2\theta^V_{aa'} + \sum_c m_c \psi^V_{aa'c}\right)\right\}$$

$$\rho = \frac{1000 + \sum_i m_i M_i}{V_\phi \sum_i m_i + \frac{1000}{\rho_w}}$$

$$\Delta V_m = V^{\text{ex}}_{\text{mix}} - yV^{\text{ex}}_1 - (1-y)\,V^{\text{ex}}_2$$

RESULTS

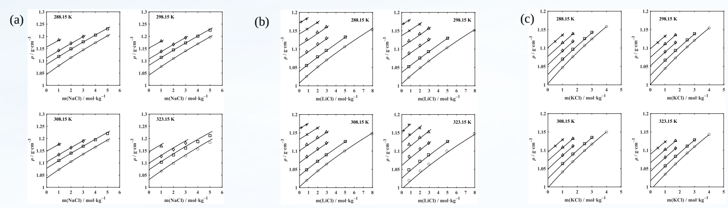

Figure 1. Comparison between experimental and modeled data of density in ternary systems (a) NaCl – KCl – H_2O, (b) LiCl – NaCl – H_2O, and (c) LiCl – KCl – H_2O from 288.15 to 323.15 K and at 101.3 kPa. (Symbols) experimental data, from this study; (—) Volumetric Pitzer model (this study).

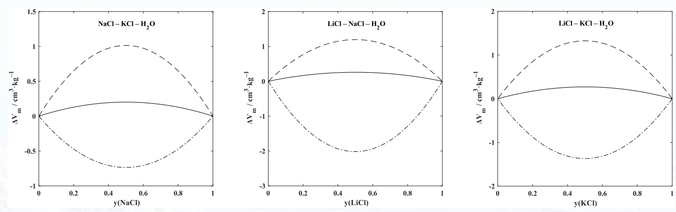

Figure 2. Calculated volume of mixing of ternary systems NaCl – KCl – H_2O, LiCl – NaCl – H_2O, and LiCl – KCl – H_2O at different ionic strengths, 298.15 K and 101.3 kPa, and as a function of ionic strength fraction y, with $y = I_1/(I_1+I_2)$. (—) I = 1 mol·kg^{-1}; (– –) I = 3 mol·kg^{-1}; (– · –) I = 6 mol·kg^{-1}.

CONCLUSIONS

Density model calibrations for the ternary systems NaCl – KCl – H_2O, LiCl – NaCl – H_2O, and LiCl – KCl – H_2O yielded fitting standard deviations of 0.08%, 0.19%, and 0.07%, respectively.

The volume of mixing values (ΔV_m) were calculated at different ionic strengths at 298.15 K in each ternary system studied. The ΔV_m values can be negative or positive depending on whether the two binary solutes have the same or different structural abilities to orient water molecules, respectively [4]. In all ternary systems studied at low to medium ionic strength, the solutes exhibit different structural abilities. However, at high ionic strength (I = 6 mol·kg^{-1}), a solute may shift to being a structure breaker of water (KCl in the NaCl – KCl – H_2O and LiCl – KCl – H_2O systems, and LiCl in the LiCl – NaCl – H_2O system).

This volumetric properties modeling in the quaternary system Li–Na–K–Cl–H_2O generates the basis for its extension to the multicomponent system representing brines extracted from the Salar de Atacama (e.g., the Li–Na–K–Mg–Cl–SO_4–B–H_2O system or Li–Seawater system).

REFERENCES

[1] P.S.Z. Rogers, K.S. Pitzer, Volumetric properties of aqueous sodium chloride solutions, J Phys Chem Ref Data 11 (1982) 15–81. https://doi.org/10.1063/1.555660.

[2] B.S. Krumgalz, R. Pogorelsky, K.S. Pitzer, Ion interaction approach to calculations of volumetric properties of aqueous multiple-solute electrolyte solutions, J Solution Chem 24 (1995) 1025–1038. https://doi.org/10.1007/BF00973519.

[3] L.M. Connaughton, F.J. Millero, K.S. Pitzer, Volume changes for mixing the major sea salts: Equations valid to ionic strength 3.0 and temperature 95 °C, J Solution Chem 18 (1989) 1007–1017. https://doi.org/10.1007/BF00647260.

[4] J.E. Desnoyers, M. Arel, G. Perron, C. Jolicoeur, Apparent molal volumes of alkali halides in water at 25 °C. Influence of structural hydration interactions on the concentration dependence, J Phys Chem 73 (1969) 3346–3351. https://doi.org/10.1021/j100844a032.

Acknowledgements

This work was funded by ANID through the Fondecyt Project N°11220731. A.N. Fuentes thanks grant ANID-Subdirección de Capital Humano/Doctorado Nacional/2023-21230277.

Organized by:

Sponsors:

POTENTIAL ELECTROACTIVE MATERIAL FOR LITHIUM-ION BATTERIES

Silvio, Ceballos Martínez[1,2], Jonathan Cisterna [1,2], Alifhers Mestra [1,2], Sergio Conejeros [1,2]

Departamento de Química, Facultad de Ciencias, Universidad de Católica del Norte, Sede Casa Central, Av. Angamos 0610, Antofagasta, Chile
[2] Centro Lithium I+D+i, Universidad Católica del Norte, Avenida Angamos 0610, 1270709, Antofagasta, Chile

Next-generation materials for energy storage are key components for the transition toward more sustainable energy sources. This work discloses the study of a new-class of quaternary chalcogenides as a promising candidate for energy storage in lithium-ion rechargeable batteries, due to its high coulombic efficiency and operational voltage. Solid-state characterization, such as X-ray diffraction (XRD) and scanning electron microscopy (SEM) were carried out to identify structural and morphological features. Additionally, potentiostatic and galvanostatic techniques were used to evaluate redox potentials, electrochemical window, reaction reversibility, and specific charge and discharge capacity.
The results revealed that the compound crystallizes in a cubic phase with $Fd\bar{3}m$ space group. Preliminary, electrochemical results point out that the material shows electrochemical activity in the 0-3 volts range vs Li/Li^+. Cyclic voltammetry measurements show a diffusion-controlled behavior in the resulting compound (94.41%). Additionally, galvanostatic charge-discharge curves demonstrate a specific discharge capacity of 1104.82 mAh g^{-1}, significantly exceeding the theoretical specific capacity- a typical electrochemical behavior of conversion materials.

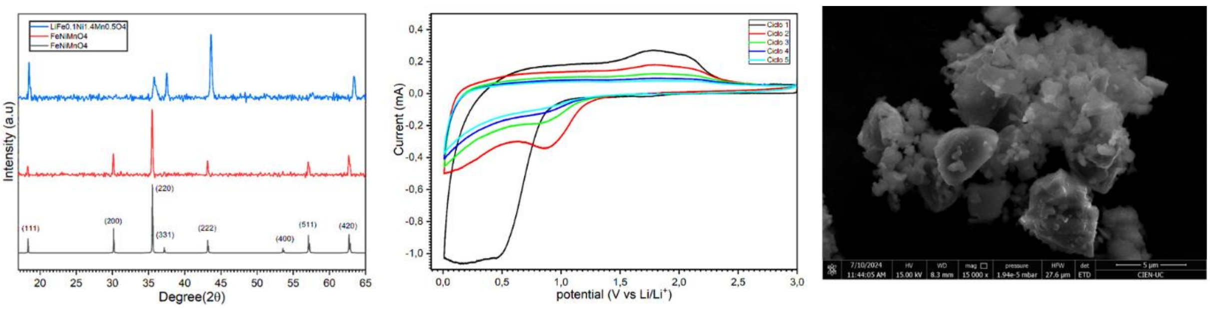

Figure 1. Structural, morphological, and electrochemical characterization of $LiFe_{0.1}Ni_{1.4}Mn_{0.5}O_4$. (a) Powder X-ray diffraction patterns, (b) cyclic voltammetry (CV) at 0.1 mV s^{-1} within a potential window of 0 to 3.0 V, (c) SEM image with 5 µm magnification.

Keywords: *conversion material, charge-discharge, diffusion-controlled processes.*

Acknowledgments: *The authors acknowledge the Departamento de Química, the Scientific Equipment Unit, MAINI and Lithium I+D+i Center at Universidad Católica del Norte.*

References:

[1] Lu, X.; Liu, H.; Shi, X.; Zhang, J. A Simple Synthesis of $Li_3Fe(MoO_4)_3$@C Composite Anode Materials with High Initial Coulombic Efficiency and High Capacity Stability for Lithium Ion Batteries. Journal of Electroanalytical Chemistry, 2022, 927, 116998. https://doi.org/10.1016/j.jelechem.2022.116998.

[2] Bin, H.; Yao, Z.; Zhu, S.; Zhu, C.; Pan, H.; Chen, Z.; Wolverton, C.; Zhang, D. A High-Performance Anode Material Based on FeMnO3/Graphene Composite. Journal of Alloys and Compounds, 2017, 695, 1223–1230.

[3] Wei, H.; Guo, Y.; Gao, C.; Wang, Z. Solvothermal Synthesis of $FeMnO_3$ Nanobelts with Excellent Electrochemical Performances for Lithium-Ions Batteries and Supercapacitors. Advanced Powder Technology, 2021, 32, 4322–4329. https://doi.org/10.1016/j.apt.2021.09.035.

POTENTIAL ELECTROACTIVE MATERIAL FOR LITHIUM-ION BATTERIES

Química UCN
Departamento de Química

Silvio, Ceballos Martínez[1], Jonathan Cisterna [2], Alifhers Mestra [1], Sergio Conejeros [2]

Departamento de Química, Facultad de Ciencias, Universidad de Católica del Norte, Sede Casa Central, Av. Angamos 0610, Antofagasta, Chile

2 Centro Lithium I+D+i, Universidad Católica del Norte, Avenida Angamos 0610, 1270709, Antofagasta, Chile

INTRODUTION

Next-generation materials for energy storage are key components for the transition toward more sustainable energy sources. This work discloses the study of a new-class of quaternary chalcogenides as a promising candidate for energy storage in lithium-ion rechargeable batteries, due to its high coulombic efficiency and operational voltage. Solid-state characterization, such as X-ray diffraction (XRD) and scanning electron microscopy (SEM) were carried out to identify structural and morphological features. Additionally, potentiostatic and galvanostatic techniques were used to evaluate redox potentials, electrochemical window, reaction reversibility, and specific charge and discharge capacity. The results revealed that the compound crystallizes in a cubic phase with space group. Preliminary, electrochemical results point out that the material shows electrochemical activity in the 0-3 volts range vs Li/Li + . Cyclic voltammetry measurements show a diffusion-controlled behavior in the resulting compound (94.41%). Additionally, galvanostatic charge-discharge curves demonstrate a specific discharge capacity of 1104.82 mAh g^{-1}, significantly exceeding the theoretical specific capacity- a typical electrochemical behavior of conversion materials.

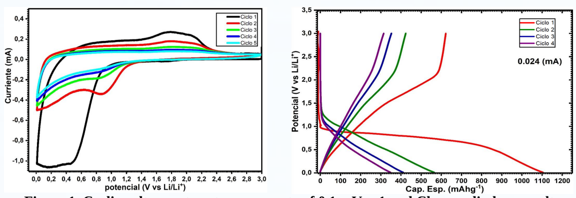

Figure 1. Cyclic voltammetry at a sweep rate of 0.1 mV s–1 and Charge–discharge voltage profiles

Table 1. Anodic and Cathodic Redox Potentials of $LiFe_{0.1}Ni_{1.4}Mn_{0.5}O_4$ at 0.1 mV·s⁻¹

Especie	Corriente (mA)	Potencial anódico (V)	Corriente (mA)	Potencial catódico (V)
Fe	0.20	1.75	-0.34	0.85
Ni	0.24	1.97	-0,3	0.96
Mn	0.23	2.07	-1.03	0.45

Table 2. Charge-Discharge Specific Capacity

$LiFe_{0.1}Ni_{1.4}Mn_{0.5}O_4$	Descarga	Carga
CORRIENTE (mA)	0.024	0.024
Cap. teórica ($mAhg^{-1}$)	132.4	--------
Cap. Esp. Ciclo 1 ($mAhg^{-1}$)	1104.82	622.42
Cap. Esp. Ciclo 2 ($mAhg^{-1}$)	565.05	423.79
Cap. Esp. Ciclo 3 ($mAhg^{-1}$)	407.47	352.59
Cap. Esp. Ciclo 4 ($mAhg^{-1}$)	348.36	314.42

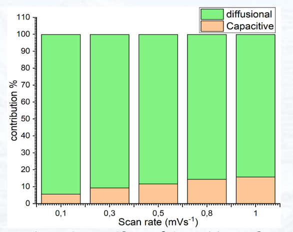

Figure 2. Bar Chart of Capacitive and Faradaic Contributions

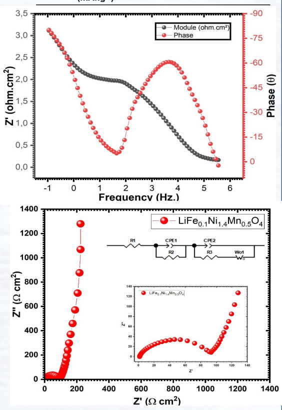

Figure 3. Nyquist and Bode plot at open circuit potential

Table 3. Resistances Associated with the Equivalent Circuit of the Cell

Parámetro	$LiFe0_{0.1}Ni_{1.4}Mn_{0.5}O_4$
R_e (Ω)	1,46
R_{ct} (Ω)	566,31
σ ($\Omega\ s^{-1}$)	309,86
D^{+}_{Li} ($cm^2 s^{-1}$)	$2,45x10^{-15}$

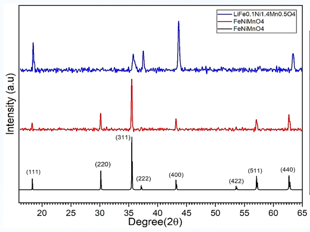

Figure 4. XRD pattern of the $LiFe_{0.1}Ni_{1.4}Mn_{0.5}O_4$ phase and characteristic signals of the $Fd\bar{3}m$ phase.

Table 4. Cell Parameters $Fd\bar{3}m$

Muestra	a(Å)	V(Å³)
$FeNiMnO_4$	8,379	588,27
$LiFe_{0.1}Ni_{1.4}Mn_{0.5}O_4$	8,309	573,697

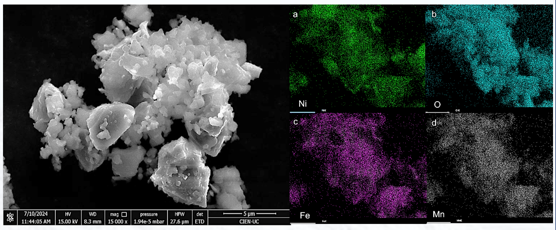

Figure 5. SEM Images at 5 µm Magnification and Mapping of $LiFe_{0.1}Ni_{1.4}Mn_{0.5}O_4$ Powder..

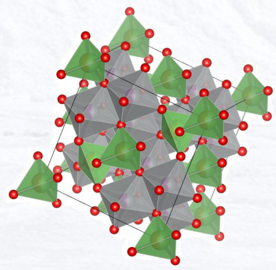

Figure 6. Crystal Structure Corresponding to the $LiFe_{0.1}Ni_{1.4}Mn_{0.5}O_4$ Phase

Figure 7. Two-Step Synthetic Route: Mechanochemical and Solid-State

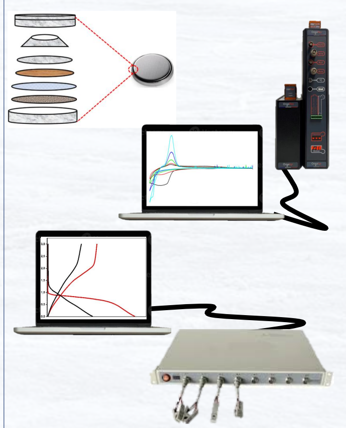

Figure 8. Electrochemical Characterization through Potentiostatic and Galvanostatic Studies

CONCLUSIONS.

- **A lithium-enriched quaternary oxide phase was synthesized and characterized using X-ray diffraction (XRD), Raman spectroscopy, and scanning electron microscopy (SEM). The results indicated that the oxide has a cubic spinel structure with the space group $Fd\bar{3}m$ and is isostructural to the lithium-free phase.**
- **It was demonstrated that $LiFe_xNi_yMn_zO_4$ is electrochemically active for lithium insertion. The discharge capacity observed during the first cycle is approximately 1104.82 mAh/g, which is significantly higher than the theoretical value of 143.97 mAh/g. This behavior is characteristic of conversion materials.**
- **Slow mobility of Li^+ ions was observed, leading to low electrochemical performance. From a future perspective, it is necessary to improve high-performance anodes by employing post-treatment methods, such as nanoparticulate materials or conductive carbon coatings.**

REFERENCES.

1. Lu, X.; Liu, H.; Shi, X.; Zhang, J. A Simple Synthesis of $Li_3Fe(MoO_4)_3$@C Composite Anode Materials with High Initial Coulombic Efficiency and Lithium-Ion Stability for Lithium-Ion Batteries. Journal of Electroanalytical Chemistry, 2022, 927, 116998. https://doi.org/10.1016/j.jelechem.2022.116998.
2. Bin, H.; Yao, Z.; Zhu, S.; Zhu, C.; Pan, H.; Chen, Z.; Wolverton, C.; Zhang, D. A High-Performance Anode Material Based on FeMnO3/Graphene Composite. Journal of Alloys and Compounds, 2017, 695, 1223–1230. https://doi.org/10.1016/j.jallcom.2016.10.249.
3. Wei, H.; Guo, Y.; Gao, C.; Wang, Z. Solvothermal Synthesis of FeMnO3 Nanobelts with Excellent Electrochemical Performances for Lithium-Ions Batteries and Supercapacitors. Advanced Powder Technology, 2021, 32, 4322–4329. https://doi.org/10.1016/j.apt.2021.09.035.

ACKNOWLEDGMENTS.

The authors acknowledge to the Departamento de Química, the Scientific Equipment Unit, MAINI and Lithium I+D+i Center at Universidad Católica del Norte.

STUDY OF ELECTROCRYSTALLIZATION OF PALLADIUM ON TITANIUM FOR WATER REDUCTION ELECTROCATALYSIS

11th IWLiME, November 27th-29th, 2024

Deellan Tello1,2, A. González1,2 , Svetlana Ushak 1,2 , Mario Grágeda 1,2

[1]*Center for Advanced Research in Lithium and Industrial Minerals, University of Antofagasta, Avenue Universidad de Antofagasta 02800, Antofagasta, Chile.*

[2]*Chemical Engineering Department, University of Antofagasta, Avenue Universidad de Antofagasta 02800, Antofagasta, Chile*

Hydrogen (H_2) has gained prominence as a clean and efficient energy source due to its high energy density, which surpasses that of fossil fuels and lithium batteries [1-2]. Its main byproduct, water, makes it an environmentally sustainable option. Among the technologies for its production, anion exchange membrane (AEM) electrolysis stands out by combining the advantages of well-established methods such as PEM and AE [3], while utilizing more accessible and cost-effective materials. In this context, palladium emerges as a promising candidate due to its lower cost and its ability to enhance catalytic properties, which could improve efficiency and reduce the costs of electrolyzers [4].

This study explores the electrocrystallization of nanostructured palladium and its impact on the electrochemical production of hydrogen in alkaline solutions such as KOH. The methodology includes palladium deposition on titanium, electrode characterization, and the analysis of palladium nucleation and growth mechanisms to optimize the process. The objective is to advance innovative technologies for green hydrogen production and the electrochemical synthesis of LiOH through water reduction.

For the experimental design, seven variables were initially considered: pH, concentration, applied potential, ON time, OFF time, number of cycles, and configuration. This would have required 128 tests (2^7), so a simplification was made by identifying the most relevant parameters based on the literature.

Cyclic voltammetry was used to identify the palladium (Pd) electrodeposition peaks and the onset potentials of the reactions, analyzing the nucleation and growth behavior of the metal through characteristic current peaks. The study identified that the optimal potential range for controlled Pd electrodeposition is between 0.0 and 0.2 V.

Subsequently, linear sweep voltammetry tests were conducted to determine the catalytic performance of palladium electrodeposits in HER activity, considering different applied effects such as concentration, potential, number of cycles, ON time, and OFF time. Experiment No. 15 demonstrated the best electrocatalytic performance, achieving higher current density values. A smooth curve without peaks was observed, confirming a uniform deposit on the electrode with particle agglomerations in the form of islands, indicating three-dimensional growth according to the Volmer-Weber model, as shown in Figure 1. The linear voltammetry, SEM, and EDX tests confirmed its superior electrocatalytic behavior.

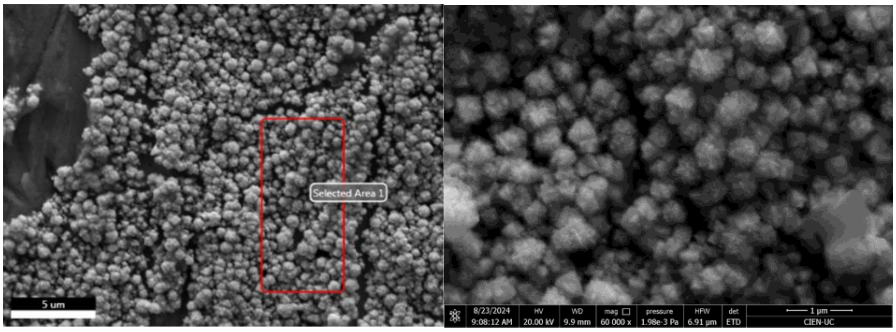

Figure 1. SEM images, Experiment 15.

References:

[1] Zakaria, Z., & Kamarudin, S. (2021). A review of alkaline solid polymer membrane in the application of AEM electrolyzer: Materials and characterization. International Journal of Energy Research, 45(13), 18337-18354. https://doi.org/10.1002/er.6983

[2] Hydrogen Council 2017, from https://hydrogencouncil.com/wp-content/uploads/2017/11/Hydrogen-scaling-upHydrogen-Council.pdf. Retrieved 27 April 2022

[3] Miller, H., Bouzek, K., Hnat, J., Loos, S., Bernäcker, C., & Weißgärber, T. et al. (2020). Green hydrogen from anion exchange membrane water electrolysis: a review of recent developments in critical materials and operating conditions. Sustainable Energy & Fuels, 4(5), 2114-2133. https://doi.org/10.1039/c9se01240k

[4] Zhang, L., Chang, Q., Chen, H., & Shao, M. (2016). Recent advances in palladium-based electrocatalysts for fuel cell reactions and hydrogen evolution reactions. Nano Energy, 29, 198-219. https://doi.org/10.1016/j.nanoen.2016.02.044

Study of Electrocrystallization of Palladium on Titanium for Water Reduction Electrocatalysis

Deellan Tello[1,2], A. González[1,2], Svetlana Ushak[1,2], Mario Grágeda[1,2]

[1]*Center for Advanced Research in Lithium and Industrial Minerals, University of Antofagasta, Avenue Universidad de Antofagasta 02800, Antofagasta, Chile.*

[2]*Chemical Engineering Department, University of Antofagasta, Avenue Universidad de Antofagasta 02800, Antofagasta, Chile*

INTRODUCTION

The research focuses on the electrocrystallization of nanostructured palladium on titanium and its influence on hydrogen production through water reduction in alkaline solutions, such as KOH and LiOH. The study employs a methodology involving the electrocrystallization of palladium on a titanium substrate and the characterization of the electrodeposits to evaluate their performance in water electrolysis.

EXPERIMENTAL PROCEDURE

- For the experimental design, seven variables were initially considered: pH, concentration, applied potential, ON time, OFF time, number of cycles and configuration. This implied performing 128 tests (2^7), so it was simplified by identifying, from the literature, the most relevant parameters.
- By means of cyclic voltammetry, the palladium (Pd) electrodeposition peaks and the starting potentials of the reactions are identified. The study identified that the optimum potential range for controlled electroposition of Pd is 0 to 0.2 V.
- Increasing the electrolyte concentration improves the initial efficiency and accelerates the growth of Pd deposits, although excessive concentrations could alter their morphology, requiring SEM analysis.

Experiment	pH (HCl M)	Concentration (mM)	Potential (V)	Time ON (s)	Particle size	Average size
9	0.1	1	0.2	1	[142,7-552,2]	306,1
12	0.1	1	0	1	[180,4-751,9]	454,2
15	0.1	3	0	1	[200,3-876,6]	407,9
19	0.1	3	0	0.1	[211,6-812,2]	473,9
20	0.1	3	0	1	[276,1-1556,3]	762,166
24	0.1	5	0.2	1	[246,5-1868,9]	1014,3

- The catalytic performance of the Pd electrodes in the HER activity was evaluated by means of linear scanning voltammetry.
- In the Linear Voltammetry plot at 1% KOH, experiment n.°15 showed the best electrocatalytic behavior, with higher current density, curve without peaks and demonstrated a uniform deposition on the electrode.

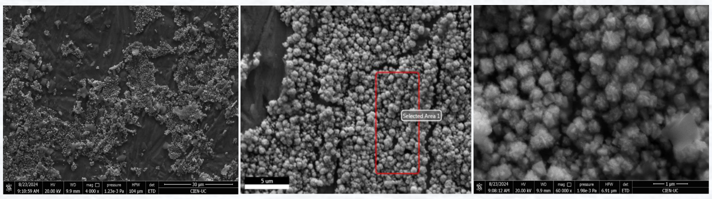

Using Statgraphics, the overpotentials obtained in the linear sweep tests were analyzed to determine the optimal deposition electrode conditions. The analysis revealed that applying a voltage of 0.2 V, using a lower concentration of 1 mM and setting an OFF time of 4 seconds significantly reduced the overpotential.

RESULTS AND DISCUSSION

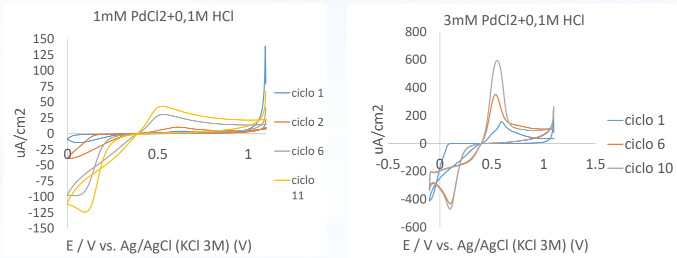

In the stage of characterization of the results, the aim is to recognize the distribution of particles deposited on the electrode and the size range of the particles formed for each experiment.

It is important to note that the pulsed electrodeposition tests (charge and discharge) presented in this poster correspond to electrodes selected with specific criteria, based on different experimental conditions.

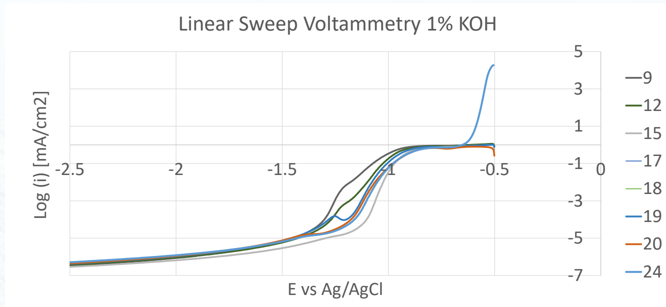

SEM images of the "Test 15" electrode show deposits of Pd particles ranging in size from 200 to 877 nm, with an average of 408 nm. The surface is observed to be uniform, with island-like agglomerations, indicating three-dimensional growth according to the Volmer-Weber model.

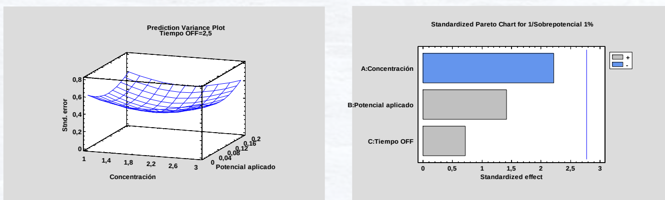

CONCLUSIONS

Electrode 15 showed the best performance in H2 production in 1% KOH solution. It was created with 3 mM $PdCl_2$ + 0.1 M HCl, a voltage of 0 V, and OFF time of 1 second. Linear voltammetry, SEM and EDRX tests confirmed its superior electrocatalytic behavior and uniform deposition, indicating a three-dimensional growth according to the Volmer-Weber model.

ACKNOWLEDGMENTS

Authors thanks to the Fondecyt Postdoctorado 2023 Nº3230474 and "Plataforma para la producción de materiales avanzados sustentables y manufactura de baterías de litio" SQM-CELIMIN Project for the financial support

Solid-liquid equilibrium modelling of Methanol + Lithium hydroxide + Water system at three temperatures

Martha Claros[1], Aldo N. Fuentes[2], Yahaira Barrueto[1], Marianela Soria[1], Yecid P. Jimenez[2] Francisca J. Justel[1]

[1]*Departamento de Ingeniería Metalúrgica y Materiales, Universidad Técnica Federico Santa María, Av. España 1680, Valparaíso, Chile*
[2]*Departamento de Ingeniería Química y Procesos de Minerales, Facultad de Ingeniería, Universidad de Antofagasta, Av. Angamos 601, Antofagasta, Chile*

The lithium industry has attracted significant attention due to the rising demand for lithium-ion batteries, driven by applications in portable electronics, electric vehicles, and renewable energy storage [1]. Lithium's unique properties, such as high electrochemical potential, low density, high heat capacity, and a low thermal expansion coefficient, make it essential in battery technology, which may be used as cathode material and/or electrolyte.
Lithium hydroxide is typically produced by solar evaporation and reaction with calcium hydroxide in aqueous solution; however, this method is both water- and energy-intensive [2]. A promising alternative is the drowning-out crystallization technique, where an organic co-solvent, such as methanol, is added to an aqueous lithium solution to induce precipitation at room temperature [3]. This method conserves energy and avoids the challenges associated with solubility changes dependent on temperature, thus providing an efficient means to crystallize high-purity lithium hydroxide [4].
The solubility diagrams and physical properties, including the co–solvent and the desired salt, are necessary since the addition of the co–solvent generates a new solubility curve, usually located below the original solvent, which allows supersaturation at the same solute concentration. However, data on the physical properties of lithium salt + water + alcohol systems are limited in the literature [5].
Therefore, this work systematically examines the solid-liquid equilibrium of the methanol + lithium hydroxide + water system at three temperatures (298.15, 303.15, and 308.15 K). Experimental solubility data were successfully correlated using the modified Pitzer model, achieving strong agreement with observed values. Figure 1 presents the solubility of the system CH_3OH + LiOH + H_2O experimentally determined at different temperatures, along with the correlation with the modified Pitzer model.

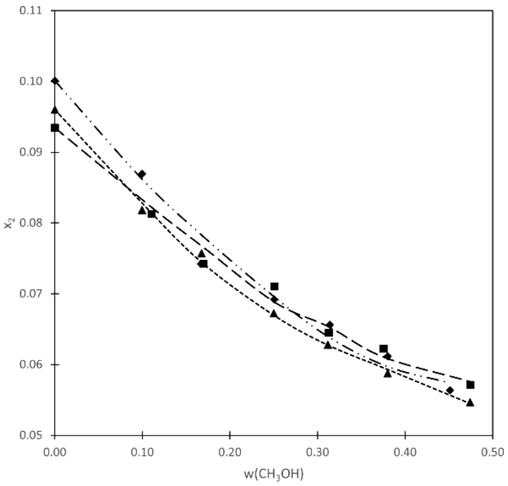

Fig. 1. LiOH solubility versus molality mass fraction of CH_3OH for the ternary system CH_3OH + LiOH + H_2O at all temperature under study: ■ 298.15 K, ▲ 303.15 K, ♦ 308.15 K and (—) calculated from the modified Pitzer model.

Adding a co-solvent reduces the solution's dielectric constant, increasing electrostatic attraction between oppositely charged ions. This enhanced interaction fosters the formation of insoluble ionic species. A critical distance exists at each dielectric constant where the electrostatic energy matches the ions' kinetic energy; below this distance, ions form stable ionic pairs that resist dissociation. Thus, introducing an organic co-solvent strengthens ionic cohesion in aqueous salt solutions, leading to precipitation.

Keywords: Lithium hydroxide, methanol, solubility, modified Pitzer model

Acknowledgment: *This work was funded by ANID through the Fondecyt Project N°11220731. A.N. Fuentes thanks grant ANID-Subdirección de Capital Humano/Doctorado Nacional/2023-21230277.*

References

[1] Gil-Alana, L.A.; Monge, M. Lithium: Production and estimated consumption. Evidence of persistence. Resour. Policy 2019, 60, 198–202, doi:10.1016/j.resourpol.2019.01.006.

[2] Kim, K.J. Recovery of lithium hydroxide from spent lithium carbonate using crystallizations. Sep. Sci. Technol. 2008, 43, 420–430, doi:10.1080/01496390701784088.

[3] Taboada, M.E.; Véliz, D.M.; Galleguillos, H.B.; Graber, T.A. Solubility, density, viscosity, electrical conductivity, and refractive index of saturated solutions of lithium hydroxide in water + ethanol. J. Chem. Eng. Data 2005, 50, 187–190, doi:10.1021/je0497449.

[4] Berry, D.A.; Dye, S.R.; Ng, K.M. Synthesis of Drowning-Out Crystallization-Based Separations. AIChE J. 1997, 43, 91–103, doi:10.1002/aic.690430112.

[5] Taboada, M.E.; Galleguillos, H.R.; Graber, T.A.; Álvarez-Benedí, J. Density, viscosity, refractive index and electrical conductivity of saturated solutions of the lithium hydroxide + ethanol + water system at 298.15 K, and thermodynamic description of the solid-liquid equilibrium. Fluid Phase Equilib. 2005, 235, 104–111, doi:10.1016/j.fluid.2005.05.022.